GEOLOGICAL SURVEY OF CANADA
BULLETIN 580

GEOLOGY OF THE DUBAWNT LAKE AREA, NUNAVUT–NORTHWEST TERRITORIES

T.D. Peterson

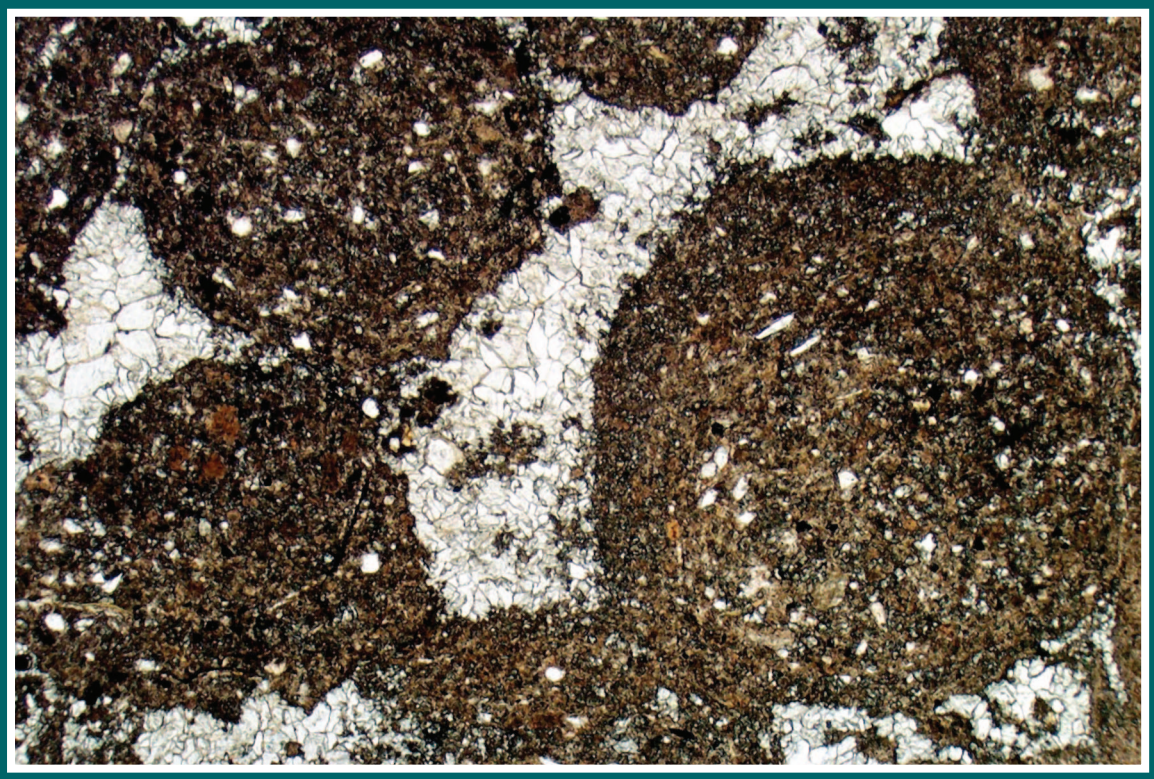

2006

Natural Resources Canada
Ressources naturelles Canada

Canada

The CD-ROM accompanying this publication contains the full report, including any oversized figures and/or A-series maps, in Portable Document Format (PDF). Oversized items may be purchased separately as paper plots from any Geological Survey of Canada Bookstore location:

Geological Survey of Canada Bookstore (Ottawa)
601 Booth Street
Ottawa, Ontario
K1A 0E8
Tel.: (613) 995-4342
Tel.: (888) 252-4301 (toll-free)
Fax: (613) 943-0646
E-mail: gscbookstore@nrcan.gc.ca
Web: http://gsc.nrcan.gc.ca/bookstore/index_e.php

Geological Survey of Canada Bookstore (Calgary)
3303-33rd Street, N.W.
Calgary, Alberta
T2L 2A7
Tel.: (403) 292-7030
Fax: (403) 299-3542
E-mail: gsc_calgary@nrcan.gc.ca
Web: http://gsc.nrcan.gc.ca/org/calgary/pub/bookstore_e.php

Geological Survey of Canada Bookstore (Vancouver)
101-605 Robson Street
Vancouver, British Columbia
V6B 5J3
Tel.: (604) 666-0271
Fax: (604) 666-1337
E-mail: gscvan@gsc.nrcan.gc.ca
Web: http://gsc.nrcan.gc.ca/org/vancouver/bookstore/index_e.php

Geological Survey of Canada Bookstore (Atlantic)
1 Challenger Drive
P.O. Box 1006
Dartmouth, Nova Scotia
B2Y 4A2
Tel.: (902) 426-4386
Fax: (902) 426-4848
E-mail: Jennifer.Bates@nrcan-rncan.gc.ca
Web: http://gsca.nrcan.gc.ca/pubprod/pubprod_e.php

Geological Survey of Canada Bookstore (Québec)
490, rue de la Couronne
Québec, Quebec
G1K 9A9
Tel.: (418) 654-2677
Fax: (418) 654-2660
E-mail: cgcq_librairie@rncan.gc.ca
Web: http://www.gscq.nrcan.gc.ca/bibliotheque/

Le CD-ROM qui accompagne cette publication renferme le rapport au complet, y compris les figures surdimensionnées ou les cartes de série A, en format PDF. Pour acheter des copies papier des éléments surdimensionnés, adressez-vous à la Librairie de la Commission géologique du Canada :

Librairie de la Commission géologique du Canada (Ottawa)
601, rue Booth
Ottawa (Ontario)
K1A 0E8
Tél. : (613) 995-4342
Tél. : (888) 252-4301 (sans frais)
Télécopieur : (613) 943-0646
Courriel : librairiecgc@nrcan.gc.ca
Web : http://cgc.rncan.gc.ca/librairie/index_f.php

Librairie de la Commission géologique du Canada (Calgary)
3303-33rd Street, N.W.
Calgary (Alberta)
T2L 2A7
Tél. : (403) 292-7030
Télécopieur : (403) 299-3542
Courriel : gsc_calgary@gsc.nrcan.gc.ca
Web : http://gsc.nrcan.gc.ca/org/calgary/pub/bookstore_f.php

Librairie de la Commission géologique du Canada (Vancouver)
101-605 Robson Street
Vancouver (Colombie-Britannique)
V6B 5J3
Tél. : (604) 666-0271
Télécopieur : (604) 666-1337
Courriel : gscvan@gsc.nrcan.gc.ca
Web : http://cgc.rncan.gc.ca/org/vancouver/ bookstore/index_f.php

Librairie de la Commission géologique du Canada (Atlantique)
1 Challenger Drive
P.O. Box 1006
Dartmouth (Nouvelle-Écosse)
B2Y 4A2
Tél. : (902) 426-4386
Télécopieur : (902) 426-4848
Courriel : Jennifer.Bates@nrcan-rncan.gc.ca
Web : http://gsca.nrcan.gc.ca/pubprod/pubprod_f.php

Librairie de la Commission géologique du Canada (Québec)
490, rue de la Couronne
Québec (Québec) G1K 9A9
Tél. : (418) 654-2677
Télécopieur : (418) 654-2660
Courriel : cgcq_librairie@rncan.gc.ca
Web : http://www.cgcq.rncan.gc.ca/bibliotheque/

GEOLOGICAL SURVEY OF CANADA
BULLETIN 580

GEOLOGY OF THE DUBAWNT LAKE AREA, NUNAVUT–NORTHWEST TERRITORIES

T.D. Peterson

2006

Catalogue No. M42-580E
ISBN 0-660-19528-3

Available in Canada from the Geological Survey of Canada Bookstore
(*see inside front cover for details*)

A copy of this publication is also available for reference by depository libraries across Canada through access to the Depository Services Program's Web site at http://dsp-psd.pwgsc.gc.ca

A free digital download of this publication is available from GeoPub:

http://geopub.nrcan.gc.ca/index_e.php

Click on "Free Download".

Cover illustration
Photomicrograph (plane-polarized light) of accretionary lapilli, sample PHA88-310, western Dubawnt Lake. The lapilli, which consist of phlogopite minette tuff mixed with quartzofeldspathic debris, were found filling in the fractures on the tops of minette flows, and represent a rare subaerial facies in this area.

Critical readers
Subhas Tella
Robert Rainbird

Author's address
Tony D. Peterson
Continental Geoscience Division
Geological Survey of Canada
601 Booth Street
Ottawa, Ontario K1A 0E8

Original manuscript submitted: 2002–08–30
Final version approved for publication: 2005–05–30

CONTENTS

Appendix A

Tables

Illustrations

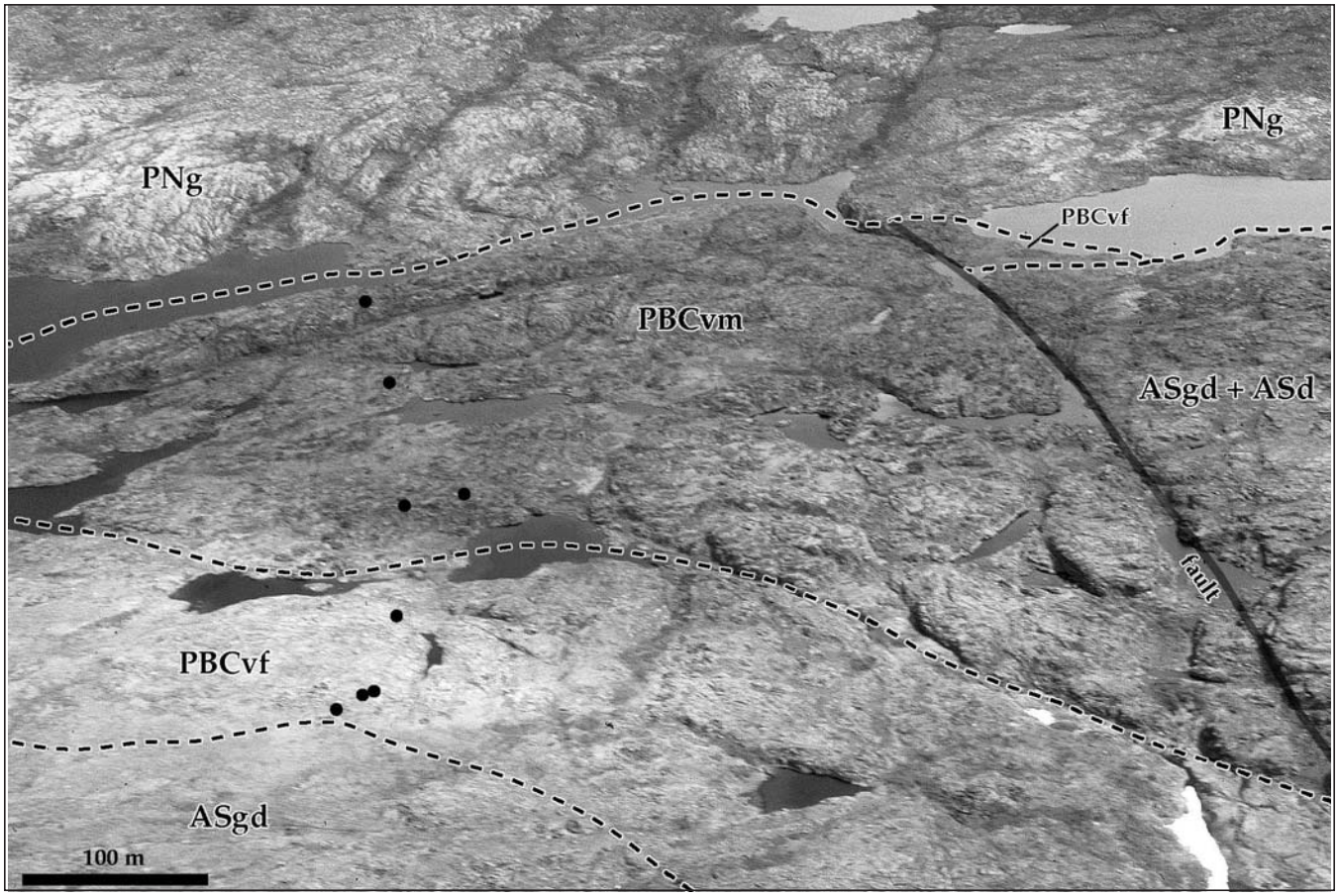

Frontispiece. *Low-angle oblique aerial view of the Slow River section of the Christopher Island Formation (NTS 65 N/3), looking northeast. Archean granodiorite and diorite (units ASgd, ASd) are overlain by early Proterozoic felsic, potassic lava flows (unit PBCvf) and olivine-phlogopite-diopside lamprophyre flows (unit PBCvm) that dip about 60°NE. The section terminates at a younger pluton of Nueltin granite (unit PNg). Black circles indicate the locations of samples PHA-89-X1 to -X8 (see 'Geochemistry' section). GSC 2002-820*

GEOLOGY OF THE DUBAWNT LAKE AREA, NUNAVUT–NORTHWEST TERRITORIES

Abstract

The bedrock of the Dubawnt Lake area mainly consists of late Archean (2.6 Ga) granite to diorite plutons, which intruded schist and gneiss (≥2.7 Ga), all overlain by early Proterozoic (1.85–1.7 Ga) siliciclastic and volcanic rocks of the Dubawnt Supergroup. Granitic plutons were emplaced on the east side of the area at ca. 1.83 and 1.76 Ga.

The northwest-trending, leucocratic, and dominantly granitic Snow River gneiss is the oldest map unit. It is overlain by metapsammitic and schistose rocks with minor mafic volcanic rocks (Clarke River schist) which record at least one deformation event at upper amphibolite facies that predates 2.6 Ga. Both units were intruded by diorite, granodiorite, megacrystic monzonite, and leucogranite of the Snow Island suite, dated at 2.602 to 2.605 Ma.

Quartzite and minor siltstone, preserved as erosional remnants in a discontinuous northeast-trending belt, were deposited on Archean basement before 1.83 Ga, and are correlated with the Aphebian Amer Group. The quartzite units contain a shallowly southeast-plunging stretching lineation, formed during upper greenschist- to lower amphibolite-facies metamorphism, which predates the Dubawnt Supergroup.

The lowermost Dubawnt Supergroup (basal Christopher Island Formation) consists of minor immature sandstone and conglomerate, and extensive flows of felsic, potassic lavas that were erupted directly onto Archean/Aphebian basement. These were transected by narrow strike-slip and normal fault valleys that were filled with mafic to felsic ultrapotassic volcanic and volcaniclastic rocks, overlain by fluvial/alluvial siliciclastic deposits of the Kunwak Formation. A felsic minette flow yielded a zircon U-Pb age of 1833 ± 3 Ga, and volcanism was probably synchronous with the emplacement of Hudson granitoid plutons within the Snow River gneiss domain.

At ca. 1.75 Ga, the eastern side of the map area was intruded by rapakivi granite (Nueltin granite). Minor rhyolite domes of the correlative Pitz Formation (middle Dubawnt Supergroup) are preserved. A period of erosion and intense chemical weathering was followed by deposition of flat-lying conglomerate and sandstone of the Thelon Formation (upper Dubawnt Supergroup) at about 1.72 Ga; a major depocentre lay to the west, under the present Thelon basin. The youngest event recognized is the emplacement of northwest-trending diabase dykes of the Mackenzie swarm at 1.72 Ga.

Résumé

Dans la région du lac Dubawnt, le substratum rocheux est constitué en majeure partie de plutons granitiques à dioritiques de l'Archéen tardif (2,6 Ga), qui recoupent des schistes et des gneiss (≥ 2,7 Ga). Le tout est recouvert de roches silicoclastiques et volcaniques qui datent du Protérozoïque précoce (1,85-1,7 Ga) et appartiennent au Supergroupe de Dubawnt. Des plutons granitiques ont été mis en place dans la partie orientale de la région il y a environ 1,83 Ga et 1,76 Ga.

Les gneiss leucocrates de Snow River, à prédominance granitique et à orientation nord-ouest–sud-est, sont l'unité cartographique la plus ancienne. Ils sont recouverts de roches métapsammitiques et schisteuses et de faibles quantités de volcanites mafiques (le schiste de Clarke River), lesquelles témoignent d'au moins un épisode de déformation au faciès des amphibolites supérieur, dont l'âge est supérieur à 2,6 Ga. Ces unités ont toutes deux été recoupées par de la diorite, de la granodiorite, de la monzonite mégacrystalline et du leucogranite appartenant à la suite de Snow Island, datant de 2,605 à 2,602 Ma.

Des quartzites et des quantités mineures de siltstone sont conservés sous forme de lambeaux d'érosion dans une ceinture de roches discontinue, d'orientation nord-est–sud-ouest. Une corrélation existe entre cette séquence, laquelle a été déposée sur le socle Archéen il y a plus de 1,83 Ga, et le Groupe d'Amer de l'Aphébien. Les quartzites comportent une linéation d'étirement plongeant légèrement vers le sud-est, qui a été formée durant une période de métamorphisme allant du faciès des schistes verts supérieur à celui des amphibolites inférieur et qui est antérieure au Supergroupe de Dubawnt.

La partie basale du Supergroupe de Dubawnt (la formation basale de Christopher Island) est constituée de quantités mineures de conglomérats et de grès immatures, de même que de vastes coulées de laves felsiques potassiques qui se sont épanchées directement sur le socle archéen et aphébien. Ces unités ont été recoupées par des vallées étroites engendrées par des décrochements et des failles normales; ces vallées sont comblées de roches volcaniques et volcanoclastiques ultrapotassiques, felsiques à mafiques, sur lesquelles reposent des dépôts silicoclastiques d'origine alluviale et fluviale de la Formation de Kunwak. Une coulée de minette felsique a donné un âge U-Pb sur zircon de 1833 ± 3 Ga, et le volcanisme aurait été synchrone avec la mise en place de plutons granitoïdes de la suite d'Hudson dans le domaine des gneiss de Snow River.

Il y a environ 1,75 Ga, un granite rapakivi (le granite de Nueltin) a recoupé la partie orientale de la région cartographique. Des dômes rhyolitiques mineurs de la formation corrélative de Pitz (section centrale du Supergroupe de Dubawnt) y sont conservés. La séquence horizontale de conglomérats et de grès de la Formation de Thelon (partie supérieure du Supergroupe de Dubawnt) a été déposée il y a environ 1,72 Ga, suivant une période d'érosion et d'altération chimique intensive. Un dépocentre majeur se trouvait à l'ouest, sous le bassin de Thelon actuel. L'intrusion de dykes de diabase (1,72 Ga) de l'essaim de Mackenzie est le dernier événement reconnu dans la région. Ces dykes sont orientés nord-ouest–sud-est.

SUMMARY

The bedrock of the Dubawnt Lake area consists mainly of late Archean (2.6 Ga) granitic to dioritic plutons intruding schist and gneiss (≥2.7 Ga), all of which are overlain by early Proterozoic (1.85–1.7 Ga) siliciclastic and volcanic rocks of the Dubawnt Supergroup. Granitic plutons were emplaced on the east side of the area at ca. 1.83 and 1.76 Ga.

The northwest-trending, leucocratic, and dominantly granitic Snow River gneiss, located in the southwest corner of the area, is the oldest map unit. It is (?unconformably) overlain on the northeast by metapsammite and schist with minor mafic volcanic rocks (Clarke River schist), which record at least one pre–2.6 Ga deformation event at upper amphibolite facies. The Clarke River schist is presumed to correlate with ca. 2.7 Ga volcanosedimentary packages to the south and east. It was extensively intruded by diorite, granodiorite, megacrystic monzonite, and leucogranite of the Snow Island suite, dated at 2.602 to 2.605 Ma.

Quartzite and minor siltstone were deposited on Archean basement before 1.83 Ga, and are now preserved as erosional remnants in a discontinuous northeast-trending belt. The belt is on strike with similar rocks to the north that make up the Aphebian Amer Group. The quartzite contains a shallowly southeast-plunging stretching lineation, formed during upper greenschist- to lower amphibolite-facies metamorphism, that is well developed in the underlying Archean rocks and is particularly strong along the northwest shore of Dubawnt Lake. The lineation, including related narrow mylonite bands, is not present in the Snow River gneiss domain. A shallowly dipping, muscovite-rich tectonic schist beneath one quartzite body may represent a northeast-vergent thrust fault related to the lineation.

SOMMAIRE

Le substratum rocheux de la région du lac Dubawnt est surtout constitué de plutons granitiques à dioritiques de l'Archéen tardif (2,6 Ga) qui recoupent des schistes et des gneiss (≥ 2,7 Ga). Le tout est recouvert de roches silicoclastiques et volcaniques du Supergroupe de Dubawnt, qui datent du Protérozoïque précoce (1,85-1,7 Ga). Des plutons granitiques ont été mis en place dans la partie orientale de la région il y a environ 1,83 Ga et 1,76 Ga.

Les gneiss leucocrates de Snow River, à prédominance granitique et à orientation nord-ouest–sud-est, se rencontrent dans le coin sud-ouest de la région; ils constituent l'unité cartographique la plus ancienne. Ils sont recouverts (en discordance (?)) dans le nord-ouest par des métapsammites, des schistes et des quantités mineures de volcanites mafiques (le schiste de Clarke River); ces roches témoignent d'au moins un épisode de déformation au faciès des amphibolites supérieur, dont l'âge est supérieur à 2,6 Ga. On présume que le schiste de Clarke River corrèle avec les assemblages volcanosédimentaires d'environ 2,7 Ga au sud et à l'est. Il a été recoupé par de nombreuses intrusions de diorite, de granodiorite, de monzonite mégacrystalline et de leucogranite appartenant à la suite de Snow Island, qui date de 2,605 à 2,602 Ma.

Des quartzites et des quantités mineures de siltstone, déposés sur le socle archéen il y a plus de 1,83 Ga, sont aujourd'hui conservés sous forme de lambeaux d'érosion dans une ceinture discontinue d'orientation nord-est–sud-ouest. Cette ceinture est parallèle à la direction de roches similaires au nord qui constituent le Groupe d'Amer de l'Aphébien. Les quartzites comportent une linéation d'étirement plongeant légèrement vers le sud-est qui a été formée durant une période de métamorphisme allant du faciès des schistes verts supérieur à celui des amphibolites inférieur. Elle est bien évidente dans les roches archéennes sous-jacentes et est particulièrement prononcée sur la rive nord-ouest du lac Dubawnt. Cette linéation ainsi que les étroites bandes mylonitiques qui lui sont associées ne sont pas observées dans le domaine des gneiss de Snow River. La présence, sous une masse de quartzite, d'un schiste tectonique riche en muscovite et à faible pendage pourrait représenter une faille de chevauchement à vergence nord-est associée à la linéation.

The lowermost Dubawnt Supergroup (basal Christopher Island Formation) consists of minor immature sandstone and conglomerate, and extensive flows of felsic potassic lava that were erupted directly onto Archean-Aphebian basement. These were transected by narrow strike-slip and normal fault valleys that were filled with mafic to felsic ultrapotassic volcanic and volcaniclastic rocks, overlain by fluvial-alluvial siliciclastic deposits of the Kunwak Formation. Faulting and dyke emplacement occurred along conjugate northwest and east-northeast directions, and may have been related to brittle indentation of the Slave Province into the Thelon tectonic zone. This activity occurred at about 1.85 to 1.81 Ga, and was probably synchronous with the emplacement of Hudson suite granitoid plutons within the Snow River gneiss domain.

At 1.76 to 1.75 Ga, the eastern side of the map area was extensively intruded by rapakivi granite (Nueltin granite). Minor rhyolite domes of the correlative Pitz Formation (middle Dubawnt Supergroup) are preserved. A period of erosion and intense chemical weathering was followed by deposition of flat-lying conglomerate and sandstone of the Thelon Formation (upper Dubawnt Supergroup) at about 1.72 Ga; a major depocentre lay to the west, beneath the present Thelon basin. The youngest event recognized was emplacement of northwest-trending diabase dykes of the Mackenzie swarm.

The ultrapotassic volcanic rocks have characteristics of both minette and lamproite, and carry mantle xenocrysts such as lherzolitic spinel, as well as cognate xenoliths consisting of high-Cr phlogopite, chrome diopside, and magnesiochromite. The Nd isotope compositions of the ultrapotassic rocks (ε_{Nd} values of –5 to –11) require a source region with long-lived enrichment in light rare-earth elements similar to continental crust. Depleted mantle Nd model ages for the Snow River gneiss, the Snow Island suite, and the Proterozoic granitoid rocks outside the Snow River gneiss domain indicate uniform crust-formation ages in the range 2.7 to 2.8 Ga. Model ages for the Christopher Island Formation, however, extend to 3.0 Ga. The ultrapotassic magmas are interpreted to originate in phlogopite-rich lithospheric mantle metasomatized by crustal components at any time from ca. 2.7 Ga onward. The production of cogenetic granite-minette associations was commonplace in the Archean hinterlands of Proterozoic collisional belts, and the Proterozoic geology of the Dubawnt Lake area reflects within-plate deformation related to the Superior-Churchill collision along the Trans-Hudson Orogen, locally complicated by eastward indentation of the Slave Province.

La partie basale du Supergroupe de Dubawnt (la formation basale de Christopher Island) est constituée de quantités mineures de conglomérats et de grès immatures, ainsi que de vastes coulées de laves felsiques potassiques qui se sont épanchées directement sur le socle archéen et aphébien. Ces unités ont été recoupées par des vallées étroites engendrées par des décrochements et des failles normales; ces vallées sont comblées de roches volcaniques et volcanoclastiques ultrapotassiques, felsiques à mafiques, sur lesquelles reposent des dépôts silicoclastiques d'origine alluviale et fluviale de la Formation de Kunwak. La formation des failles et la mise en place des dykes ont eu lieu selon des directions conjuguées nord-ouest–sud-est et est-nord-est–ouest-sud-ouest et pourraient être reliées à un épisode de renfoncement cassant de la Province des Esclaves dans la zone tectonique de Thelon. Cet événement, daté d'environ 1,85 à 1,81 Ga, a probablement été synchrone avec l'intrusion de plutons granitoïdes de la suite d'Hudson dans le domaine des gneiss de Snow River.

Il y a environ 1,76 à 1,75 Ga, la partie orientale de la région cartographique a été copieusement recoupée par un granite rapakivi (le granite de Nueltin). De petits dômes rhyolitiques de la formation corrélative de Pitz (section centrale du Supergroupe de Dubawnt) y sont conservés. Il y a environ 1,72 Ga, suivant une période d'érosion et d'altération chimique intensive, la séquence horizontale de conglomérats et de grès de la Formation de Thelon (partie supérieure du Supergroupe de Dubawnt) a été déposée. Un dépocentre majeur était situé à l'ouest, sous le bassin de Thelon actuel. L'intrusion de dykes de diabase de l'essaim de Mackenzie est le dernier événement reconnu dans la région; ces dykes ont une orientation nord-ouest–sud-est.

Les roches volcaniques ultrapotassiques présentent certaines caractéristiques de la minette et de la lamproïte. Elles contiennent des xénocristaux mantelliques, telle la spinelle lherzolitique, et des xénolithes syngénétiques constitués de phlogopite riche en chrome, de diopside chromique et de magnésiochromite. Les données isotopiques de Nd provenant des roches ultrapotassiques (valeurs ε_{Nd} de -5 à -11) indiquent que la source a encouru un enrichissement prolongé en lanthanides légers, comme c'est le cas d'une croûte continentale. Les âges modèles de Nd d'un manteau appauvri pour les gneiss de Snow River, la suite de Snow Island et les granitoïdes du Protérozoïque à l'extérieur du domaine des gneiss de Snow River indiquent que l'origine de la croûte terrestre remonte à entre 2,8 et 2,7 Ga. Toutefois, les âges modèles de la Formation de Christopher Island remontent jusqu'à 3,0 Ga. L'origine des magmas ultrapotassiques est attribuée au métasomatisme d'un manteau lithosphérique riche en phlogopite par des composantes de la croûte, qui aurait eu lieu à partir d'environ 2,7 Ga. La genèse de granite et de minette cogénétiques était chose courante dans les arrière-pays archéens des ceintures orogéniques du Protérozoïque. La géologie du Protérozoïque dans la région du lac Dubawnt est représentative d'une déformation intraplaque associée à la collision entre la Province du lac Supérieur et celle de Churchill le long de l'orogène trans-hudsonien, et compliquée localement par le renfoncement vers l'est de la Province des Esclaves.

INTRODUCTION

The rocks described in this report are Archean gneissic, schistose, and granitoid rocks, and early Proterozoic dykes and granitic and supracrustal rocks of the Dubawnt Lake area, all older than 1.3 billion years (Table 1). The Archean rocks are mainly dioritic to granitic plutons that intruded a polydeformed, mostly metasedimentary supracrustal sequence, which may overlie an older gneiss terrane. These rocks were deformed by Paleoproterozoic dextral shearing and possibly northeast-vergent thrust faulting, then faulted during the formation of intracratonic extensional basins that were filled to a thickness of 3 km or more with ultrapotassic volcanic rocks and alluvial sedimentary rocks. Dubawnt Lake (*see* Fig. 1 for location), at 3850 km^2, is the third largest lake in Nunavut and the Northwest Territories. It straddles the treeline, which is deflected northward along the Dubawnt River beyond its usual limit in the District of Keewatin. Dubawnt Lake is part of an historical canoe route leading from Lake Athabasca to Hudson Bay via the Thelon River (Tyrrell, 1898). Tyrell reported extensive ice cover with narrow shore leads in August of 1893, but the lake was mostly ice free by mid-July during the field seasons when fieldwork was being carried out for this report (1988–1989, 1991–1994).

The northwestern shore of Dubawnt Lake forms part of the eastern boundary of the Thelon Game Sanctuary. One grizzly bear was seen within the reserve, and wolves were seen east of Outlet Bay (Fig. 2). A single male muskox summered in 1988 and 1989 on a grassy peninsula at the north end of the lake. In 1993, a herd of approximately 20 muskoxen summered on Dumb-bell island (unofficial name) near the west shore of the lake (*see* Fig. 3 for location map).

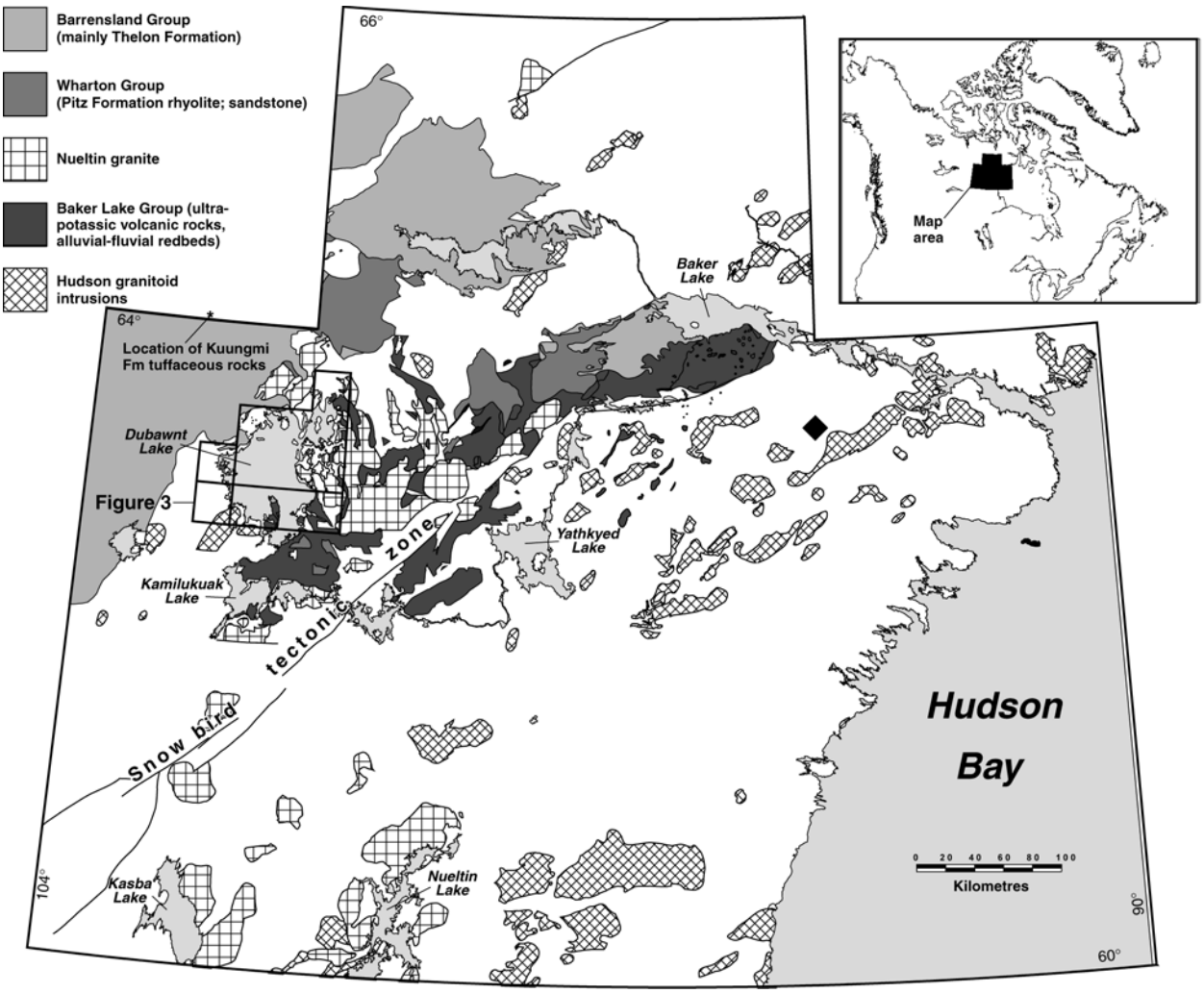

Figure 1. *Location of the study area, which contains the intersection of four 1:250 000 map sheets (65 K, 65 L, 65 M, 65 N). Also shown are the distributions of the lower Dubawnt Supergroup (Baker Lake Group) and middle Dubawnt Supergroup (Wharton Group). A portion of the Thelon basin, containing the upper Dubawnt Supergroup (Barrensland Group) is shown. The black diamond indicates the position of the diamondiferous Akluilâk minette dyke..*

Table 1. Table of formations, Dubawnt Lake area.

Lithology	Map unit	Radiometric age
PROTEROZOIC		
Mackenzie diabase dykes	PM	1276 Ma (LeCheminant and Heaman, 1989)
----------Intrusive contact----------		
Dubawnt Supergroup		
Barrensland Group		
Lookout Point Formation (dolostone)	PRL	
Kuungmi Formation (potassic tuff)	PRU	
Thelon Formation (sandstone, conglomerate)	PRT	1720 ± 6 Ma (Miller et al., 1989)
----------Erosional unconformity----------		
Wharton Group		1750–1765 Ma (Peterson and van Breemen, 1999)
Nueltin granite plutons, dykes	PNg	
Nueltin basaltic dykes	PNb	
----------Intrusive contact----------		
Pitz Formation (rhyolite, sandstone)	PWPv	1750–1765 Ma (Peterson and van Breemen, 1999)
*Amarook Formation (eolian sandstone)	PWS	
----------Erosional unconformity----------		
Baker Lake Group		
Kunwak Formation (sandstone, conglomerate)	PBK	1785 ± 3 Ma (Rainbird et al., 2003)
Christopher Island Formation	PBC	ca. 1.83 Ga (references in Peterson and van Breemen, 1999)
Aphanitic felsic lava flows	PBCva	
Siltstone	PBCsl	
Conglomerate-sandstone	PBCs	
Lamprophyre lava flows, tuff, and breccia	PBCvm	
Porphyritic felsic lava flows	PBCvf	1833 ± 3 Ma (Rainbird et al., 2003)
Basal conglomerate	PBCb	
*Kazan Formation (arkose)	PBZ	
*South Channel Formation (conglomerate)	PBS	
----------Erosional unconformity----------		
**Hudson intrusions (monzonite to granite)	Pg	ca. 1.84 Ga (Peterson et al., 2000)
----------Contact not exposed----------		
Amer Group		
Chloritic schist	PAs	
Quartzite	PAq	
----------Erosional unconformity----------		
ARCHEAN		
Snow Island Suite		
Biotite leucogranite	ASl	2602 ± 2 Ma (Roddick, unpub. data, 1989)
Hornblende leucogranite	ASlh	
Megacrystic monzonite to granite	ASm	2605 ± 5 Ma (LeCheminant and Roddick, 1991)
Granodiorite	ASgd	
Diorite	ASd	
----------Intrusive contact----------		
Clarke River Schist		
Metapsammite and iron formation	ACs2	
Pelitic schist and iron formation	ACs1	
Amphibolite	ACv	
Peridotite	ACp	
----------?Unconformity ----------		
Snow River Gneiss		
Melanocratic orthogneiss	ARo	
----------Intrusive contact----------		
Granitic paragneiss, schist, amphibolite	Arn	

* Not present in the Dubawnt Lake area.

**Contact relations with Dubawnt Supergroup unknown.

Local relief rarely exceeds 50 m and outcrop is generally sparse, there being considerable sand cover, especially within the game sanctuary and near river inlets and outlets. The bedrock south of Outlet Bay is almost completely obscured by heaved outcrop and hummocky glacial outwash. The most prominent rock exposures are rounded, glacially polished outcrops of Archean megacrystic granite and leucogranite, and of siliceous lava flows in the upper and lower felsic volcanic members of the Christopher Island Formation (*see* Frontispiece).

The geology of the Dubawnt Lake area (Fig. 2; Map 2021A, on CD-ROM) was first investigated by Tyrrell (1898), who highlighted the spectacular exposures of alluvial conglomerate on islands near the western shoreline, which he placed within the Athabasca sandstone. Operation Thelon (Wright, 1955, 1967) saw one of the first uses of helicopters in Canada for geological mapping; this project produced a 1:1 000 000-scale geological map of the western District of Keewatin and led to the recognition of the Dubawnt Group (now Supergroup; Gall et al., 1992; Rainbird et al., 1999).

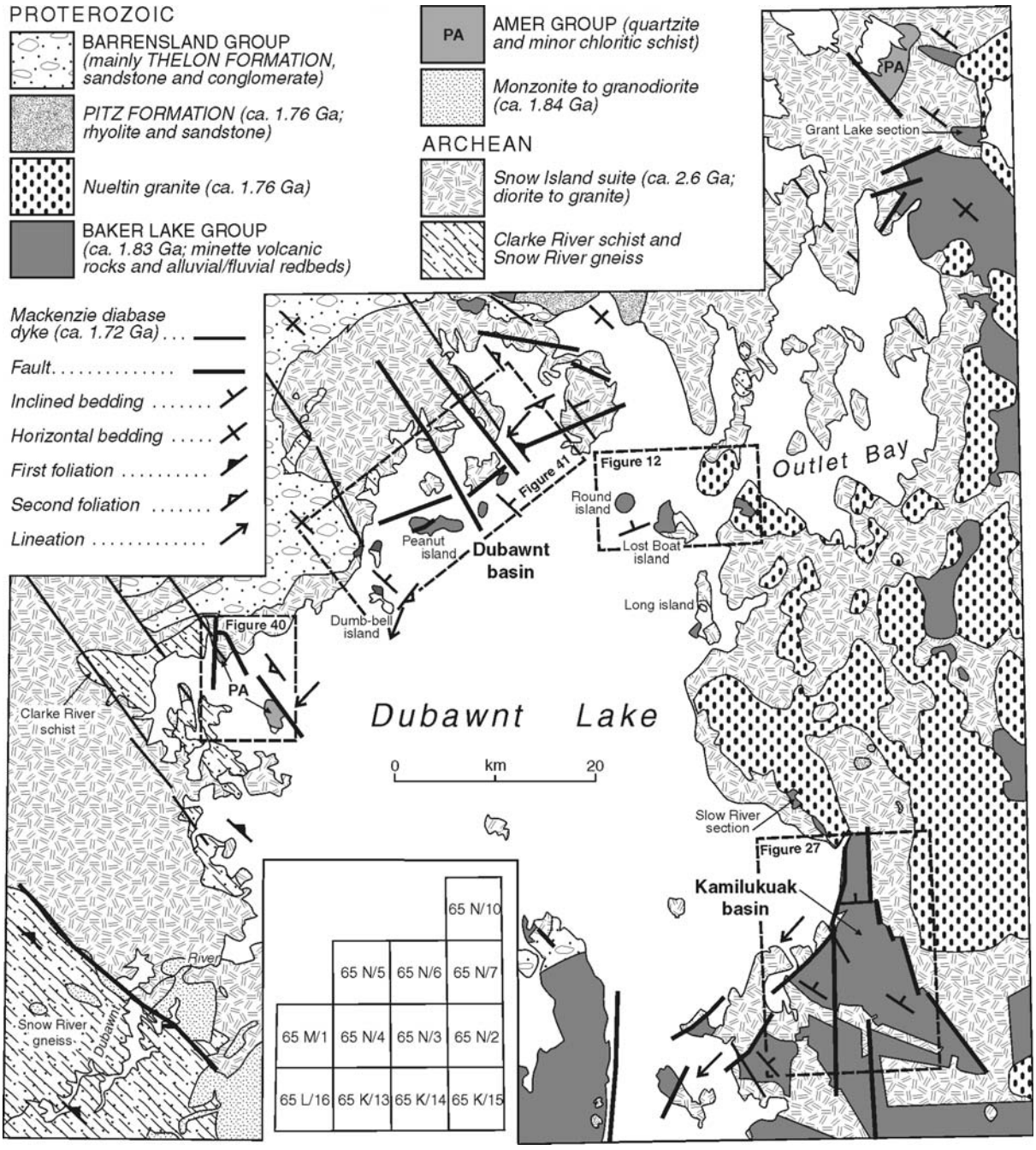

Figure 2. *Simplified geology of Dubawnt Lake, Nunavut–Northwest Territories.*

Stratigraphic studies by Donaldson (1965, 1967, 1969) led to the description of a major unconformity below the Thelon Formation (Barrensland Group, upper Dubawnt Supergroup). Further studies in the District of Keewatin demonstrated that several unconformities are present within the Dubawnt Supergroup, and that some of the mafic volcanic rocks of the lower Dubawnt Supergroup are strongly potassic (LeCheminant et al., 1979; Blake, 1980). A lower age limit of ca. 1.72 Ga was assigned to the Thelon Formation by Miller et al. (1989). The age of the middle Dubawnt Supergroup (Pitz Formation, Wharton Group) was fixed near 1.75 Ga by Loveridge et al. (1987). The maximum age of the ultrapotassic volcanic rocks (Christopher Island Formation, Baker Lake Group) has been estimated at ca. 1.85 Ga or slightly younger (Peterson and van Breemen, 1999). The measured range of ages overlaps that of the Hudson granitoid plutons, which are widespread throughout the western Churchill Province and dated at ca. 1.85 to 1.81 Ga (Peterson et al., 2000).

Dubawnt Lake lies at the western extremity of a complex of structurally separated sub-basins of the Baker Lake Group, which extends from Baker Lake southwest to Kamilukuak Lake (Fig. 1). Dubawnt Lake also overlaps the southwestern end of the known extent of the Wharton Group, and lies on the eastern edge of the Thelon basin. It is therefore well situated for studies of Proterozoic volcanism, sedimentation, and basin development in the western Churchill Province.

Mapping for this study was mostly conducted by boat and foot traverses, with transportation to about 10% of the traverses being provided by fixed-wing aircraft. The principal objectives were to:

- provide an accurate description of the stratigraphy of the Paleoproterozoic supracrustal rocks, and to interpret the development of the basins containing them;
- determine the nature and origin of the ultrapotassic volcanic rocks; and
- determine the lithological domains and principal structural features of the Archean rocks.

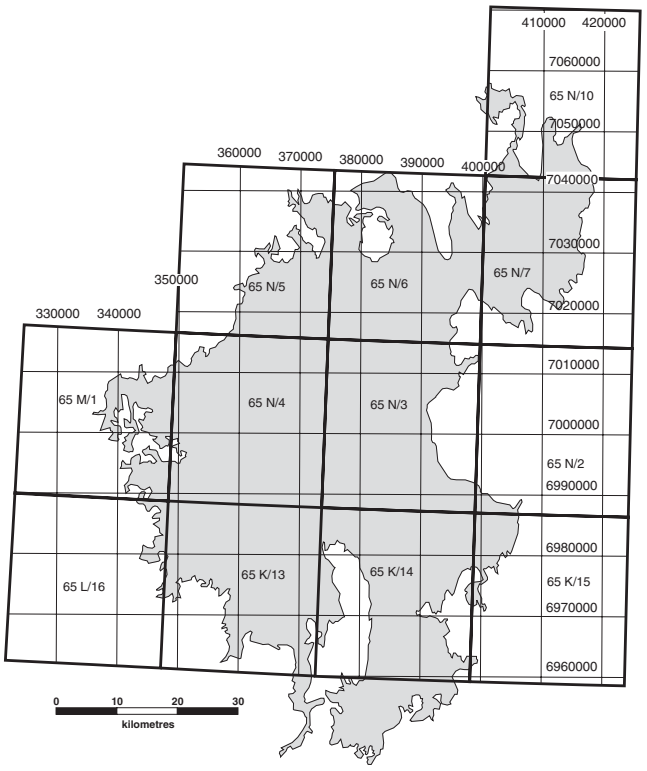

Figure 3. *UTM grid used for location references.*

Acknowledgments

The following students are gratefully acknowledged for their assistance in the field: Natalie Morisset, Robert Spark, Andrew Conly, Michael Neville, Robert Moroz, and Alex Ivanoff. Robert Rainbird, Bruce Kjarsgaard, Quentin Gall, Chris Lee, and Peter Born acted as senior assistants. Paul Wallace (University of California, Berkeley) visited camp for three weeks in 1989 and provided valuable input regarding the petrology and geology of the ultrapotassic rocks. Anthony LeCheminant assisted with mapping in 1988, and Al Donaldson visited camp in 1988 and 1989 to continue his studies of the Thelon Formation. I particularly thank Anthony LeCheminant for advice during all stages of this project.

GENERAL GEOLOGY

Archean

Snow River gneiss (unit ARn)

The oldest rocks recognized in the area belong to a polydeformed, mixed gneiss unit (unit ARn; Fig. 4) exposed along the Dubawnt River in NTS 65 L/16. The Snow River gneiss is named after a small river which drains into the Dubawnt River. The unit is dominated by leucocratic quartzofeldspathic gneiss, consisting mainly of white-weathering, 1 to 10 m thick bands of biotite granite separated by mesocratic bands containing minor amphibole and biotite, and thinner (0.01 to 5 m) amphibolitic layers and boudins. Thin pelitic layers are

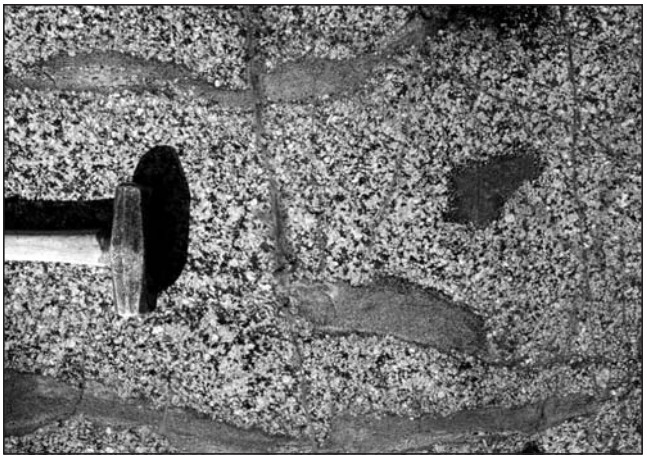

Figure 4. *Xenoliths of psammitic and amphibolitic Snow River gneiss (unit ARn) in Snow Island granodiorite (unit ASgd). GSC 2002-821*

abundant in the northeast part (structural top) of the unit. The amphibolite is commonly rimmed by white quartzofeldspathic segregations that are deformed with the amphibolite in centimetre- to metre-scale intrafolial folds. The unit appears to form a gently northeast-dipping homocline, and is interpreted as a succession of meta-arkose with minor mafic volcanic rocks, fining upward to the northeast.

After development of the gneissic foliation, unit ARn was intruded by a semiconcordant melanocratic orthogneiss (unit ARo1), which now consists of quartz-feldspar lenses with granulated edges in a schistose, biotite amphibolite matrix. This unit occurs along, and is cut by, a high-strain zone that forms the northeastern boundary of unit ARn, subparallel to the gneissic fabric. The orthogneiss is typically separated from the paragneiss by a 10 cm layer of coarse, white pegmatite. Both gneisses (units ARn, ARo1) are cut by dykes of pink-weathering leucogranite, ranging from 5 to 50 cm in width, that commonly have diffuse gradational contacts with the granitic bands of the paragneiss.

The gneissic fabric of unit ARn is nearly orthogonal to the main northeast structural trend of the Dubawnt Lake area, which is demonstrably Proterozoic (post–Amer Group) in age. Folds of the gneissosity with 1 m amplitude and 1 to 10 m wavelength have shallowly plunging (0–20°), undulating axes that are typically parallel to the Proterozoic fabric.

Clarke River schist (units ACs1, ACs2, ACv, ACp)

A 10 km raft of biotite schist (unit ACs1) and paragneiss (unit ACs2) in younger granite and granodiorite is exposed along the southwestern shore of Dubawnt Lake (NTS 65 L/16, 65 M/1). The southern margin of this raft consists of subequal amounts of strongly foliated quartzofeldspathic gneiss and biotite-muscovite schist; the abundance of schist increases to the northeast. The gneiss, which is similar to unit ARn, is intruded by a plagioclase-phyric melanocratic rock that is included in unit ARo (subunit ARo2). The foliation is intensely crenulated, and it is unclear whether the transition from gneiss to schist is stratigraphic or structural. The northern margin of the raft (in NTS 65 M/1) was intruded and metasomatized ('granitized') by pink leucogranite.

Unit ACs1 consists mostly of schist, identical to that present in a large body of metasedimentary and volcanic rocks exposed to the north, in a bay on the west side of Dubawnt Lake (Peterson and Born, 1994). The body consists of a biotite±muscovite metapelite with bands of sparsely micaceous, grey-weathering, quartzofeldspathic metapsammite (unit ACs2) and minor amphibolite pods (unit ACv). The schist is rich in weakly deformed muscovite-bearing leucosome and coarse pegmatitic pods of muscovite and white feldspar. Portions of the schist near the metapsammite contain numerous segments of disrupted meta–iron-formation rich in pyrite and almandine garnet. These generally are concentrated in trains, suggesting original stratigraphic control, but they cannot be traced for more than a few tens of metres.

On its western margin, the Clarke River schist terminates in plutons of the younger Snow Island intrusive suite. The northeastern boundary of the metasedimentary rocks is marked by a schistose, greenschist-facies, high-strain zone, interpreted as a west-dipping fault that separates Archean rocks from quartzite that is correlated with the Proterozoic Amer Group. Remnants of the Clarke River schist, enclosed in plutons of the Snow Island suite, occur east of this fault, along the northwest shoreline of Dubawnt Lake. The quartzofeldspathic and schistose remnants are extensively resorbed (revealing their presence mainly as a relict foliation within leucogranite), but extensive outcrops of mafic rocks, also found in this area, produce prominent magnetic anomalies. Notable among these is a weakly deformed, coarse plutonic peridotite body (unit ACp) exposed on an island (NTS 65 N/5, UTM 376200E, 7030900N). The peridotite contains minor phlogopite but is strongly depleted in incompatible elements (sample PHA89-7, Appendix 1), and is therefore unlikely to be related to Proterozoic mafic alkaline volcanism. The west side of the peridotite grades into a graphic anorthosite, which separates the peridotite from Snow Island megacrystic granite.

Snow Island Suite (units ASd, ASgd, ASm, ASl, ASlh)

A plutonic suite consisting of diorite, granodiorite, megacrystic monzonite to granite, and leucogranite dominates Archean rocks in the map area. The suite is named after an island in NTS 65 N/4 described by Tyrell (1898). A U-Pb (zircon) age of 2605 ± 5 Ma was obtained for megacrystic granite in northwestern Dubawnt Lake (LeCheminant and Roddick, 1991); a nearby leucogranite sample yielded an age of 2602 ± 2 Ma (Roddick, unpub. data, 1989). Felsic members of the suite intruded the more mafic members; the only exception noted was rare dykes of megacrystic granite in leucogranite. All phases of the Snow Island suite contain resorbed inclusions and rafts of older supracrustal rocks. Fabrics within the centres of the plutons are usually faint, but their margins typically have a strong relict foliation, and contain screens of amphibolitic supracrustal rocks that were strongly flattened parallel to the contact. Units ASd and ASgd are strongly concentrated on the south side of the study area.

Dioritic rocks (unit ASd) of this suite are hornblende and clinopyroxene bearing, medium to coarse grained, and distinguished by blue-white-weathering plagioclase feldspar. They occur in small (<2 km wide) plutons that are enclosed within larger granodiorite or megacrystic granite bodies and invariably display a strong positive magnetic anomaly. Commingling with more felsic rocks is common (Fig. 5).

The most common variety of granodiorite (unit ASgd) is equigranular and medium grained; however, sparsely potassium-feldspar-phyric rocks with a mesocratic matrix were observed in NTS 65 M/1. The porphyritic granodiorite grades into potassium-feldspar-megacrystic monzonite to granite (unit ASm; Fig. 6) containing accessory biotite, hornblende, and titanite. Outcrops of unit ASm are commonly cut by dykes of pink-weathering biotite leucogranite (unit ASl); large bodies of unit ASl are invariably in contact with unit

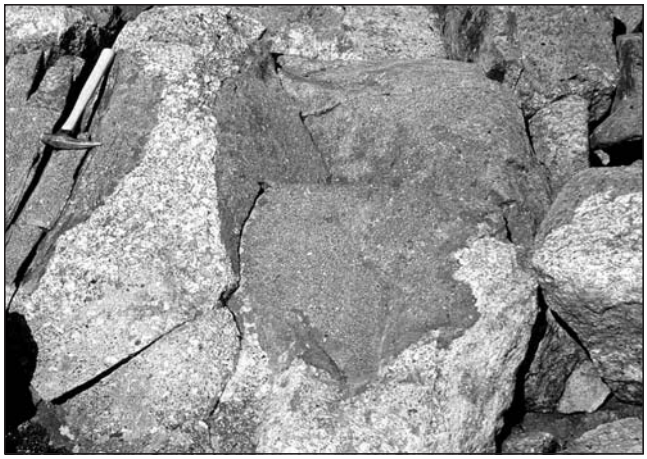

Figure 5. *Mingled enclaves of Snow Island diorite (unit ASd) in megacrystic granite (unit ASm). GSC 2002-822*

Figure 6. *Megacrystic granite of the Snow Island intrusive suite (unit ASm). GSC 2002-823*

ASm. Unit ASl is equigranular and fine to medium grained. The north side of NTS sheet 65 L/16 contains an almandine- and hornblende-bearing granite with yellow plagioclase (unit ASlh) that was not observed elsewhere.

Paleoproterozoic: pre–Dubawnt Supergroup

Amer Group (units PAq, PAs)

Orthoquartzite was mapped north of Dubawnt Lake during Operation Thelon (Wright, 1967), and is also exposed in two large outcrop areas on the west side of the lake (Fig. 2). This train of exposures is on strike with synformal keels of Paleoproterozoic metasedimentary rocks in the Amer Lake area, assigned to the Amer Group by Tippet and Heywood (1978). A large island straddling NTS 65 N/4 and 65 M/1 consists almost entirely of white orthoquartzite with minor muscovite and sparse wisps of dark minerals. The contact with Archean rocks (unit ACv) is hidden in a narrow topographic notch; there is no evidence of a fault, so the inferred contact may be an unconformity. Bedding, recognized from semipelitic and heavy-mineral bands and crossbed truncations, is poorly preserved in most outcrops. A strong, shallowly southwest-plunging lineation is developed everywhere on the island. Undeformed staurolite and biotite are present in semipelitic bands, indicating peak metamorphism at lower amphibolite facies. The northeast side of the island contains north-northwest-trending bands of strongly crenulated, tectonic muscovite schist with slivers of quartzite.

Quartzite is also exposed on the shoreline northwest of this island. It is separated from underlying Snow Island leucogranite by an approximately 1 m thick muscovite schist containing abundant slivers of both granite and quartzite. The quartzite is cut off on the west side by a west-dipping fault. This fault underlies a body of grey-green-weathering chloritic slate (unit PAs), which in turn underlies a second fault to the west that separates the slate from Archean Clarke River schist. The relatively low metamorphic grade of the slate is inconsistent with an Archean age. It resembles a grey-green slate unit overlying a quartzite unit in the Beverly Lake area (LeCheminant et al., 1984), and is assigned here to the Amer Group. Its exact stratigraphic position is uncertain.

Hudson granitoid plutons (unit Pg)

The Hudson granitoid rocks (Peterson and van Breemen, 1999) are an extensive suite of 1850 to 1810 Ma monzonite to granite plutons mainly exposed west of Hudson Bay, between latitude 60°N latitude and the Wager Bay area. They are represented in the southeastern part of NTS 65 L/16 by poorly exposed stocks of pink-weathering, magnetite-bearing granitoid (mostly biotite granodiorite and quartz monzonite). These are continuous with Proterozoic granitoid stocks to the east (NTS 65 K/13), mapped by Tella and Eade (1980, 1985). They show a pronounced magnetic anomaly pattern (Fig. 7) identical to that of a pluton near Mosquito Lake, in central NTS 65 L, that was dated at ca. 1.84 Ga (Peterson et al., 2000).

The Hudson intrusions in 65 L/16 are petrographically similar to the leucogranite of the Snow Island suite and, together with numerous pink-weathering semiconcordant dykes within unit ARn, were initially interpreted as Archean (Peterson and Lee, 1995); however, they cut a Proterozoic shear zone (*see* 'Structural geology and metamorphism' section). The Hudson granitoid rocks in the study area are not in contact with any other Proterozoic rocks, so their relationship with the lower Dubawnt Supergroup, thought to be of similar age, is unknown.

Proterozoic: Dubawnt Supergroup

The Dubawnt Lake area contains numerous excellent exposures of flat-lying to steeply dipping volcanic and sedimentary rocks of the Dubawnt Supergroup (Fig. 8). The Baker Lake Group, which locally consists of mafic (lamprophyric) to felsic ultrapotassic volcanic rocks (Christopher Island Formation) plus alluvial fan and fluvial deposits (Kunwak Formation), is mainly exposed in island and shoreline outcrops. The younger Pitz Formation (rhyolite and minor sandstone) and Thelon Formation (sandstone-conglomerate) are mostly exposed in mainland outcrops.

Baker Lake Group (units PBC, PBK)

The Baker Lake Group in the Dubawnt Lake area consists of the Christopher Island Formation (unit PBC) and the Kunwak Formation (unit PBK). The Christopher Island Formation is named after an island at the east end of Baker Lake (Donaldson, 1965). There are several well exposed, steeply dipping sections on the east side of Dubawnt Lake, as well as flat-lying rocks on the eastern mainland. Lamprophyre dykes are common in Archean rocks on the east side of the lake, but they are rare on the west side and were not observed within the Snow River gneiss. A U-Pb age of 1833 ± 3 Ma was obtained from five zircon fractions from a sanidine-porphyritic felsic lava flow southeast of Dubawnt Lake, in NTS map 65 K/15 (sample PHA-89-81, UTM 411070E, 6975670N) (Rainbird et al., unpub. data, 2004). The overlying Kunwak Formation (type area on the Kunwak River; LeCheminant et al., 1979) forms a sequence with an apparent thickness of 10 km on the west side of the lake. Altogether, four structurally separated basins around Dubawnt Lake contain thick, continuous exposures or fragmented sections of the Christopher Island and Kunwak formations:

- the Dubawnt basin, which extends across numerous islands and the mainland in northern Dubawnt Lake, an area measuring approximately 40 by 20 km;

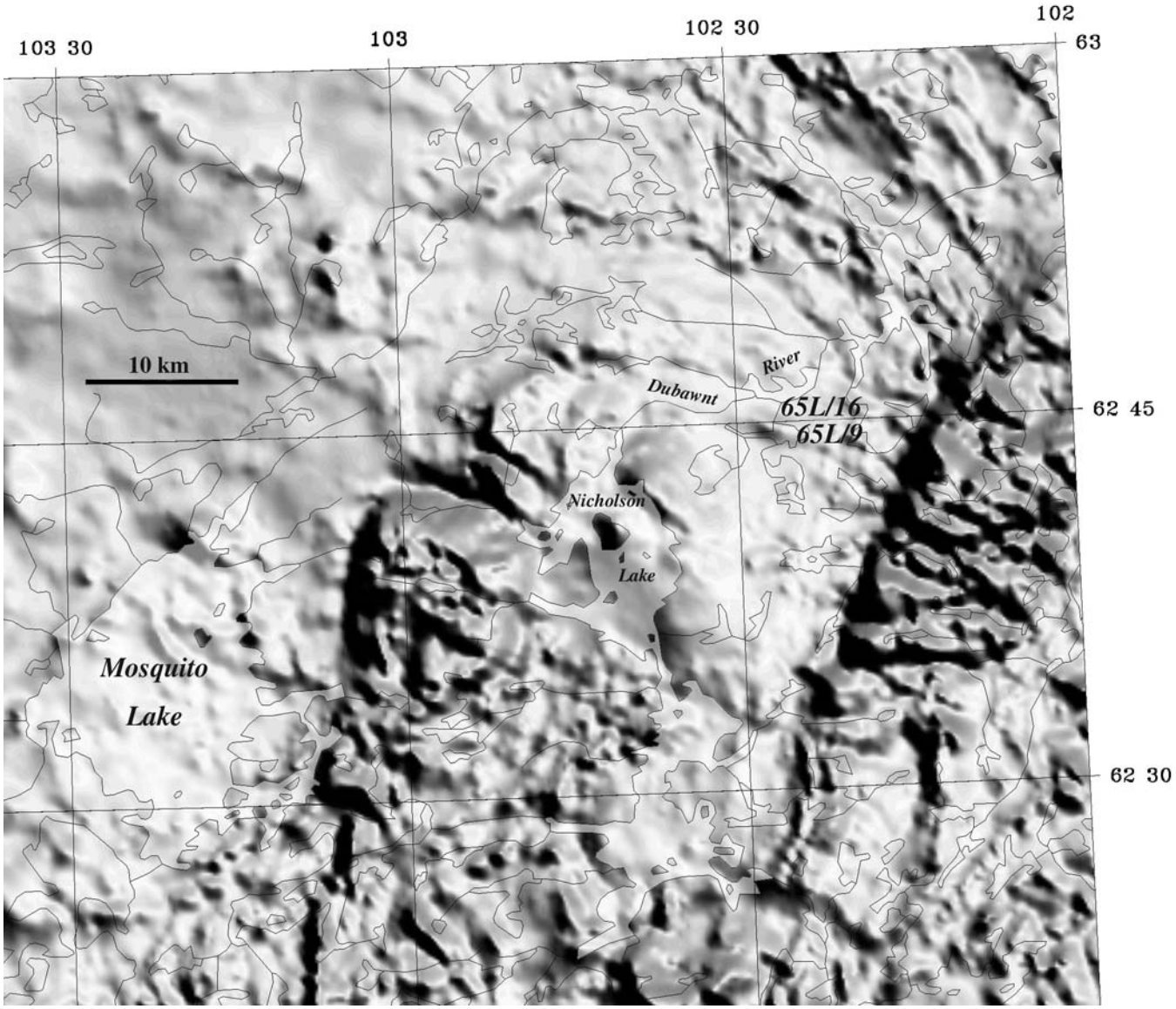

Figure 7. *Shaded aeromagnetic anomaly map of the northeast corner of NTS 65L. The anomaly between Mosquito Lake and Nicholson Lake is due to a granodiorite pluton dated at ca. 1.84 Ga by Peterson and van Breemen (Peterson et al., 2000). The anomaly appears identical to that extending across the east edge of the figure (NTS 65 L/9 and /16), which correlates with a granitoid pluton that crosses a northwest-trending shear zone. Both plutons appear to have one or two dyke-like extensions to the south.*

- the Kamilukuak basin, a triangular wedge about 2500 km^2 in area and extending from the Slow River (NTS 65 N/2) south to northern Kamilukuak Lake;
- the Outlet Bay field, consisting of widespread, isolated outcrops of flat-lying felsic flows south and east of Outlet Bay; and
- the Grant Lake section, exposed along the Dubawnt River between Outlet Bay and Grant Lake.

Several lithostratigraphic elements are common to these basins, and the most complete section is exposed on Lost Boat island (*see* Fig. 2 for location). The composite section shown in Figure 9 is essentially the same as that of Lost Boat island, together with the lower felsic volcanic member that is present in most other sections (Fig. 10).

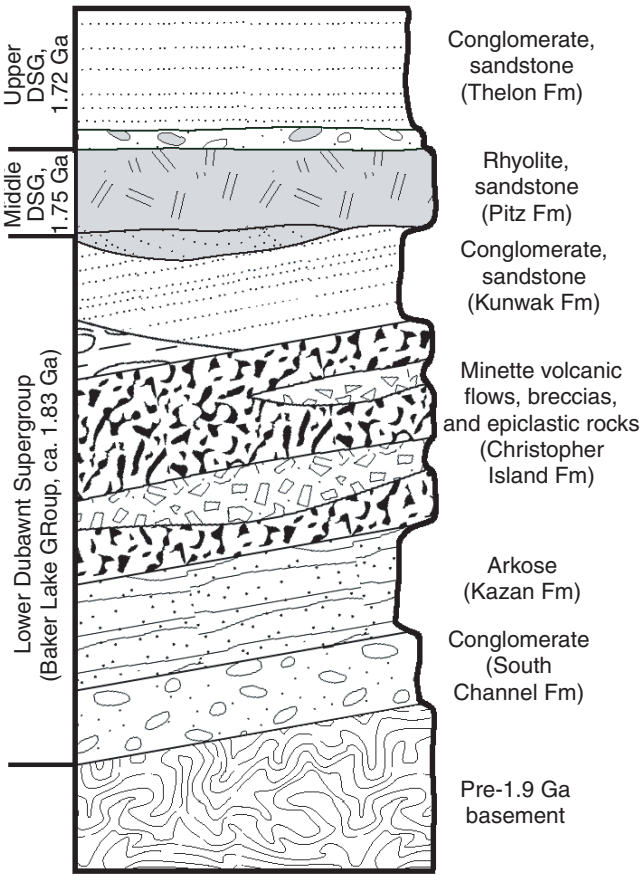

Figure 8. *Simplified stratigraphic section for the Dubawnt Supergroup (unit DSG). Thicknesses of individual units vary greatly; maximum thicknesses are approximately 2 km for the South Channel and Kazan Formations; 2 km for the Christopher Island Formation; 2 km for the Kunwak Formation 0.5 km for the Wharton Group; and 2 km for the Thelon Formation. Not shown are the thin (<200 m thick) units overlying the Thelon Formation (Kuungmi and Lookout Point formations).*

Dubawnt basin

The Dubawnt basin (Fig. 11, 12) contains the greatest variety of sedimentary and igneous rock types, and has the best exposures on shorelines. It consists of 1) a northeast-facing section (west side), dominated by a very thick sequence (approx. 10 km apparent thickness) of Kunwak Formation alluvial-fan facies; and 2) a northwest-facing section (east side), dominated by a thick section (approx. 2.5 km) of Christopher Island Formation volcanic flows and epiclastic rocks, with overlying Kunwak Formation fluvial facies.

Lost Boat island (Fig. 11) contains all members of the Christopher Island Formation, except for the lower felsic flows. The basal unconformity on this island can be traced for about 200 m, and its irregularity indicates about 10 m of

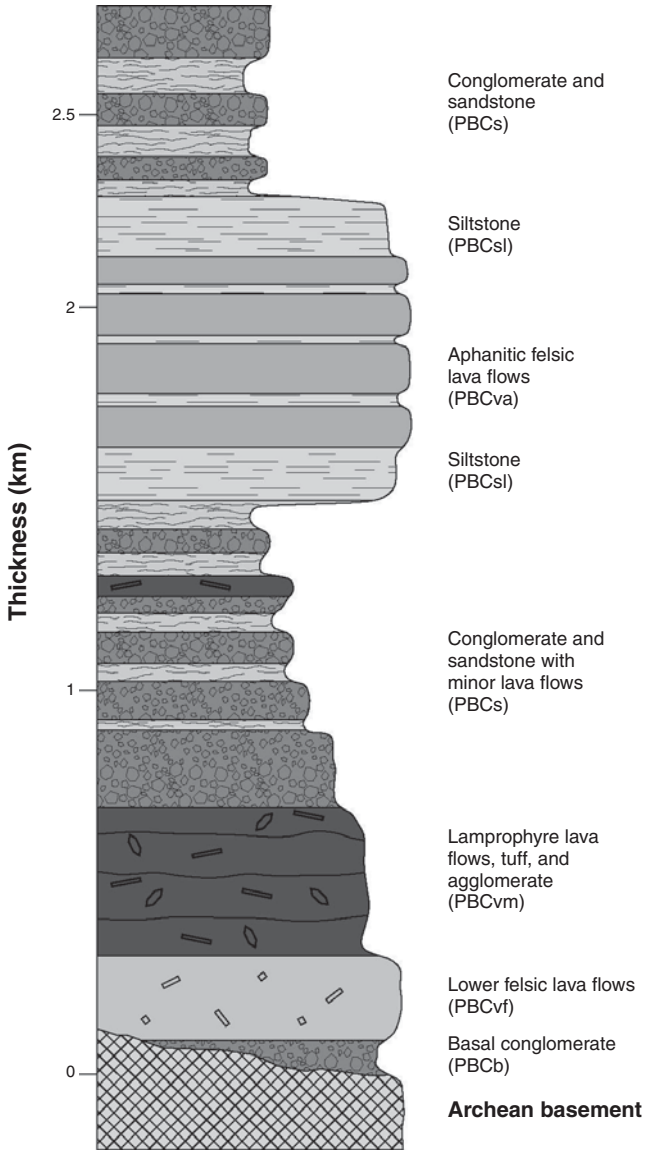

Figure 9. *Composite stratigraphic section for the Christopher Island Formation at Dubawnt Lake.*

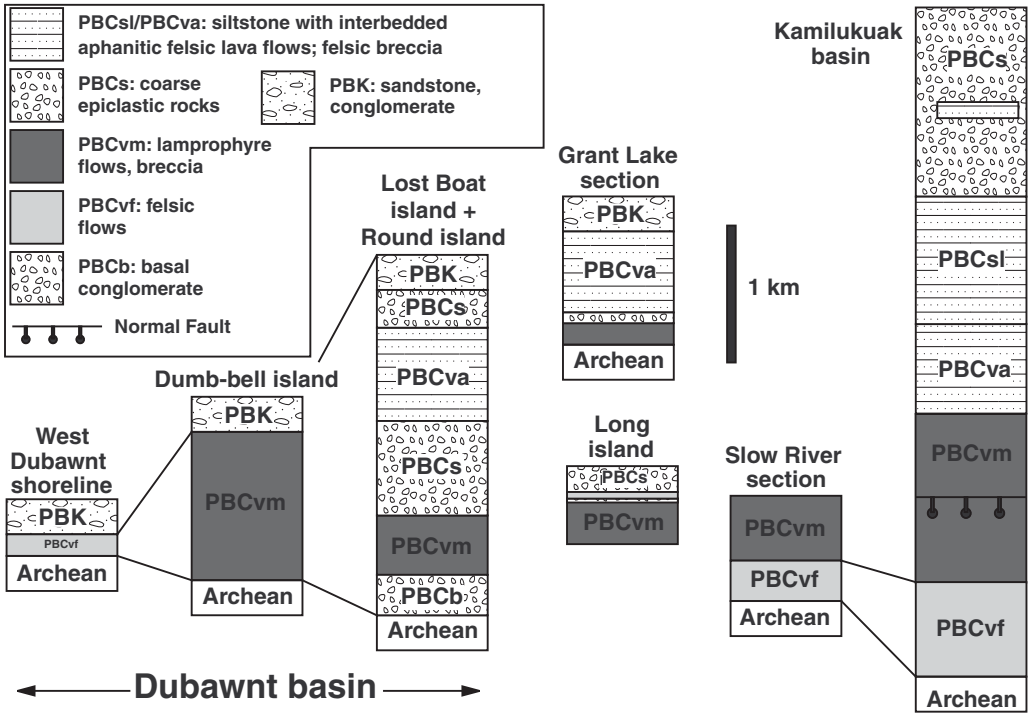

Figure 10. *Stratigraphy of individual sections of the Christopher Island Formation. Only the Long island and Lost Boat island sections were measured; the others are derived from 1:50 000-scale mapping. The west Dubawnt section is from the western shoreline of Dubawnt Lake. All of the volcanic members are dominated by subaerial facies, except those at Lost Boat island, which are entirely subaqueous. Although some members are absent from some sections, the overall sequence conforms to that in Figure 10. Within the Kamilukuak basin, strike-parallel faults have increased the apparent thickness of unit PBCvm (lamprophyre lava flows). Unit PBCs at the top of the Kamilukuak basin section is thicker than depicted, but is probably also fault thickened. The extremely coarse talus deposits near the top may be part of the Kunwak Formation (unit PBK).*

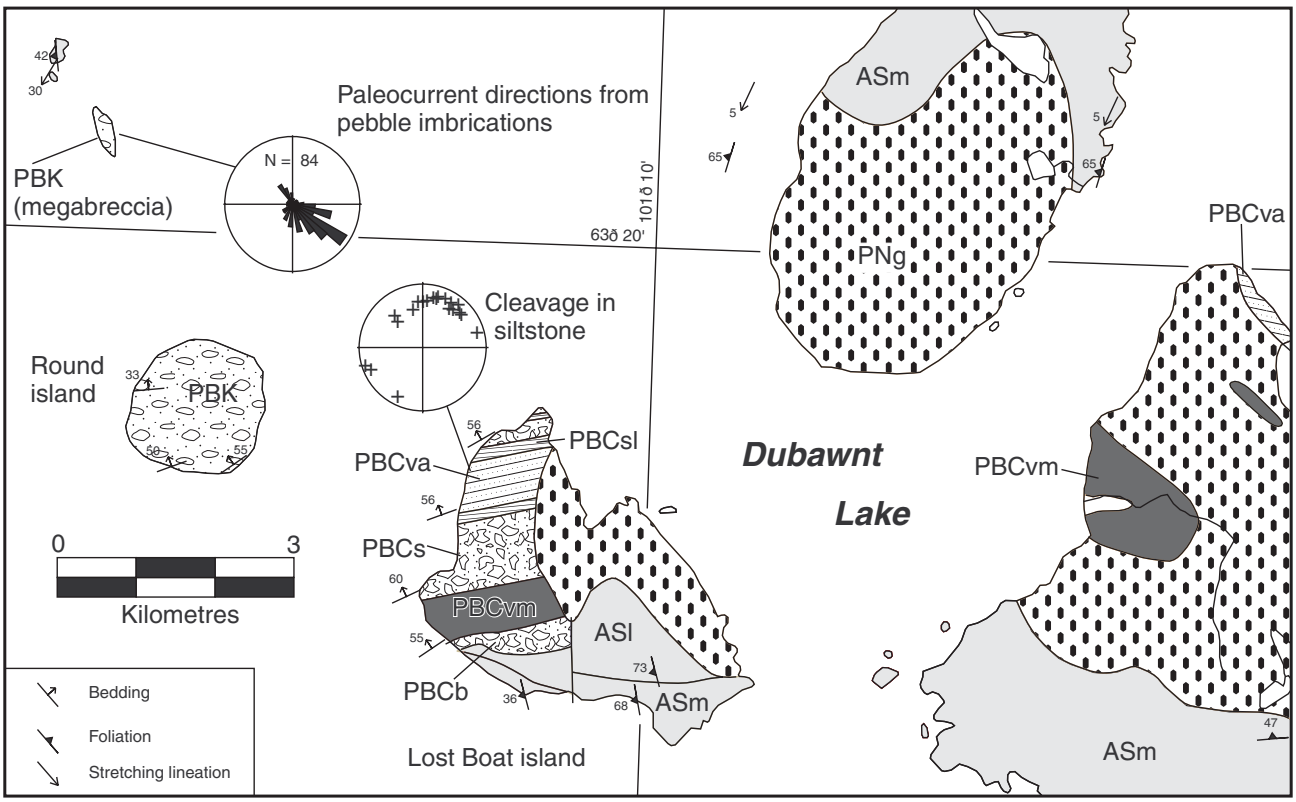

Figure 11. *Geology of the east side of the Dubawnt basin.*

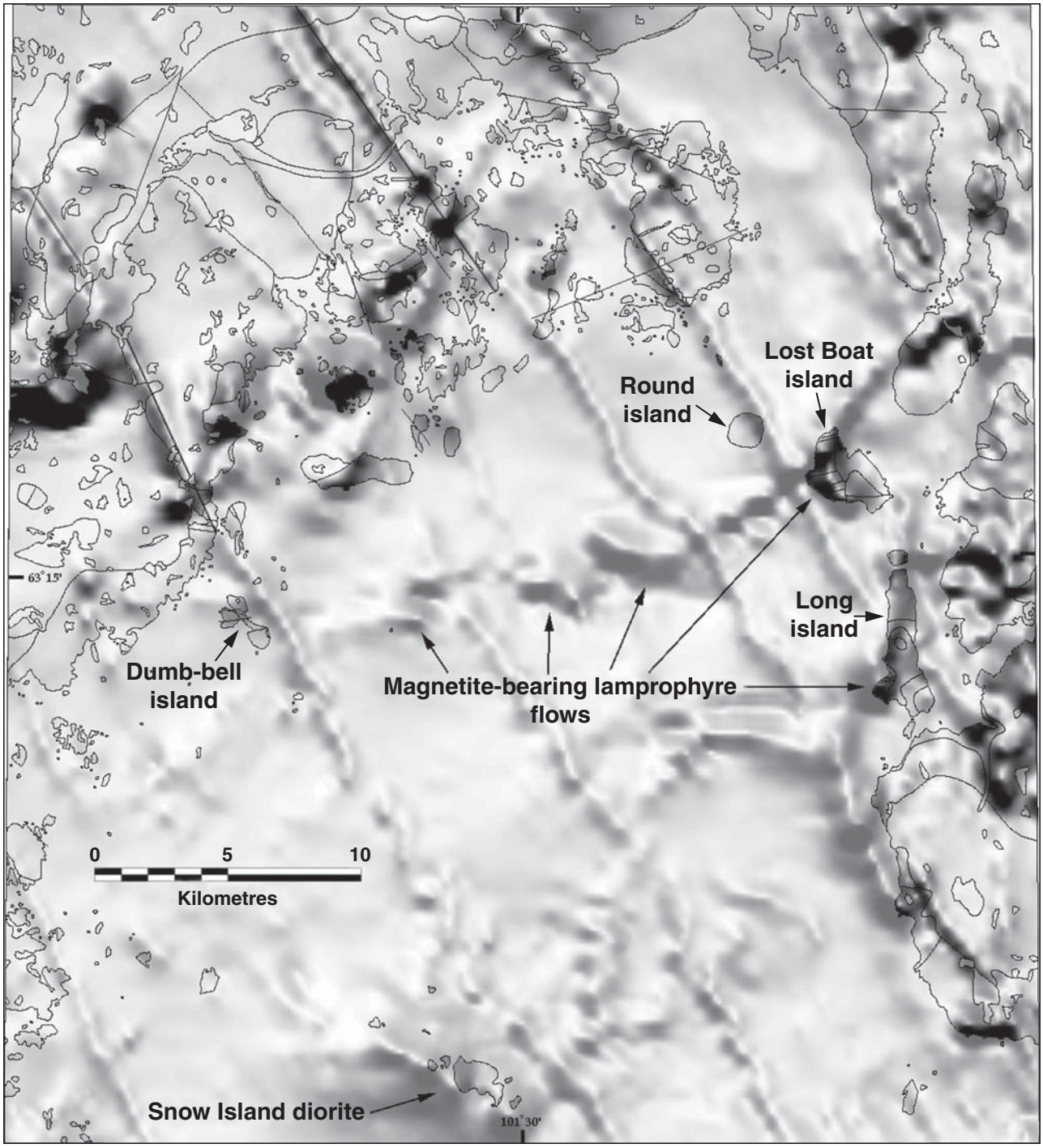

Figure 12. *Shaded relief aeromagnetic map (illumination direction 000°) of northwestern Dubawnt Lake (NTS 65 N/2, /3, /4, /5), with shorelines and geological contacts superimposed. Areas covered by water have been given reduced contrast. The prominent linear features trending 135° are Mackenzie dykes. A band of strongly magnetic rocks extends from the Lost Boat island volcanic section (east side) across the lake in an arc to Dumb-bell island (west side), where it becomes less prominent. This feature is interpreted as a continuous horizon of lamprophyre flows at the base of the Dubawnt basin, which thins to the west. The magnetic anomaly appears to continue along the unexposed northern edge of the Nueltin granite body that cuts across Lost Boat island. Offsets of the horizon are consistent with subsequent sinistral movements on north- to northwest-trending faults. The magnetically low, flat region immediately north of the flows corresponds to an extensive blanket of Kunwak Formation. Northwest of the basin, intensely magnetic rafts of amphibolite and peridotite in granite are exposed on the mainland and nearshore islands. The intense anomaly in the south is associated with the Snow Island diorite, exposed on a large island.*

paleotopographic relief. The unconformity intersects the shoreline, but is not exposed there. The basal unit (unit PBCb) consists of planar-bedded, pale purple-brown-weathering siltstone and fine sandstone with thin layers and lenses of poorly sorted pebble conglomerate (Fig. 13). The clasts are angular and consist of unweathered granitoid rocks, and minor vesicular lamprophyre. The stratigraphically lowermost outcrops exposed on the shoreline consist of thin, vesicular, phlogopite-clinopyroxene (±olivine) lamprophyre flows and angular breccia in a poorly sorted, sandy volcanogenic matrix that lacks any organized sedimentary structures (unit PBCvm; Fig. 14). The lamprophyre weathers in shades of purple-pink to dark brown-black (fresher). Well developed chill margins on flows, rounded pillow-like bulges on some flow tops, and dark, aphanitic volcanic clasts resembling spalled glassy rinds are consistent with a subaqueous environment.

Unit PBCvm is overlain by a fining-upward sequence of very coarse (clasts ≤50 cm) purple-brown-weathering epiclastic rhythmites that resemble turbidites (Fig. 15, 16; unit PBCs). The unit is organized into bed sets of conglomerate to siltstone, each up to 2 m thick, with prominent load features beneath the basal conglomerate layers and sand and silt draped over their tops. The clasts are mostly of vesicular phlogopite-clinopyroxene lamprophyre; feldspar porphyry clasts are uncommon (<1%), and Archean granitoid clasts are rare. Crossbedding was not observed, and there is no evidence for reworking of the tops of the cycles. Therefore, this portion of the section is interpreted as a series of proximal slumps deposited on a deep lake bottom. The lamprophyre clasts have moderate sphericity and are well rounded, but this is interpreted to reflect the ease with which the glassy, vesicular volcanic blocks were abraded into smooth shapes, rather than extensive transport. Thin (1 m) lamprophyre lava flows are present near the top of this unit.

Unit PBCs gradually fines upward to grey- and tan-weathering, thinly bedded siltstone and fine sandstone (unit PBCsl) that consist of subequal amounts of quartz and feldspar. The silt displays dewatering structures such as ball-and-pillow structures (Fig. 17), and homoclinal folds

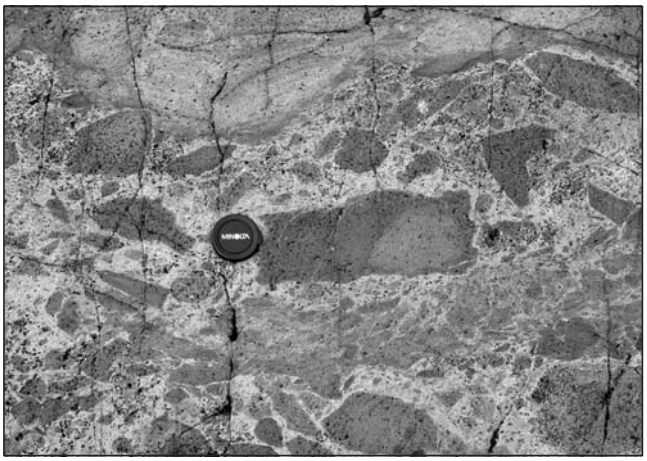

Figure 14. *Subaqueous lamprophyre flow-breccia, Lost Boat island (unit PBCvm). Stratigraphic top is toward the top of the photo. GSC 2002-825*

Figure 15. *Lamprophyre conglomerate, Lost Boat island (lower part of unit PBCs). Stratigraphic top is toward top of photo. GSC 204724-B*

Figure 13. *Unit PBCb (basal Christopher Island Formation) on Lost Boat island. Stratigraphic top is toward the top of the photo. GSC 2002-824*

Figure 16. *Conglomeratic rhythmite, Lost Boat island (middle part of unit PBCs), beneath shallow water. Stratigraphic top is to the right. GSC 2002-826*

and synsedimentary faults. Traction features are absent. The central portion of the siltstone package contains 1 to 3 m thick interbeds of grey-weathering, aphanitic volcanic flows (unit PBCva). These form prominent outcrops, and give a strong 'phonolite ring' when struck with a hammer. The upper third of each flow is rich in centimetre-sized amygdules filled with quartz and epidote (Fig. 18). Some flow tops and bottoms incorporated xenoliths of highly convoluted siltstone, suggesting that the flows may have been injected into unconsolidated sediment. The siltstone sequence coarsens upward over about 200 m, until pink-purple-weathering, normally graded conglomerate-sandstone cycles (with minor thin lamprophyre flows) are re-established. This upper PBCs unit contains a large proportion of aphanitic and porphyritic felsic volcanic clasts, as well as approximately 5% Archean granitoid clasts.

A very similar section of lamprophyre and grey-yellow siltstone with grey aphanitic flows (Fig. 19) is exposed on the southwestern shoreline of Long island, south of Lost Boat island (*see* Fig. 2 for location). The section is structurally separated from the Dubawnt basin and is relatively compressed, but the same sequence is preserved. The lower part of the lamprophyre unit in the Long island section consists of

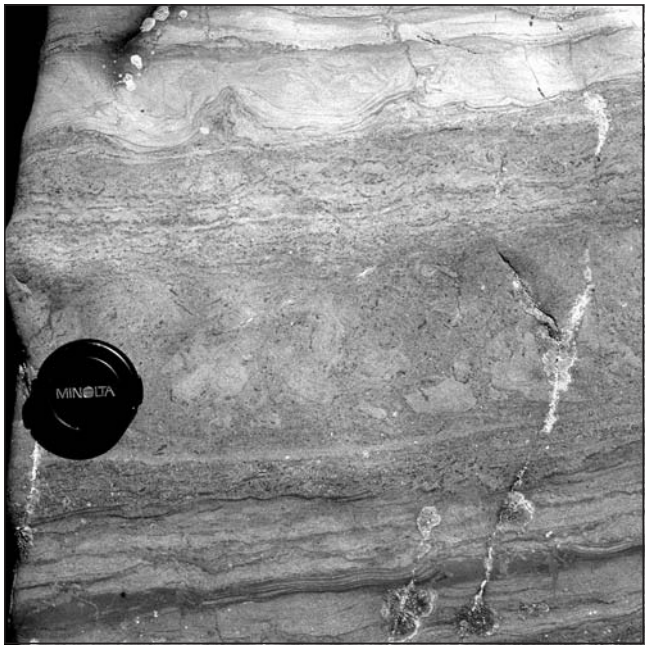

Figure 17. *Laminated siltstone with disrupted beds (ball-and-pillow structures; unit PBCsl), Lost Boat island. Stratigraphic top is toward the top of the photo. GSC 2002-827*

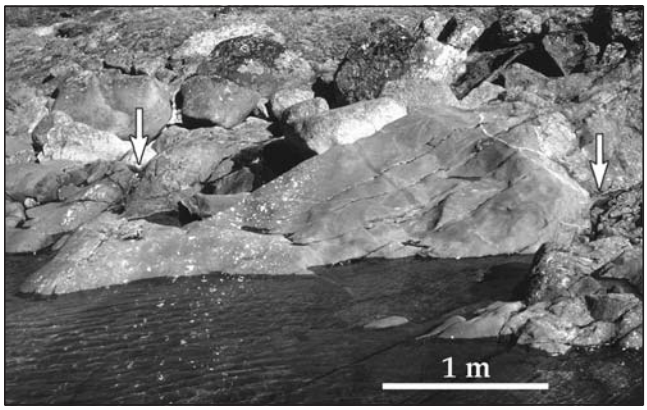

Figure 18. *Aphanitic lavas (unit PBCva) with quartz-filled vesicles concentrated near the top of one flow (boundaries indicated by arrows; up is to the left). GSC 204724-J*

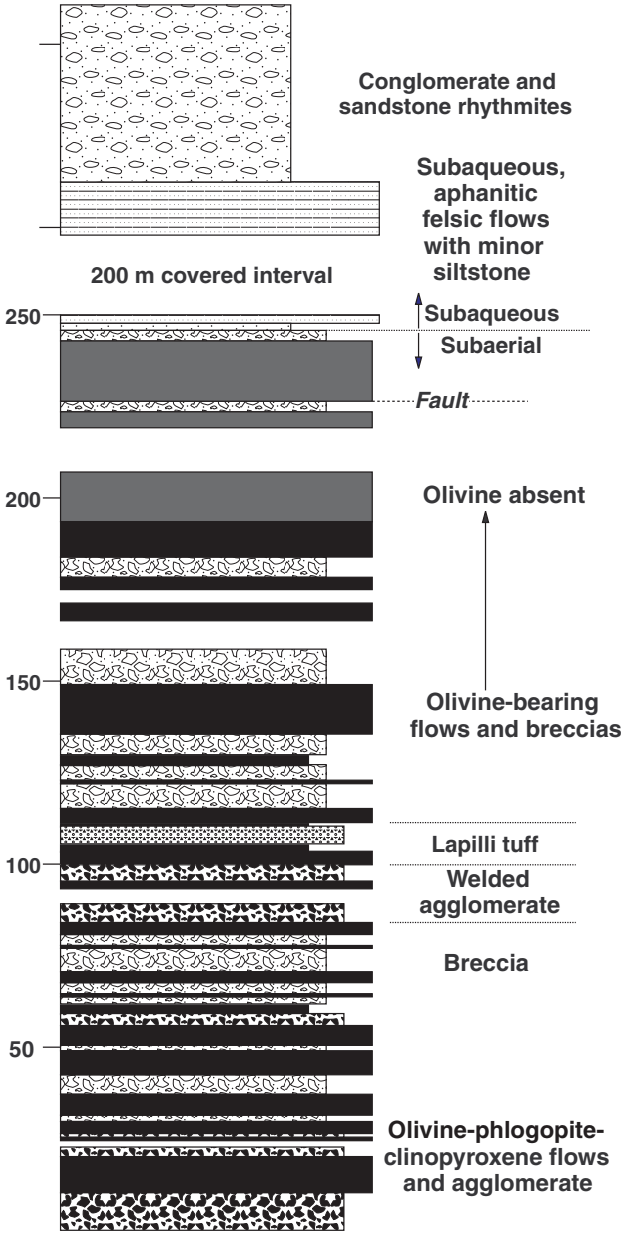

Figure 19. *Detailed stratigraphic section for southwestern Long island, NTS 65 N/3. Exceptional outcrops of welded agglomerate and lamprophyre lapilli tuff occur near the 100 m point. Section measured by R. Rainbird.*

olivine- and phlogopite-rich lava flows and breccia units, lapilli tuff, and coarse welded agglomerate (Fig. 20, 21). The lamprophyric part of the section is entirely subaerial, but the upper felsic unit (unit PBCva) is sandwiched between units of siltstone that are interpreted as subaqueous epiclastic rocks. The upper conglomerate unit contains some quartz-rich pebbly conglomerate clasts (Fig. 22). These clasts may be derived from the South Channel or Angikuni Formations of the lowermost Baker Lake Group (Blake, 1980).

The northern tip of Lost Boat island is on strike with the southeastern edge of a large island to the west (Round island), which consists entirely of conglomerate with interbedded sandstone and siltstone (Fig. 11). These rocks appear to stratigraphically overlie the Lost Boat island section and are assigned to the Kunwak Formation (unit PBK; Rainbird and Peterson, 1990). Outcrops on the southeastern edge of Round island consist of poorly sorted and weakly bedded conglomerate with equal amounts of lamprophyre and basement clasts. Over an interval of about 100 m, the volcaniclastic conglomerate passes into quartzofeldspathic conglomerate and pebbly sandstone redbeds with prominent trough crossbedding, current ripples, and mud rip-ups (Fig. 23). They commonly form the bases of metre-scale, fining-upward cycles that are capped by vivid red-brown silty tops with desiccation cracks. Clasts are almost entirely of local granitoid rocks (mostly from units ASm and ASl). A small island northwest of Round island (cut by a Mackenzie diabase dyke) consists partly of clast-supported, megalithic (up to 2 m) conglomerate with veined and brecciated granitoid clasts. This is interpreted as a talus breccia deposited at the edge of the Dubawnt basin.

Exposures of Kunwak Formation on the west side of the Dubawnt basin are similar to those on the east side, except in outcrops that are near the contact with Archean rocks (which is underwater). There, the formation consists of extremely coarse (up to 1 m) and crudely bedded conglomerate (Fig. 24); individual beds are 1 to 3 m thick and occasionally have thin layers rich in carbonate cement, interpreted as caliche caps. The clasts, consisting solely of local Archean rock types, are

Figure 20. *Olivine-phlogopite-clinopyroxene lamprophyre agglomerate and welded tuff, Long island. Stratigraphic top is to the right. Range pole is marked in 10 cm segments. GSC 2002-828*

Figure 22. *Clast from the upper portion of unit PBCs, Long island (NTS 65 N/3). This clast resembles a quartz-rich pebbly conglomerate exposed in a small outcrop in NTS 65 N/2 that directly overlies Archean rocks. GSC 2002-830*

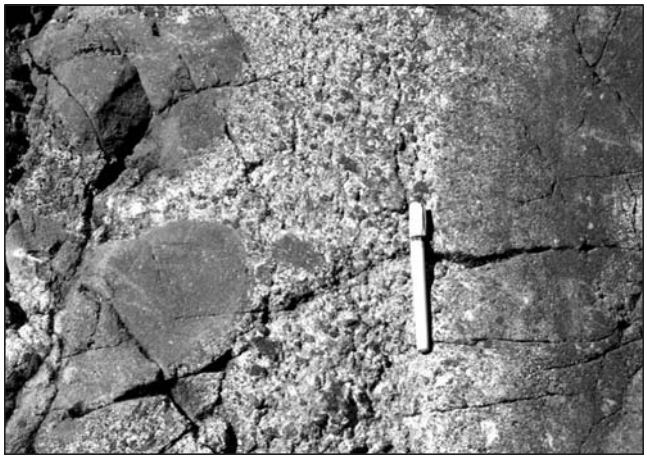

Figure 21. *Graded lamprophyre lapilli tuff, Long island. Stratigraphic top is to the right. GSC 2002-829*

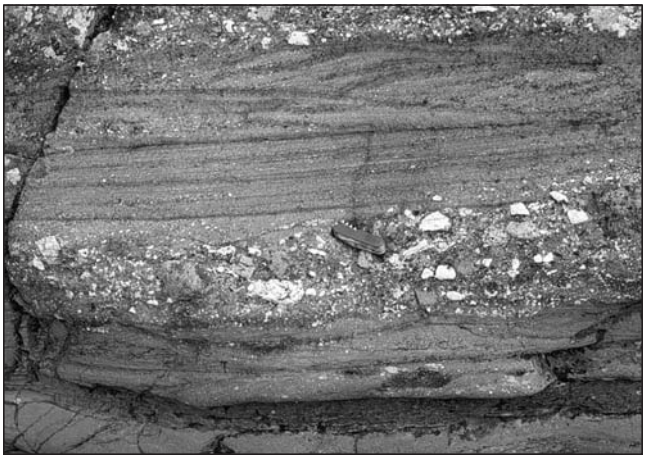

Figure 23. *Kunwak Formation fluvial facies, Round island. Pen knife for scale. GSC 2002-831*

moderately rounded but have low sphericity. Discoid clasts are sufficiently imbricated to yield paleocurrent data, which indicate transport predominantly toward the basin centre. These rocks are interpreted as alluvial-fan deposits that originated from basin-margin fault scarps (Rainbird and Peterson, 1990).

Exposures of the Christopher Island Formation on the west side of the Dubawnt basin are thin and discontinuous. The basal sedimentary member is absent, but a felsic volcanic member (unit PBCvf), overlain by lamprophyre flows, is observed in contact with Archean rocks. The felsic flows are pale grey-pink weathering and flinty, and are rich in rounded, 0.1 to 5 cm xenoliths of foliated crystalline rocks that are not from local bedrock. All xenoliths were partially melted and are separated from the felsic host by a 0.5 cm wide leucocratic rind that quenched mainly to plagioclase. Subaerial accretionary lapilli (Fig. 25) were observed filling fractures in the top of a lamprophyre flow on the west side of Dubawnt Lake (NTS 65 N/5, UTM 361000E, 702200N). They consist of phlogopite, oxidized volcanic glass, and quartzofeldspathic sand, and may correlate with the upper part of unit PBCvm. Subaqueous volcanic facies were not identified on the western side of the basin.

Kamilukuak basin

The Kamilukuak basin (Fig. 26) is a fault-bounded, south-opening triangle with its apex located on the southeast side of Dubawnt Lake. Bedding dips to the northeast at 35 to 75°. In the southern part of the map area, massive, flinty, grey to pink felsic volcanic flows (unit PBCvf) unconformably overlie Archean granodiorite (unit ASgd). Lamprophyre flows (unit PBCvm) above the felsic unit are massive and not visibly bedded. Outcrops of unit PBCvm are cut by a series of strike-parallel, chloritic, schistose faults with steep southerly dips. Some of these faults repeat the stratigraphy (including the unconformity), and they are interpreted as south-side-down normal faults.

Near the apex of the basin, units PBCs, PBCsl, and PBCva are present, but discontinuous along strike. Unit PBCva contains a breccia facies that resembles a subaerial deposit of juvenile bombs and ash (Fig. 27). The apex of the basin contains lamprophyre flows and an unsorted, clast-supported deposit composed of angular blocks of Archean rocks up to 5 m in size, interpreted as talus. The Slow River section, north of the apex of the Kamilukuak basin, is well exposed over a distance of 1 km, extending from the unconformity to an intrusive contact with Nueltin granite (unit PNg). In this section, felsic flows overlie the unconformity and are themselves overlain by mafic lamprophyre flows.

A notable deposit of travertine occurs on the west edge of the Kamilukuak basin, on a small island in NTS 65 K/11 (UTM 395000E, 6957800N). The outcrop, which is substantially heaved, consists of flat-lying breccia or coarse pebbly deposits of lamprophyre, cemented and overlain by a few metres of chemogenic deposits. These vary from decimetre-scale, acicular crystalline sprays in a coarse calcite matrix to disrupted, millimetre- and centimetre-scale layers of microcrystalline calcite and red silt (Fig. 28). Some broken laminae are upturned and form the cores of additional laminar overgrowths. Many of the disrupted laminae were tightly folded before lithification (Fig. 29); they may have been kept cohesive by mats of bacteria, which can mediate the deposition of laminated travertine (Chafetz and Guidry, 1999). From its stratigraphic position, the travertine could be in the upper Christopher Island Formation, but may be younger. Carbonate in the travertine has been dated at 1785 ± 3 Ma (Rainbird et al., unpub. data, 2004).

Figure 24. *Kunwak Formation alluvial-fan facies, west Dubawnt Lake. GSC 2002-832*

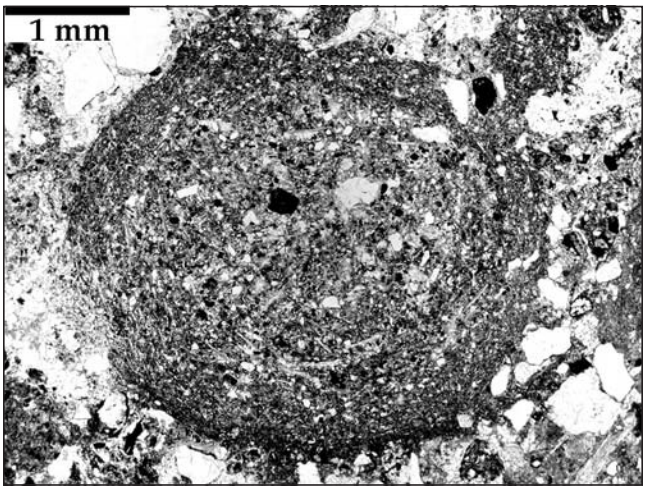

Figure 25. *Accretionary lapillus composed of phlogopite, fine volcanic ash, and quartz sand, west side of Dubawnt Lake (sample PHA-88-310; NTS 65 N/5, UTM 361000E, 702200N).*

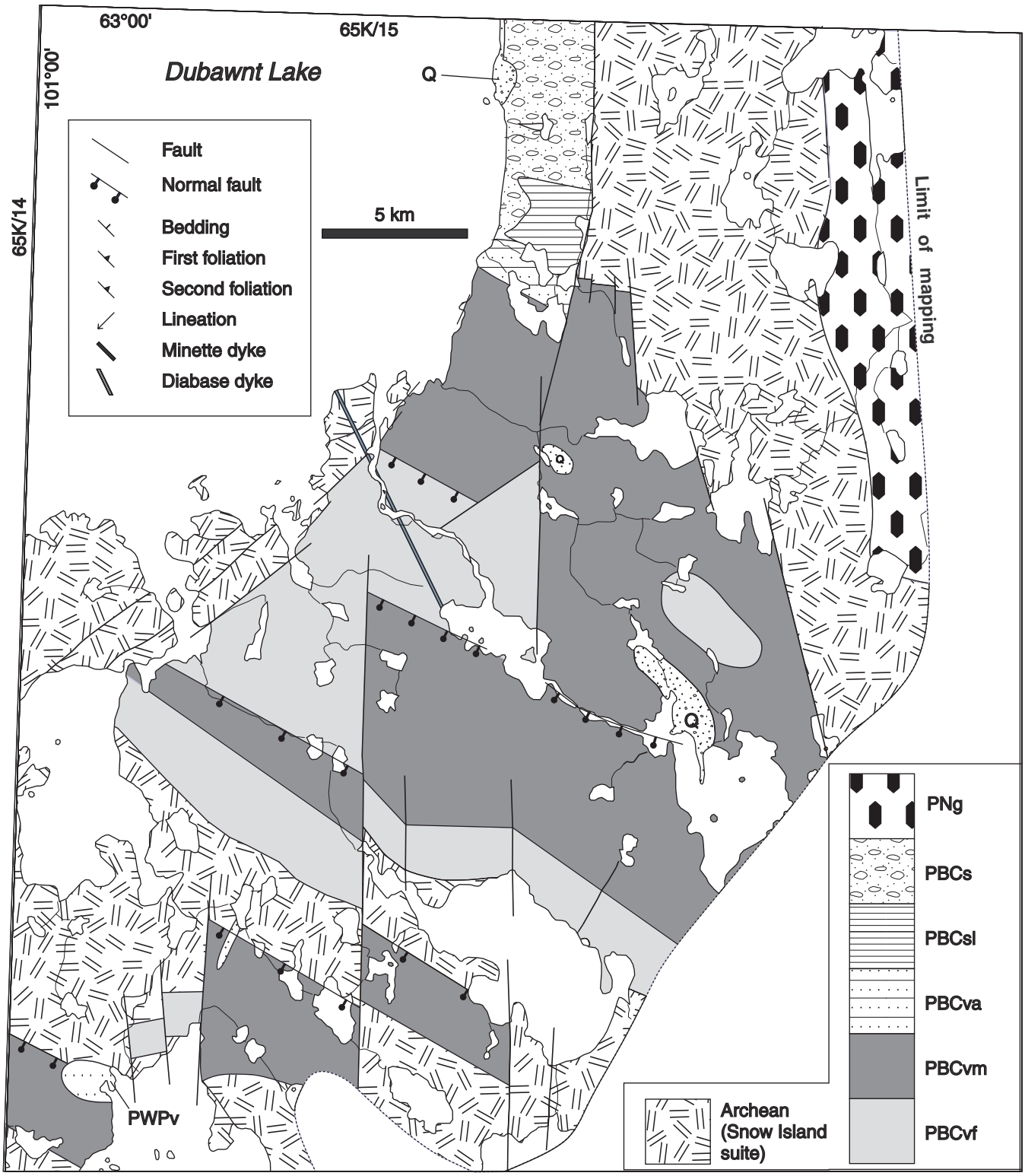

Figure 26. *Geology of the apex of the Kamilukuak basin, southeastern Dubawnt Lake. Abbreviations: PWPv, Pitz Formation anorthoclase-phyric rhyodacite flow; Q, Quaternary sand and gravel.*

Outlet Bay field and Grant Lake section

The Outlet Bay volcanic field occupies a poorly exposed area south and east of Outlet Bay (Fig. 2). Flat-lying, pale purple-pink-weathering, aphanitic felsic flows, which strongly resemble unit PBCvf in the Dubawnt and Kamilukuak basins, directly overlie Archean granitoid intrusive rocks. Lamprophyric and sedimentary units are absent. The Grant Lake section is well exposed along the north shore of the Dubawnt River downstream from Outlet Bay. The volcanic rocks of this section have an unusually strong and penetrative, north-northeast-trending fracture cleavage. A rapid but continuous transition to Kunwak Formation pebbly conglomerate is observed on both banks of the river, upstream from Grant Lake. The section terminates at a Nueltin granite pluton that underlies Grant Lake.

Dykes and intrusive breccias

Lamprophyre dykes that are petrographically identical to the flows are common on the east side of Dubawnt Lake but are rare on the west side. They are 0.1 to 1 m wide and show chilled margins with phlogopite phenocrysts aligned parallel to the contacts. Phlogopite- and clinopyroxene-phyric dykes are common. Aphanitic felsic dykes are less abundant and feldspar porphyry bodies are rare. The dykes can be traced for up to hundreds of metres, with offsets every 10 to 30 m. Many dykes contain crustal xenoliths, 1 to 5 cm in size, which are highly rounded and composed of tonalitic or gneissic rocks not representative of local bedrock (Fig. 30). These were probably derived from the lower crust, and became rounded by thermal ablation during ascent. Some phlogopite-rich dykes contain 1 to 3 cm long ellipsoidal glimmerite nodules that probably precipitated from high-Mg melts in the upper mantle (Peterson and LeCheminant, 1993).

An intrusive breccia exposed on the southeastern shore of Outlet Bay is composed mostly of angular fragments of Christopher Island Formation, emplaced along a cataclastic fault in megacrystic granite (NTS 65 N/7, UTM 417820E, 7037250N). The breccia is an unsorted lithic and crystal tuff

Figure 27. *Unsorted deposit of black-weathering, aphanitic volcanic bombs in a fine-grained green-black sandy matrix, northern Kamilukuak basin (unit PBCva). The outcrop is interpreted as a juvenile subaerial deposit. Hammer handle is 60 cm long. GSC 2002-833*

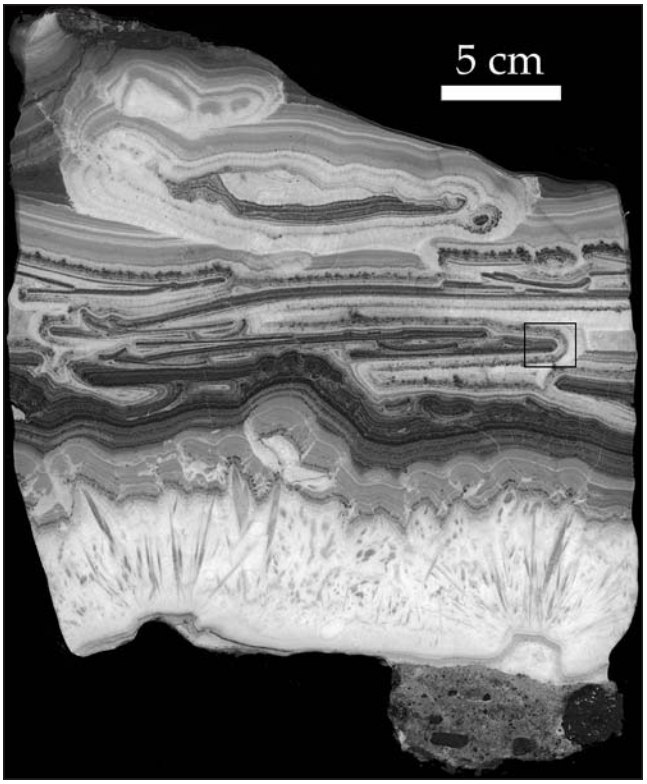

Figure 28. *Polished slab of travertine from the Kunwak Formation (sample PHA-89-40), southern Dubawnt Lake. Stratigraphic top is toward the top of the photo. A piece of the underlying lamprophyre conglomerate is clinging to the corner at bottom right. The small rectangle indicates the location of Fig. 29. GSC 2002-834*

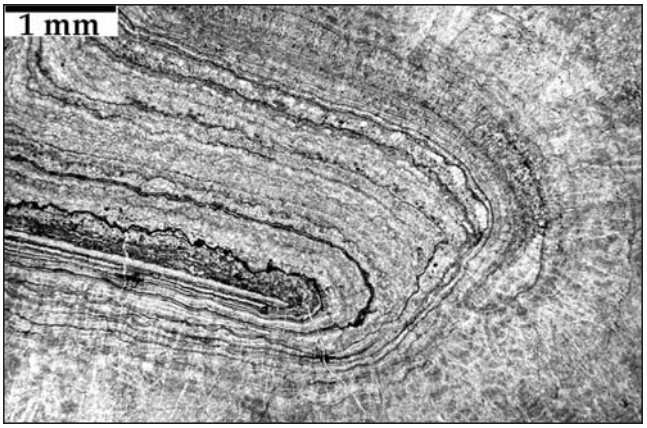

Figure 29. *Folded layers of microcrystalline calcite in travertine. The thin section was taken from the location indicated in Fig. 28.*

Figure 30. *Lamprophyre dyke with ablated gneissic xenoliths, western margin of Kamilukuak basin. GSC 2002-835*

consisting of decimetre- to metre-size fragments of granite and lamprophyre in a coarse, pebbly to sandy matrix of the same composition. In thin section, some of the volcanic clasts appear glassy, and the breccia was partially welded. No primary bedding features are preserved, but large phlogopite grains are preferentially oriented and slightly folded, suggesting minor compaction. At least three varieties of lamprophyre are present (*see* 'Petrology of Proterozoic igneous rocks' section); judging from the relative plasticity of the clasts and the composition of the matrix, the juvenile component was a phlogopite-diopside lamprophyre.

Wharton Group

Pitz Formation (units PWPs, PWPv)

The Pitz Formation consists mainly of brick-red to purplish-red-weathering quartz and alkali-feldspar porphyritic rhyolite (Fig. 31), and minor dark-brown-weathering, carbonate-cemented sandstone and conglomerate. The sandstone, which underlies the rhyolite, occurs only near the southern edge of NTS 65 K/14. The rhyolite units in the map area are altered, and most are closely associated with the overlying Thelon Formation. Rhyolite units near the Thelon-Pitz contact are heavily kaolinized, hematized, and laced with quartz veins, and are difficult to distinguish from similarly altered Snow Island leucogranite (unit ASl). On the west edge of NTS 65 N/5 (at UTM 356200E, 7040000N), an elongated paleotopographic high extending southeast from the edge of the Thelon basin consists of this altered material.

Two felsic domes within the Kamilukuak basin (one shown in Fig. 26, unit PWPv) overlie lamprophyre flows but their contacts are unexposed. They are anorthoclase porphyry bodies that lack quartz phenocrysts and petrographically resemble felsic dykes of the Christopher Island Formation; however, one sample (PHA-89-303) contains high SiO_2 (71.3%) and very low TiO_2 (0.17%), and is compositionally more similar to Nueltin granite. South of the study area, similar outcrops were mapped by Tella and Eade (1980, 1985) as part of the Pitz Formation. This precedent was followed here but may require revision.

Nueltin granite suite (units PNg, PNb)

The youngest plutonic rocks in the area are hypersolvus, quartz-porphyritic, undeformed, salmon-weathering granite stocks and associated porphyry dykes. They are part of a widespread suite of granitic rocks, dated at 1765 to 1750 Ma (Peterson and van Breemen, 1999), that extends southwest from the west end of Baker Lake to Kasba Lake (NTS 65D; Fig. 1). They are named after a large pluton at Nueltin Lake (Eade, 1972). Pluton margins and dykes are chilled, are rich in quartz and alkali-feldspar phenocrysts, and strongly resemble rhyolite of the Pitz Formation. Rapakivi texture is locally developed in the coarse interiors of plutons (Fig. 32). The granite intrusions are leucocratic, contain sparse magnetite, and have minor, late-crystallizing, strongly oxidized biotite associated with apatite, zircon, titanite, and fluorite. The

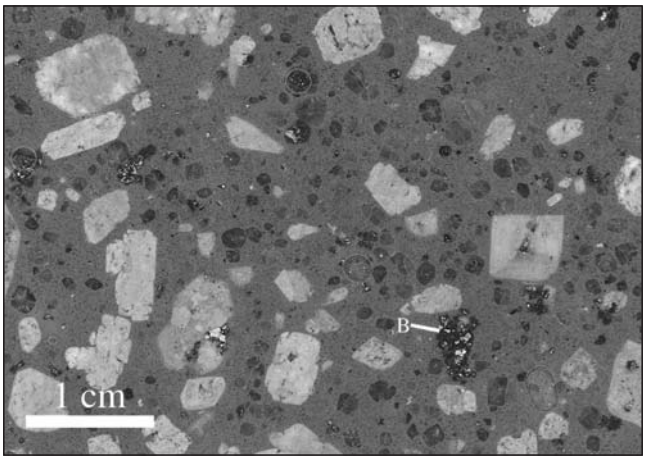

Figure 31. *Pitz Formation rhyolite porphyry (sample PHA-89-PZ). Polished slab from a 50 cm cobble, collected south of the mouth of the Slow River. Feldspar phenocrysts (white) are anorthoclase and sanidine. Abbreviation: B, basaltic bleb. GSC 2002-836*

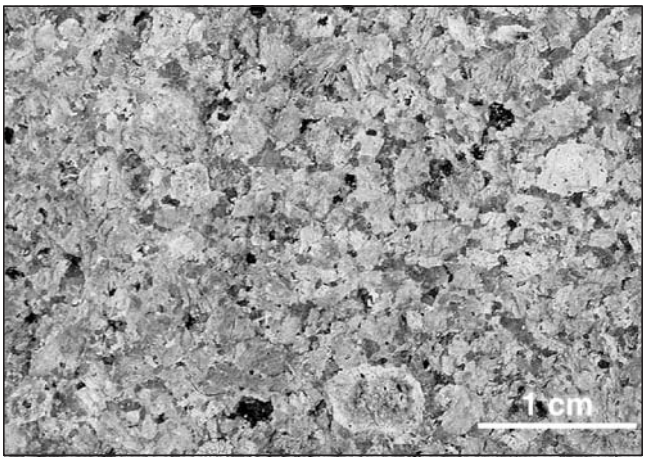

Figure 32. *Outcrop of rapakivi granite (unit PNg), eastern Dubawnt lake. Note the white plagioclase rim on the ovoid, grey, potassium-feldspar phenocryst in the bottom centre of the photo. GSC 2002-837*

larger plutons are restricted to the east side of Dubawnt Lake and are poorly exposed. Where the contacts are hidden, they were inferred to correspond to the limit of the smooth, negative magnetic anomaly that is associated with exposed portions of the plutons (Geological Survey of Canada aeromagnetic maps 7843G and 7829G). There appears to have been no structural control on emplacement of the plutons, except for the one north of the mouth of the Slow River (65 N/3, Fig. 2), which is an elongate body lying along an extrapolation of a southeast-trending fault that bounds the Kamilukuak basin.

On the west side of Dubawnt Lake, near the mouth of the Dubawnt River (NTS 65 L/16, Fig. 2), several small stocks and irregular dykes of porphyritic, salmon-weathering granite occur in an east-northeast-trending zone. They are petrographically identical to the Nueltin plutons. At UTM 647300E, 6878100N, a dyke of this granite is cut by a mesocratic rock comprising quartz xenocrysts and minor plagioclase phenocrysts in a fine-grained matrix of clinopyroxene, plagioclase, and magnetite (Fig. 33). This rock resembles basaltic and gabbroic rocks, commingled with Nueltin granite, near McRae Lake and Wharton Lake (LeCheminant et al., 1981). Enclaves of chilled basalt are common in Pitz Formation rhyolite at Pitz Lake (Booth, 1983), and millimetre- to centimetre-scale basaltic blebs with pyrite inclusions are ubiquitous in the rhyolite at Dubawnt Lake (Fig. 31). The mesocratic dykes and granitic rocks are considered part of a bimodal basalt-rhyolite igneous assemblage (LeCheminant et al., 1979).

Barrensland Group

Thelon Formation (unit PRT)

The map area includes the southeast edge of the Thelon basin. The Thelon Formation here consists of two members: 1) a basal matrix-supported conglomerate (Fig. 34), about 10 m thick and composed of well rounded pebbles in a lithic, arenaceous matrix; and 2) flaggy, planar bedded to crossbedded lithic and quartz arenite (Fig. 35). Both members are buff to pale maroon weathering and poorly indurated, and typically contain abundant pale orange reduction spots approximately 1 cm in diameter. Locally, the polymictic basal conglomeratic unit is dominated by clasts of either quartzite (most common) or local Archean granitoid rocks, with minor amounts of detritus from the Pitz Formation. Both members are typically cemented by kaolinite and other clay minerals.

Figure 34. *Basal conglomerate of Thelon Formation, containing clasts of quartzite and Pitz Formation rhyolite (dark clast in the centre of the photo). GSC 2002-838*

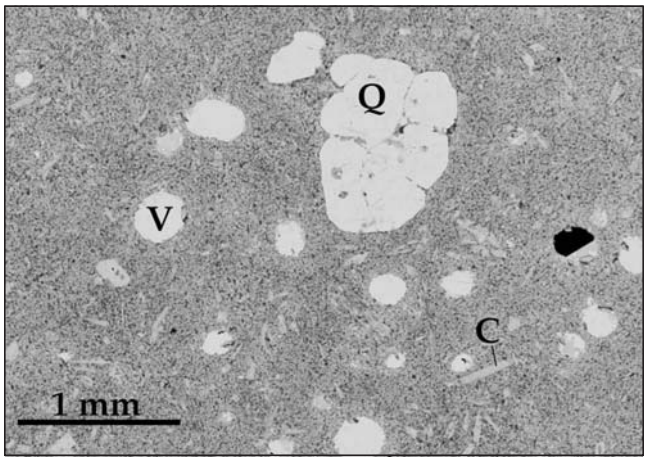

Figure 33. *Photomicrograph of mesocratic, basaltic rock associated with Nueltin granite (sample PHA-94-124c). Abbreviations: V, vesicle filled with calcite±magnetite; C, clinopyroxene; Q, quartz xenocryst.*

Figure 35. *Flaggy beds of Thelon Formation pebbly lithic and quartz arenite, above the basal conglomerate. The large-scale crossbeds, up to 10 m across, are interpreted as aeolian in origin. GSC 2002-839*

Kuungmi Formation

Outcrops of dark grey to brown-purple, aphanitic volcanic flows overlie the Thelon Formation on the large peninsula in NTS 65 K/14, and similar rocks occur in small, isolated outcrops near the west edge of the Kamilukuak basin. Analysis of one sample (PHA-89-R5, Appendix 1) collected during this study, and of others by Tella and Eade (S. Tella, pers. comm., 2001), revealed that these flows are shoshonitic, with moderate SiO_2 (50%) and MgO (6%). They appear to be correlative with phlogopite-bearing crystal and lithic tuff overlying the Thelon Formation near Retort Lake (Peterson, 1995; Fig. 1, map 66 D/2, lat. 64°04'N, long. 102°58'W). The base of the tuffaceous rocks, which are contaminated with up to 50% quartz sand (Fig. 36), has an irregular contact with the underlying Thelon Formation and is commonly vesicular (Fig. 37). The sandy tuff is interpreted as a phreatomagmatic deposit, produced by eruption of magma through wet, unconsolidated sand. It is overlain by well bedded, shoshonitic crystal tuff with olivine, clinopyroxene, sanidine, and altered interstitial glass. The degree of welding increases with stratigraphic height, and the outcrops are capped by relatively resistant rocks that superficially resemble lava flows; the total exposed thickness of the tuff units is about 15 m.

Lookout Point Formation

Donaldson (1969) identified a siliceous, stromatolitic dolostone south of the Thelon River, representing a late marine incursion into the Thelon basin. It is best exposed in an area of raised beaches immediately west of, and at higher elevation than, exposures of the Kuungmi Formation tuff (Gall et al., 1992). It consists of silicified and finely crystalline, cryptalgal dolostone and thin-bedded, medium-grained siliceous arenite, gradationally overlain by a thicker section of silicified stromatolitic dolostone with minor arenite interbeds. The basal contact is not exposed. Stromatolites near the base are both discrete and laterally linked domal forms, commonly with a synoptic relief of 5 to 10 cm, and rarely 30 cm. Some beds are dominated by well laminated, low-relief, hummocky ('egg carton') stromatolites. The upper half of the section contains fewer quartzose sandstone interbeds and more laminar cryptalagal dolostone. Teepee structures, oncolites, edgewise conglomerate beds, desiccation cracks, and hopper crystal casts are common in the upper parts of the section.

Mackenzie diabase dykes

Wide (50–100 m) diabase dykes of the Mackenzie swarm are prominent in the north half of the map area. Outcrops of diabase are absent in the domain containing the Snow River gneiss, although magnetic anomaly maps indicate that some thin dykes are present there. The Mackenzie dykes have distinctive features that are attributed to their lengths (approx. 1500 km), and have an inferred source near the Coppermine homocline (LeCheminant and Heaman, 1989). The dykes are exceptionally straight, with few apophyses, and have well developed chilled margins about 30 cm wide. Evidence for wall-rock ablation and contamination is absent; only the porous Thelon sandstone shows any visible thermal effects adjacent to the contacts. The dyke centres are heterogeneous, with internal chilled contacts, weak banding due to crystal sorting, and abundant patches and veins of pink granophyre resulting from crystal differentiation. Mackenzie dykes in this area are part of a recognized subswarm that is both more mafic and more alkaline than average (Baragar et al., 1996).

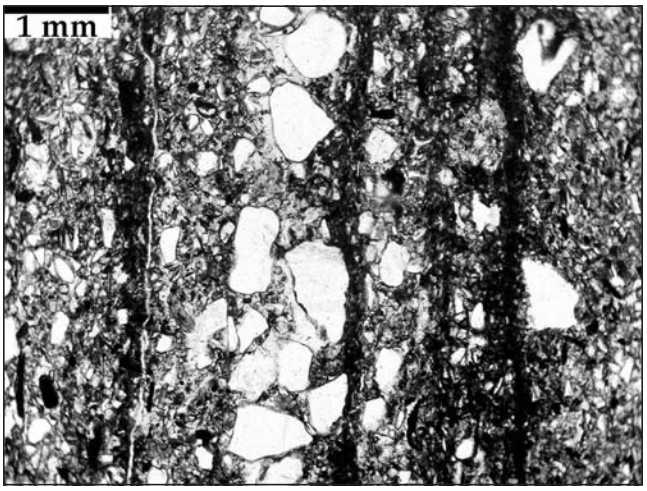

Figure 36. *Photomicrograph of sandy tuff, Kuungmi Formation (sample PHA-93-K6). Layers of angular grains of broken quartz and quartz cement are interbedded with silt-size, hematized volcanic glass and phlogopite crystals. Stratigraphic top is to the left.*

Figure 37. *Three beds of Kuungmi Formation sandy tuff. The uppermost is dark, hematitic, and vesicular. The middle, grey tuff (beneath the pen) is mixed with a large proportion of quartz sand. The lowermost, quartz-rich sand has erosional features (small arrow). The lower two beds are cut by a breccia dyke (large arrow) that resembles the vesicular tuff. GSC 1994-741C*

STRUCTURAL GEOLOGY AND METAMORPHISM

Deformation and metamorphism in the Dubawnt Lake area occurred in six stages: 1) at least one deformation event at amphibolite facies prior to 2.6 Ga; 2) emplacement of the extensive, 2.6 Ga, Snow Island intrusive suite; 3) post–Amer Group, pre–Dubawnt Supergroup development of a strong, southwest-plunging stretching lineation, and possible northeast-vergent thrust faulting, at upper greenschist to lower amphibolite facies; 4) brittle extensional faulting and local ductile shearing, concurrent with Baker Lake Group volcanism and sedimentation (ca. 1830 Ma); 5) emplacement of the Nueltin granite suite at ca. 1760 Ma, with local contact metamorphism and resetting of some radiological clocks; and 6) minor normal faulting after 1760 Ma.

Pre–2.6 Ga deformation

Intrusions of the Snow Island diorite to granite suite, dated at ca. 2605 Ma (LeCheminant and Roddick, 1991), cut a strong mineral and gneissic foliation in the Snow River gneiss, and a schistose fabric in the Clarke River schist. Both older units have mineral assemblages consistent with these fabrics developing at upper amphibolite facies. Partial melting and metamorphic segregation generated muscovite-feldspar pegmatite bodies in the schist, and felsic rinds on amphibolitic layers in the Snow River gneiss. Centimetre-scale recumbent folds are present in amphibolitic portions of the Snow River gneiss. Large-scale folds were not identified in the gneiss.

2.6 Ga deformation

Intrusion of the Snow Island suite was accompanied by extreme flattening of septa of adjacent host rocks at high metamorphic grade. The septa, typically consisting of layered amphibolite with lit-par-lit injections of granitic melt (?and partial melts of wall rock) display foliations subparallel to the pluton margins. At a few localities, the foliation wraps around feldspathic augen, but rotations of these are not discernible. The internal portions of the plutons invariably are massive and undeformed, except where cut by discrete Proterozoic shear bands (*see* following section), or where they contain a relict foliation inherited from older wall rocks.

Post–Amer Group, pre–Dubawnt Supergroup deformation

Sedimentary strata, correlative with the Paleoproterozoic Amer Group, were affected by regional low-grade metamorphism and contain muscovite-bearing tectonic schist, discrete northeast-trending mylonite bands, and a shallowly southwest-plunging stretching lineation within the mylonite foliation. A peak lower amphibolite facies metamorphic grade is indicated by a semipelitic band in quartzite from west-central Dubawnt Lake, which contains quartz+muscovite+staurolite+ opaque minerals+zircon. Biotite and alkali feldspar are absent. An oxidized band in the semipelite is rich in hematite, and staurolite is coated with rims of Fe-Ti oxides, possibly as a result of re-equilibration with fluids during retrograde metamorphism. The peak metamorphic mineral assemblages are polyvariant, but indicate a temperature between 525 and 675°C, bracketed at low temperature by the reaction chloritoid + Al_2SiO_5 → staurolite + quartz, and at high T by the reaction staurolite + quartz → almandine + sillimanite.

Four fault zones, characterized by muscovite schist, are present in the western Dubawnt Lake area. From north to south they are

1) a narrow (1 m wide), vertical, muscovite-bearing, northeast-trending fault zone cutting through Snow Island megacrystic granite and leucogranite (NTS 65 N/6, UTM 380500E, 7030500N; *see* Fig. 2), which appears to be an extension of the boundary between the Kunwak Formation and Archean rocks on the west side of the lake;

2) a nearly flat-lying muscovite schist separating Amer quartzite from Archean leucogranite northeast of the Clarke River schist (NTS 65 M/1, UTM 346700E, 7011000N; Fig. 38);

3) a northwest-trending, crenulated muscovite schist on the northeast edge of a large island underlain by Amer quartzite (NTS 65 N/4, UTM 350000E, 7003000N); and

4) a strongly crenulated muscovite schist, dismembered by younger brittle faulting and quartz veining, on the northwestern segment of the northwest-trending shear zone that forms the northern boundary of the Snow River gneiss (NTS 65 L/16, UTM 330000E, 6983000N).

In each case the muscovite was developed from earlier quartz-feldspar assemblages in granite or quartz-rich arenite. None of these schist units is in contact with Dubawnt Supergroup rocks, so their ages can only be constrained as post–Amer Group. Penetrative deformation is rare in the Dubawnt Supergroup and occurred at sub-greenschist facies, consistent with the muscovite schist being older.

Figure 38. *Tectonic schist developed between Amer Group quartzite and Snow Island leucogranite. Compass is pointing north; minor folds trend approximately 210°, parallel to a regionally developed Proterozoic lineation in underlying crystalline rocks. GSC 2002-840*

The tectonic schist north of the Clarke River schist (example 2, above) has an anastomosing fabric that wraps around centimetre-scale bands of quartzite and Snow Island leucogranite. The schist appears to entirely underlie a band of quartzite, forming a small klippe (Fig. 39). This quartzite is cut off on the west side by an east-dipping, chloritic, schistose fault hosted in a grey-green slate. It is in the footwall of this fault that a strong, south-southwest-plunging stretching lineation, characteristic of the entire northwest side of Dubawnt Lake, first becomes prominent. The fold axes in the tectonic schist are parallel to this lineation in the underlying granite.

The northwest quadrant of the Dubawnt Lake area is notable for having numerous, 1 to 10 m thick bands of steeply dipping, south-southwest-striking mylonite that contain the shallowly (15–30°) south-southwest-plunging stretching lineation (Fig. 40). The lineation is present in Amer Group quartzite but not in younger rocks, and is commonly well developed in rocks with no planar fabric, such as fine-grained Snow Island leucogranite (unit ASl). In the leucogranite mylonite, deformed biotite is replaced and overgrown by chlorite. The lineation is difficult to discern in coarse-grained megacrystic granite (unit Asm), which instead displays an anastomosing foliation that wraps around potassium feldspar phenocrysts. Shear-sense indicators are rare in the anastomosing fabric and in the mylonite. In north-central Dubawnt Lake (NTS 65 N/6, UTM 380750E, 7030700N), pink feldspar pegmatite bands, 1 cm in width, define intrafolial Z-folds within a northeast-trending mylonite (Fig. 41) and cut the mylonite, suggesting formation during dextral shear.

The widespread association between prominent muscovite schist within and beneath the Amer Group, and penetrative lineations in contiguous rocks, suggests they developed nearly simultaneously. The muscovite schist separating quartzite from leucogranite north of the Clarke River schist may be interpreted as a décollement, itself folded and cut by a pair of younger, east-vergent faults that placed chlorite slate and Archean rocks over quartzite.

Deformation at ca. 1830 Ma

There are no widely developed ductile deformation features that postdate the regional southwest-trending stretching lineation described above. Two types of brittle faults affect lower Dubawnt Supergroup and older rocks. Extensional faults with substantial quartz stockworks are associated with Baker Lake Group basin margins, particularly the northeast edge of the Kamilukuak basin. These may be developed within older ductile deformation zones, particularly those present along the west edges of the Dubawnt and Kamilukuak basins. Within the latter basin, zones of sub-greenschist-facies anastomosing cleavage, which dip southward at about 60°, are sporadically exposed along east-trending topographic breaks. They are interpreted as south-side-down normal faults, which are responsible for repetitions of the Archean-Proterozoic unconformity and of the contact between lower felsic (unit PDCvf) and mafic minettes (unit PDCvm; *see* Fig. 26).

Subaqueous volcanic flows and clastic deposits from the middle and upper Christopher Island Formation, plus very coarse megabreccia (?talus) deposits, are present in the northern apex of the Kamilukuak basin; similar megabreccia is exposed on an island on the north edge of the Dubawnt basin (Fig. 11). South of the apex, exposures consist almost entirely of lava flows, with no interbedded sedimentary rocks. The distribution of lithofacies in the Kamilukuak basin indicates that erosional and depositional rates increased with time and toward the north. The present geometry, and distribution of facies and faults, approximate that of an idealized basin produced by north-south extension during east-west indentation of a competent block (Fig. 42). In such a situation, the basin apex undergoes large relative downdropping and should be the site of both coarse alluvial sedimentation and subaqueous lithofacies. North-south extension within the wedge must be accommodated on faults at a high angle to the extension direction, and these faults are presumably represented by the south-dipping, anastomosing cleavage zones. Late, north-trending normal faults that crosscut these features may be related to postindentation extension.

It cannot be demonstrated that the faults bounding the Kamilukuak basin were active solely at ca. 1830 Ma, and they may have been reactivated at a later time. Nevertheless, the northwest-trending fault bounding the east side of the Kamilukuak basin is on strike with the Bathurst fault of the Thelon tectonic zone. The northwestern shore of Dubawnt Lake, which intersects the extrapolation of this fault, is the site of sinistral offsets of the western side of the Dubawnt basin (which are clearly visible in offsets of a band of strongly magnetic Archean metavolcanic rocks, *see* Geological Survey of Canada, 1972), and is also the site of a high concentration of fault-parallel Mackenzie diabase dykes. The faults bounding the Kamilukuak basin can be viewed as a conjugate set: the conjugate nature of faulting in the area at this time is reflected in the bimodal distribution of lamprophyre dyke trends (Fig. 43). The Dubawnt basin has important features similar to the Kamilukuak basin (e.g. extremely coarse, clast-supported conglomerate at the northern apex) and may have had a similar origin, although the inferred faulted contacts are obscured by the lake and by intrusions of Nueltin granite. Rainbird and Peterson (1990) interpreted the thick succession of Kunwak Formation conglomerate on the west side as representing a northeast-prograding alluvial stack that developed against an escarpment that coincided with a dextral strike-slip fault, consistent with easterly directed indentation. Paleocurrents inferred from pebble imbrication studies suggest transport along this margin toward a depocentre located somewhere beneath north-central Dubawnt Lake (Fig. 11, 40).

Whatever the nature of syndepositional faulting for the Baker Lake Group, the timing of its initiation is suggested by the orientations and locations of the lower felsic (unit PBCvf) unit. This unit directly overlies Archean rocks, with no intervening sediment, and contains no clastic sedimentary interbeds. The lower part of unit PBCvf is not present in the most steeply dipping sections, particularly within the eastern Dubawnt basin. An idealized cross-section through the Dubawnt basin (Fig. 44) suggests a likely scenario, in which eruption of the lower felsic flows preceded basin development. The lamprophyre and upper felsic flows, in contrast, were deposited within active basins during and after rapid sedimentary deposition. The interpreted environment is similar to that in the

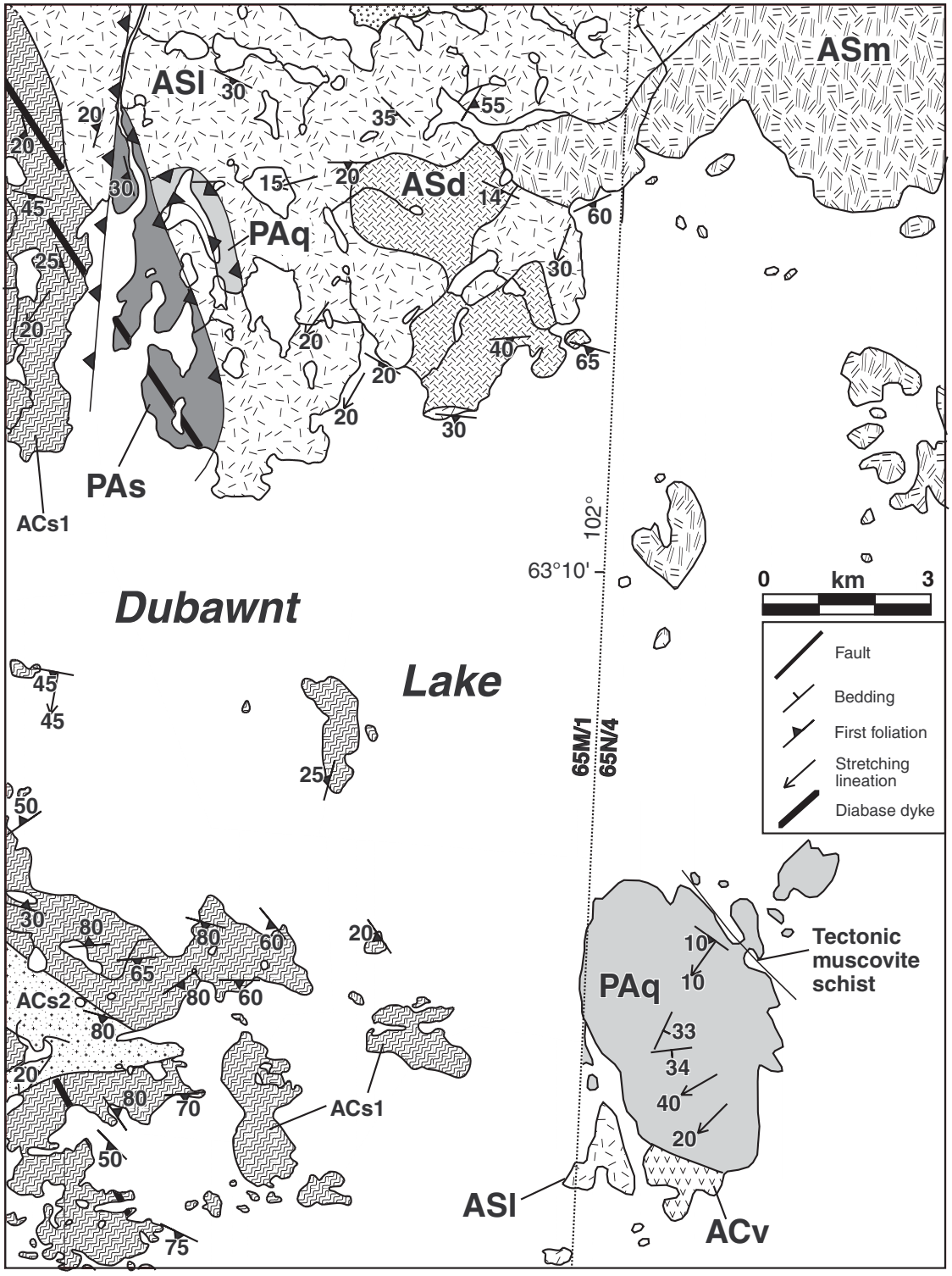

Figure 39. *Geology of west-central Dubawnt Lake. Abbreviations: ACS1, Clarke River schist; ACS2, Clarke River psammite; ASl, Snow Island leucogranite; ASm, megacrystic granite; ASd, diorite; PAq, Amer Group quartzite; PAs, Amer Group chloritic schist. It is not known whether the contact between ACv and PAq on the large island is a fault or an unconformity.*

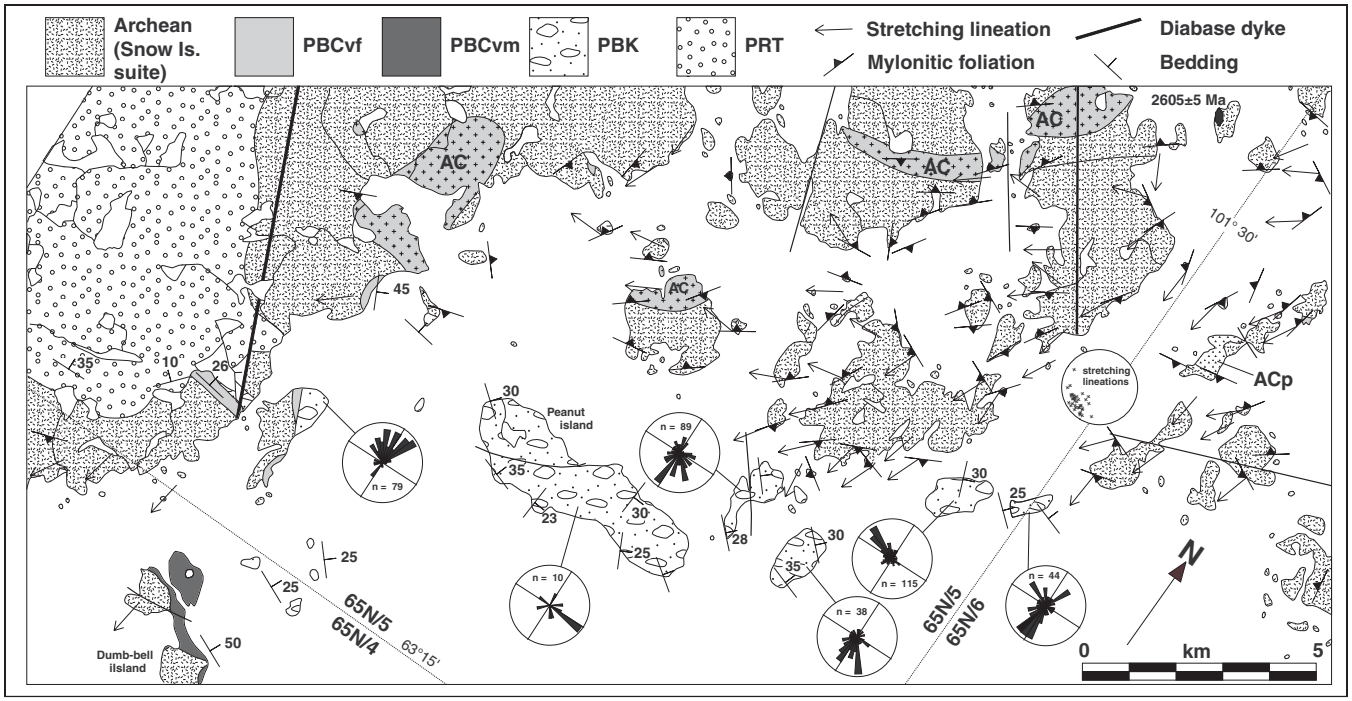

Figure 40. *Geology of northwestern Dubawnt Lake, showing the strongly lineated Archean rocks along the western side of the Dubawnt basin. Abbreviations: AC, undivided Clarke River schist (ACp, peridotite); ASm, Snow Island megacrystic granite (with U-Pb zircon age of 2.605 Ma), ASl, leucogranite. Outcrops of lower felsic flows (PBCvf) are restricted to the extreme west edge of the basin. Note that the PBCvm member on Dumb-bell island dips twice as steeply as the overlying Kunwak Formation (PBK). The Thelon Formation (PRT) locally has moderate dips due to minor faulting. Rose diagrams for the Kunwak Formation are current vectors measured from cobble imbrications.*

Figure 41. *Transposed syntectonic pegmatite vein with Z-folds in strongly lineated mylonite of Snow Island leucogranite, northwestern Dubawnt Lake. The near-vertical foliation trends 335°. GSC 2002-841*

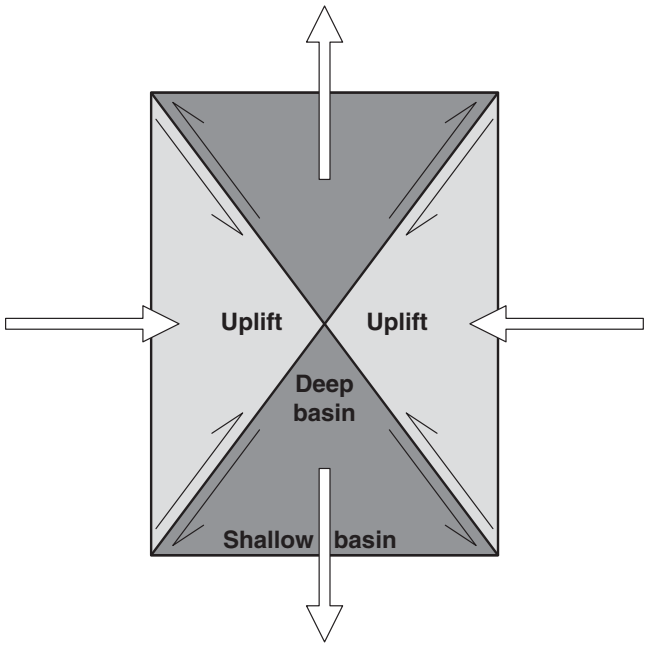

Figure 42. *Idealization of basins resulting from north-south extension during east-west indentation of a competent block. The basin margins are escarpments that are steepest near the apex, and are potential sites for the formation of large alluvial fans.*

Karakorum fault zone on the western flank of the Tibetan Plateau, where ultrapotassic volcanic rocks and fluvial-alluvial sediments are currently being deposited in narrow basins bounded by active faults (Pognante, 1990).

Post–1830 Ma deformation and metamorphism

Some open folds and cleavages within the Christopher Island Formation, all developed at sub-greenschist facies, may have developed synchronously with basin development or later. Sinistral shear on a northwest-trending surface is demonstrated by a lamprophyre dyke in Outlet Bay (NTS 65 N/7, UTM 407800E, 7031800N), which contains thin parallel quartz veins that were transposed into a southeast-vergent S-fold (Fig. 45). Northeast of this dyke, grey felsic lava flows (unit PBCva) of the Grant Lake section contain a well developed, closely spaced, north-northeast-trending slaty cleavage. A widely spaced, mostly northwest-trending fracture cleavage is prominent in the upper felsic lavas and siltstone at Lost Boat island.

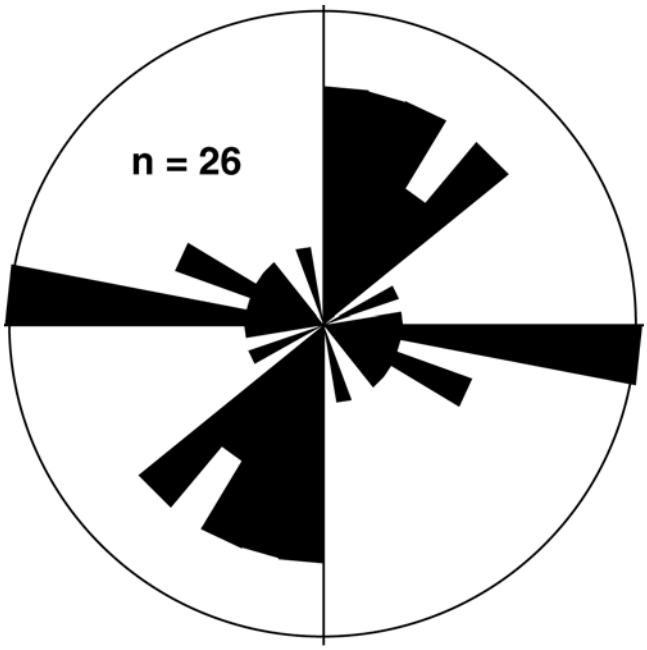

Figure 43. *Rose diagram of lamprophyre dyke trends, Dubawnt Lake area. Dykes with one of the two prominent trends (035°, 100°) are uniformly distributed on the east side of Dubawnt Lake.*

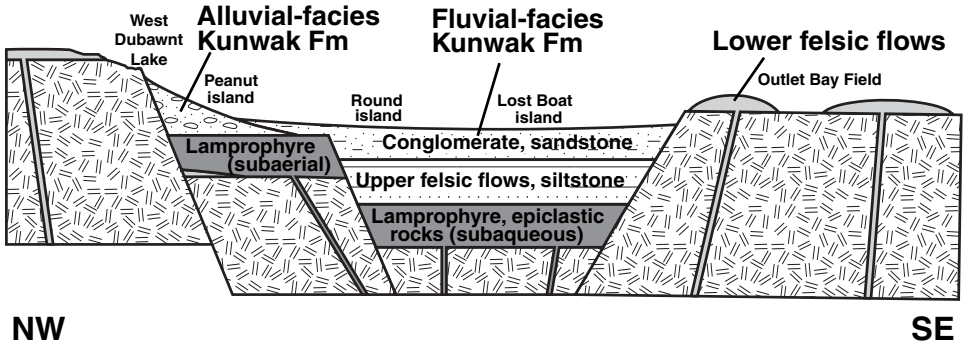

Figure 44. *Idealized cross-section through a Dubawnt-style basin, before tilting at 30 to 60°. Lower felsic flows (unit PBCvf) erupted directly onto crystalline basement, followed by normal faulting, extension, and downdropping of a graben that accumulated lamprophyre volcanic and epiclastic rocks (PBCvm). Upper felsic lavas (PBCva) and lacustrine sediments accumulated on the east side only, due to further downdropping of the east side of the basin. Alluvial-fan deposits of the Kunwak Formation accumulated along a prominent fault escarpment on the west side, which developed along an older ductile shear zone. Fluvial-facies conglomerate and sandstone covered the volcanic rocks on the basin floor. The approximate locations of some prominent stratigraphic sections and outcrop areas are indicated.*

Map-scale, post–Baker Lake Group faulting in the area is mainly restricted to a set of north-trending faults, with a dextral component of movement. These are prominent in the south half of the lake, where they segment the Kamilukuak basin. They also form the east side of a large peninsula west of the Kamilukuak basin that is underlain by a north-younging succession of the Dubawnt Supergroup. The relationship of this peninsula to the nearby Kamilukuak basin is unknown, and the age of the faults is also unknown.

No deformation event can be positively correlated with deposition of the Wharton Group. Peterson and Rainbird (1990) speculated that an elongated pluton in 65 N/3 was emplaced along a reactivated fault. In 65 L/16, trains of small Nueltin granite stocks and associated mesocratic dykes trend about 120°, subparallel to one major set of minette dykes (Fig. 46), but this direction is also parallel to the foliation of the enclosing gneiss and to a major shear zone to the north. Hence, the location of these intrusions may not be controlled by active faulting. It has long been recognized that a low-grade thermal metamorphic event of this age (i.e. ca. 1.76 Ga) is widespread in the western Churchill Province (Loveridge et al., 1988). It is demonstrated by a Rb-Sr isochron age obtained from the Christopher Island Formation (*see* 'Geochemistry' section), and by a U-Pb age of 1750 Ma obtained from metamorphic titanite in lamprophyre from Long island, a few metres away from a Nueltin granite contact (R. Parrish, unpub. data, 1990). The Nueltin granite and Pitz Formation are themselves undeformed. Minor post-Thelon faulting affects the margins of the Thelon basin.

PETROLOGY OF PROTEROZOIC IGNEOUS ROCKS

Christopher Island Formation

Petrography and mineralogy

Flows and dykes of the Christopher Island Formation range from lamprophyre with abundant phenocrysts of olivine, phlogopite, diopside, and apatite (Fig. 47), to leucocratic and felsic aphanitic rocks, and sanidine or anorthoclase porphyry. The matrix of the lamprophyre typically consists of poikilitic, Ba-rich potassium feldspar enclosing microphenocrysts of phlogopite, clinopyroxene, and magnetite, or of sanidine laths with interstitial phases that are consistent with peralkaline residua (carbonate, alkali amphibole, and sodic clinopyroxene). Phenocrysts and microphenocrysts of leucite (pseudomorphed by alkali feldspar±quartz) are rare but present in both mafic and felsic rocks.

There are five principal rock types:

1) olivine-phlogopite-clinopyroxene lamprophyre, which typically has a groundmass of fine-grained potassium feldspar, clinopyroxene, biotite, and magnetite; extrusive samples are concentrated in the lower part of unit PBCvm;

2) phlogopite-clinopyroxene lamprophyre, in which the matrix may consist of fine-grained phlogopite+clinopyroxene+feldspar+magnetite, or of small phenocrysts of potassium feldspar; this is the most common type of lamprophyre (middle and upper units PBCvm);

3) sanidine porphyry (unit PBCvf), which contains a high proportion of felsic groundmass and a population of oxidized and resorbed phenocrysts of phlogopite and clinopyroxene; it is the only lava type that contains significant plagioclase;

4) aphanitic felsic volcanic rocks, consisting of fine-grained alkali feldspar with interstitial mafic minerals; and

5) felsic flows with resorbed phenocrysts of anorthoclase and phlogopite, and abundant groundmass leucite.

Types (4) and (5) are from the upper felsic unit (PBCva).

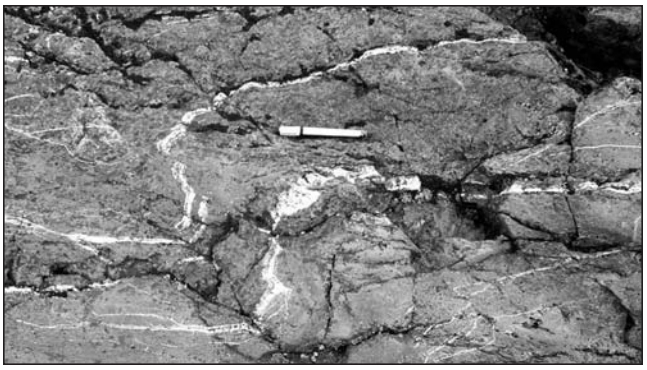

Figure 45. *Folded quartz veins in a minette dyke trending 343°, Outlet Bay. The axial plane of the fold is parallel to the dyke. The veins initially developed parallel to the dyke contacts, which are also folded. GSC 2002-842*

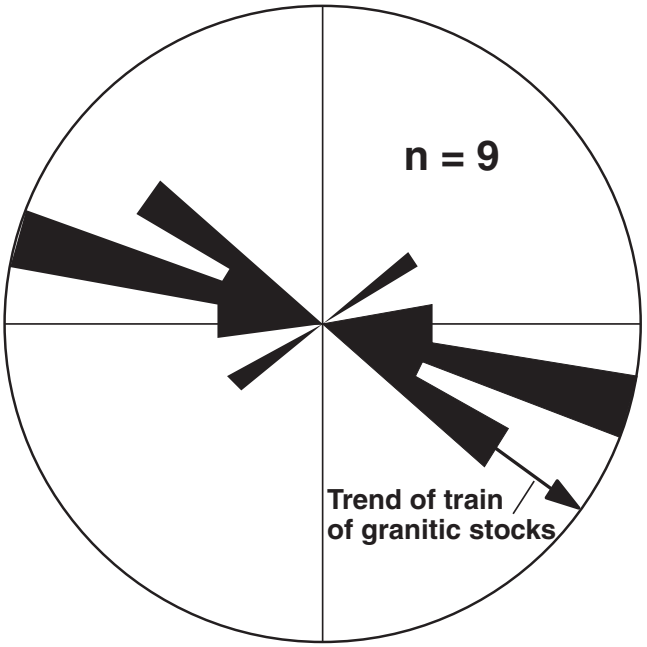

Figure 46. *Rose diagram of trends of mafic dykes associated with Nueltin granite stocks and net-vein intrusions, NTS 65 L/16. Also shown is the trend of a train of four granite intrusions.*

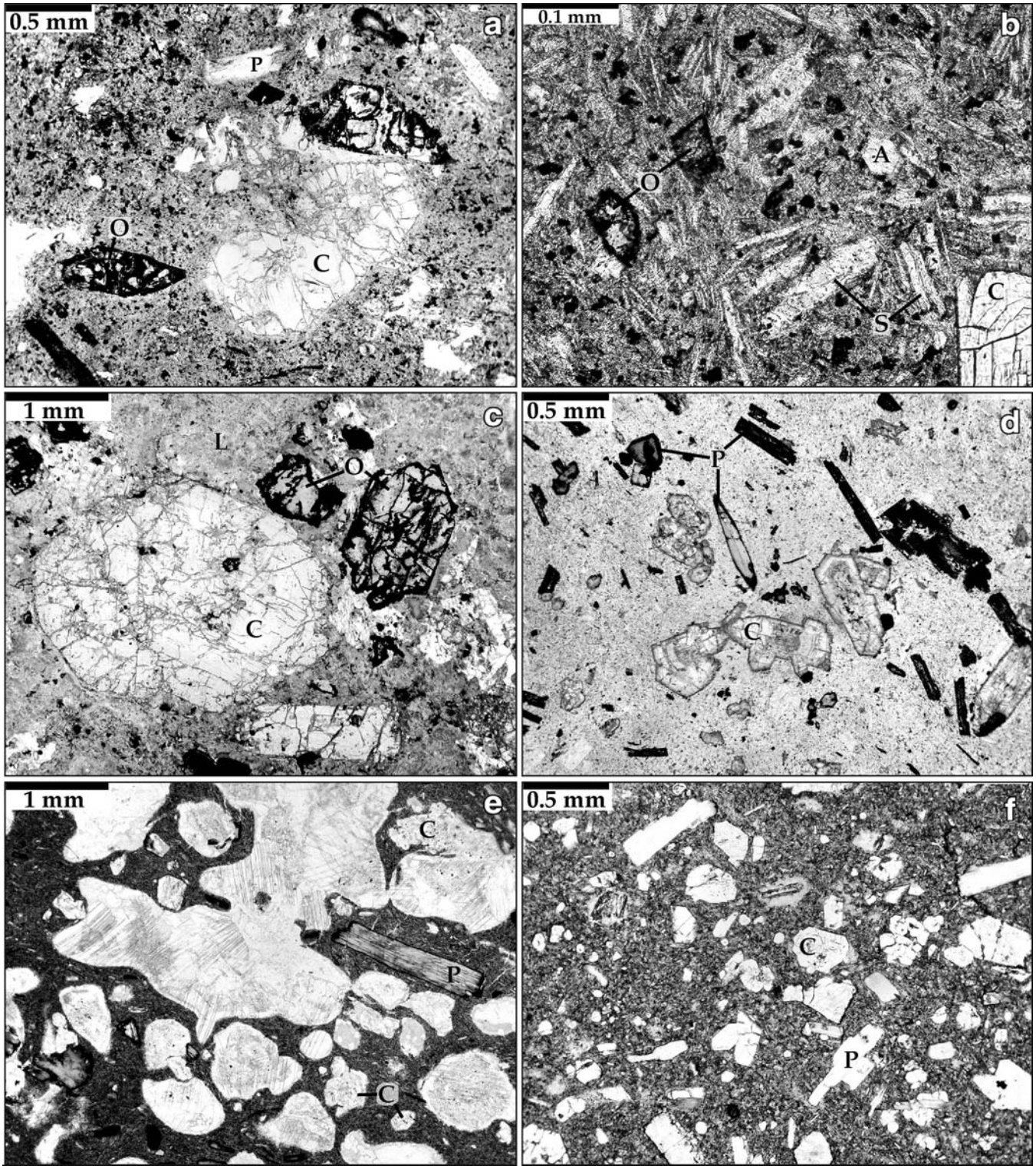

Figure 47. *Photomicrographs of mafic lamprophyre from the Christopher Island Formation (abbreviations: C, clinopyroxene; P, phlogopite; O, altered olivine; S, sanidine; A, apatite; L, leucite pseudomorphs): a) olivine-clinopyroxene-phlogopite lamprophyre dyke (sample PHA-91-21), north of Outlet Bay; b) groundmass of olivine-phlogopite-clinopyroxene lamprophyre (sample PHA-91-150), Outlet Bay breccia; c) olivine-clinopyroxene-leucite cumulate (?dyke; sample PHA-89-137), Outlet Bay (*see also *Fig. 55); d) phlogopite-clinopyroxene lamprophyre with groundmass rich in strongly oxidized mica and potassium feldspar, Outlet Bay breccia; e) vesicular phlogopite-clinopyroxene lamprophyre (the large vesicles filled with calcite), Outlet Bay breccia; f) phlogopite-clinopyroxene lamprophyre with phlogopite-rich groundmass, Outlet Bay breccia.*

Most samples have undergone significant alteration. Olivine-bearing rocks, in particular, may be largely replaced by carbonate or silica, and fresh phenocrystic feldspar is rare. Alteration is particularly intense adjacent to Nueltin granite plutons.

Olivine

Unaltered olivine was not found in any of the samples. Serpentine, carbonate, and quartz pseudomorphs are mostly irregular, indicating that most olivine phenocrysts underwent resorption and oxidation during transport to the surface. Most of the pseudomorphs are less than 1 mm long, although megacrysts up to 1.5 cm occur in sample PHA-91-18. Olivine always occurs in phlogopite-rich rocks and is usually associated with clinopyroxene and sometimes leucite. The only inclusions noted in olivine are of apatite.

Phlogopite and amphibole

Phlogopite phenocrysts (≤1 cm) commonly define a trachytic texture in lamprophyre dykes and flows. They are mostly a golden brown or slightly reddish brown, and commonly have strongly oxidized rims studded with magnetite. The phenocrysts display a continuous spectrum of compositions (Table 2); Mg/(Mg+Fe) is not strongly correlated with any other compositional variable in the phenocrysts. The Al_2O_3 contents of the phenocrysts (11–13.5%) are relatively high, typical of phlogopite from minette (Mitchell and Bergman, 1991). The phenocryst to groundmass trends, however, parallel those of lamproite (Fig. 48). Mica with high Ti and Fe, low Al, polysynthetic twinning (Fig. 49), and yellow-brown to pink pleochroism is present in some flows in unit PBCva and in clasts from overlying epiclastic rocks (e.g. Table 2, sample PHA-89-16). This mica resembles groundmass tetraferriphlogopite in some lamproite bodies.

Glimmerite xenoliths found in the Dubawnt Lake area are not mineralogically diverse, and are mostly altered. Figure 48 includes data for glimmerite xenoliths occurring throughout the western Churchill Province (Peterson and LeCheminant, 1993). Phlogopite from the glimmerite nodules forms a separate compositional group that overlaps only slightly with the phenocrysts. It defines a trend parallel to that of mica from Group II kimberlite bodies (orangeite; Mitchell and Bergman, 1991). This mica has low TiO_2 (<1.25%), high MgO, and highly variable Cr_2O_3 (usually >0.5%) and Al_2O_3, and is considered to have precipitated from highly magnesian and CO_2-rich melts near their source region in the upper mantle.

Amphibole is an uncommon primary constituent of the lamprophyre. Richteritic amphibole occurs in the groundmass of a few samples (Table 3). Secondary tremolite commonly replaces clinopyroxene, especially near the contacts with younger granite bodies.

Table 2. Electron-microprobe analysis of phlogopite phenocryst cores and rims, and groundmass from flows and dykes of the Christopher Island Formation, Dubawnt Lake area.

PHA-	89-K8	89-K8	89-K8	89-K8	89-16	89-16	89-27B	89-27B	89-27B	89-27B	89-73	89-73	89-81	89-81	89-81	89-81	89-82	89-82	89-82	89-82	89-X8	89-X8	89-X8
Sample type	**c**	**c**	**r**	**r**	**c**	**c**	**c**	**c**	**g**	**g**	**c**	**c**	**c**	**c**	**r**	**r**	**c**	**c**	**r**	**r**	**g**	**c**	**c**
SiO_2	38.77	40.97	37.66	40.3	39.63	37.67	41.91	41.57	41.96	41.58	38.59	38.1	38.94	40.3	38.7	39.31	39	38.99	39.88	38.63	39.22	40	41.01
TiO_2	2.61	2.67	2.72	2.93	3.54	2.46	2.1	2.22	1.84	1.77	3.48	3.44	1.8	1.82	2.43	4.32	1.59	1.16	1.24	1.7	1.43	1.83	1.67
Al_2O_3	11.62	11.77	11.53	11.37	10.39	11.28	11.95	11.94	12.02	12.19	12.6	12.61	12.59	13.4	13.11	12.09	13.09	12.86	12.74	12.78	12.51	12.27	12.7
Cr_2O_3	0.2	0.18	0.05	0.1	0.03	0.02	0.14	0.12	0.01	0.1	0.08	0.08	0.1	0.15	0.08	0.03	0.14	0.91	0.05	0.11	0.17	0.18	0.2
FeO	6.8	6.44	8.89	7.73	11.84	12.65	3.44	3.66	3.96	3.81	4.98	5.36	12.95	7.23	12.29	12.23	7.67	5.77	6.14	9.65	7.13	6.75	5.67
MnO	0.05	0.01	0.02	0.09	0.34	0.24	0.15	0.1	0.05	0.19	0.1	0.09	0.15	0.22	0.28	0.13	0.05	0.07	0.08	0.1	0.21	0.06	0.05
MgO	22.02	22.25	21.15	21.25	18.13	20.47	24.91	24.62	26.09	26.14	22.59	22.15	18.1	22.23	18.18	17.4	21.95	23.3	24.06	20.8	21.79	22.54	23.74
CaO	0.02	0	0.04	0.07	0.11	0.11	0.02	0.02	0.07	0.02	0.01	0	0.01	0.02	0.04	0	0.01	0.02	0	0.01	0.17	0.03	0.04
Na_2O	0.02	0.05	0.09	0.09	0.13	0.11	0.19	0.16	0.1	0.12	0.2	0.19	0.25	0.37	0.17	0.41	0.48	0.34	0.46	0.43	0.04	0.03	0.23
K_2O	10.39	10.18	9.73	9.93	9.28	6.5	9.74	9.88	8.81	8.86	9.93	9.78	8.8	9.36	9.37	8.79	9.62	9.92	9.85	9.45	9.56	10.06	10.05
BaO	0.29	0.33	0.18	0.72	0.38	0.13	0.27	0.4	0.14	0.07	0.87	0.8	0.31	0.43	0.57	0.34	0.22	0.38	0.19	0.42	0	0.21	0.4
F	2.11	2.18	2.51	1.31	1.51	1.26	0.85	0.87	1.11	1.38	0.77	0.86	0.72	1.1	0.82	0.79	0.76	0.82	1.21	0.79	0.62	0.61	0.85
O=F*	-0.89	-0.92	-1.05	-0.55	-0.32	-0.32	-0.36	-0.37	-0.47	-0.58	-0.32	-0.36	-0.3	-0.46	-0.34	-0.33	-0.32	-0.34	-0.51	-0.33	-0.26	-0.26	-0.36
Total	94.00	96.10	93.51	95.34	94.26	94.26	95.3	95.19	95.71	95.66	93.89	93.1	94.42	96.16	95.69	95.51	94.26	94.18	95.39	94.53	92.6	94.32	96.25

Sample types: c, phenocryst core; r, phenocryst rim; g, groundmass. *Oxygen equivalent of fluorine

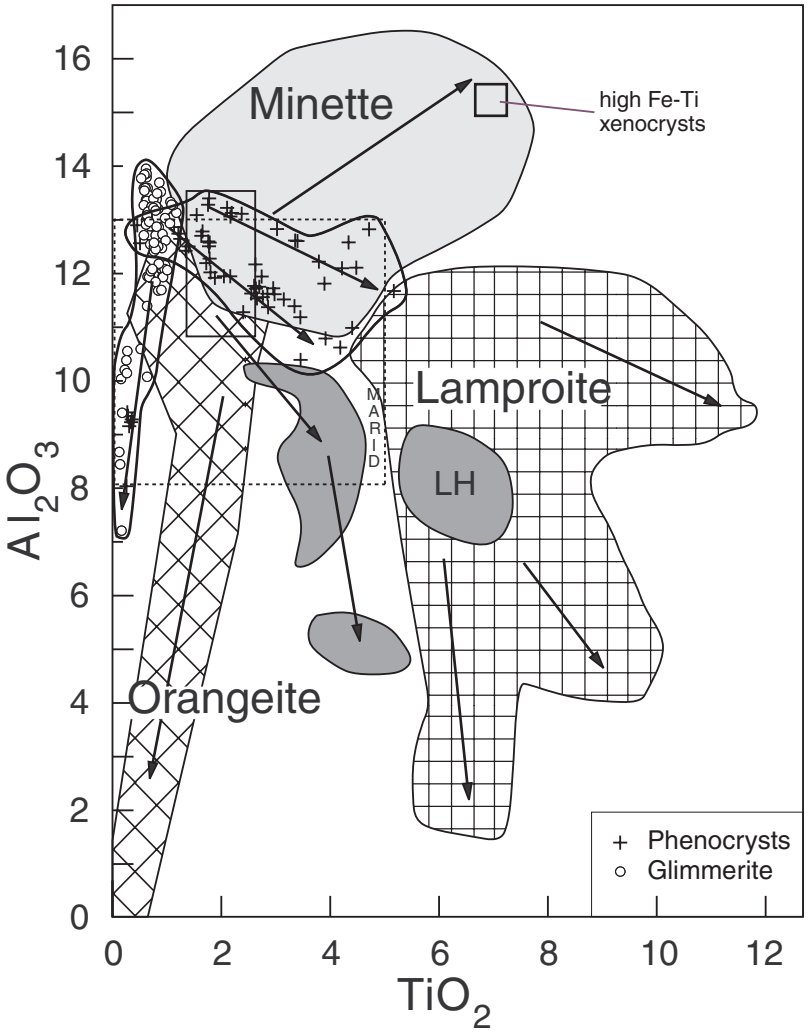

Figure 48. *Phlogopite compositions for the Christopher Island Formation and other ultrapotassic rocks (*modified from *Mitchell and Bergman, 1991). Orangeite is Group II (micaceous) kimberlite. The MARID box is the range in compositions from mica-amphibole-rutile-ilmenite-diopside nodules in kimberlite. Arrows point in the direction of magmatic evolution, from core to rim and groundmass. Abbreviation: LH, Leucite Hills.*

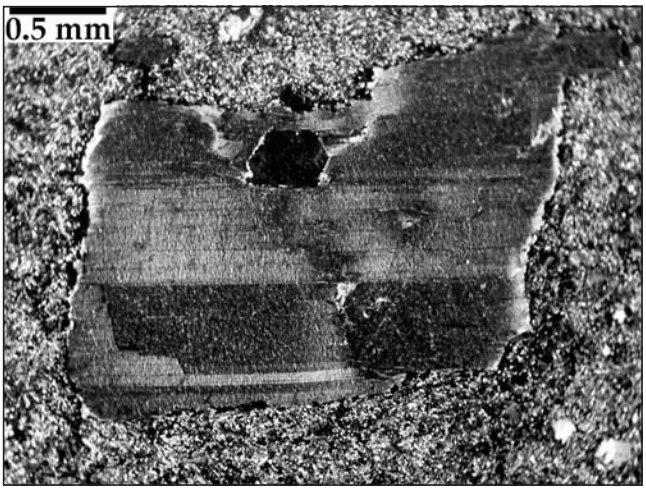

Figure 49. *Partially resorbed phlogopite phenocryst in leucite-bearing upper felsic flow (sample PHA-89-LBIF), Lost Boat island. The phlogopite has polysynthetic twinning and pink-orange pleochroism, characteristic of Ti-rich, Al-poor phlogopite in lamproites.*

Table 3. Electron-microprobe analysis of groundmass and secondary amphibole from flows and dykes of the Christopher Island Formation, Dubawnt Lake area.

PHA-	88-303A				89-K8	89-82			89-81		89-73		89-27B	
Sample type	1	1	1	1	2a	2b	2b	2b	3	3	4a	4a	4b	4b
SiO_2	57.81	56.63	57.76	57.04	56.89	51.05	51.00	51.20	54.32	54.44	56.20	56.64	58.73	56.13
TiO_2	0.58	0.61	0.62	0.65	0.92	3.28	2.00	0.15	0.07	0.25	0.08	0.09	0.09	0.17
$Al2O_3$	0.93	1.13	0.97	1.10	0.11	1.04	1.32	0.70	1.38	2.14	1.62	0.92	0.58	1.05
Cr_2O_3	0.00	0.06	0.00	0	0.04	0.00	0.01	0.04	0.08	0.01	0.01	0.10	0.06	0.03
Fe_2O_3	5.68	6.55	6.41	6.27	7.23	2.08	2.56	11.63	1.42	0.00	2.20	3.05	1.87	4.71
FeO	0.00	0.00	0.00	0	2.79	8.82	6.91	11.57	8.95	9.23	0.85	0.00	0.00	0.47
MnO	0.12	0.17	0.17	0.14	0.14	0.13	0.23	0.51	0.48	0.36	0.19	0.28	0.22	0.27
MgO	21.15	20.74	21.00	21.12	17.88	16.32	17.47	9.46	17.11	17.33	22.44	23.27	23.49	21.41
ZnO	0.00	0.06	0.00	0.04	0.04	0.00	0.11	0.17	0.16	0.10	0.02	0.05	0.05	0.08
CaO	5.62	5.43	5.45	5.56	0.62	5.29	6.54	3.97	12.53	13.18	12.77	12.12	12.14	11.22
Na_2O	5.70	5.86	5.72	6.00	7.7	6.58	5.94	5.15	0.42	0.35	0.57	0.54	0.95	1.22
K_2O	0.85	0.87	0.90	0.87	3.83	1.23	1.15	0.14	0.11	0.30	0.14	0.15	0.17	0.23
BaO	0.05	0.14	0.02	0.00	0.13	0	0.03	0.00	0.00	0.02	0.08	0.00	0.00	0.03
F	0.85	1.01	1.24	0.87	0.18	2.60	2.65	0.06	0.16	0.00	0.25	0.29	0.25	0.38
O≡F*	-0.36	-0.42	-0.52	-0.37	-0.07	-1.10	-1.12	-0.02	-0.07	0.00	-0.10	-0.12	-0.10	-0.16
sum	98.96	98.81	99.73	99.31	98.42	97.32	96.80	94.72	97.11	97.70	97.32	97.37	98.49	97.22
Principal components	ric-eck	ric-eck	ric-eck	ric-eck	eck-ric	eck-ric	eck-ric	eck-ric	tre-hnb	tre-hnb	tre-hnb	tre-hnb	tre-hnb	tre-hnb

Sample types: 1, groundmass in alkaline high-Mg rock; 2a and 2b, groundmass in alkaline low-Mg rock; 3, secondary after clinopyroxene; 4a and 4b, secondary after phlogopite.
Principal components: ric, richterite; eck, eckermannite; tre, tremolite; hnb, hornblende
*Oxygen equivalent of fluorine

Clinopyroxene

Three types of clinopyroxene are present (Table 4). Colourless, diopside-rich phenocrysts and microphenocrysts are optically homogeneous or display weak oscillatory zoning, although strongly zoned large phenocrysts do occur. On average, the crystals are normally zoned with relatively Fe-rich rims, but abrupt variations in MgO are observed and are consistent with magma mixing or disruption of cognate xenoliths from dyke walls and cumulate bodies. These are preserved as pyroxenite clumps (≤2 cm long) with minor phlogopite (Fig. 50). Apatite and magnetite are common inclusions in clinopyroxene.

A small fraction of colourless diopsidic phenocrysts contains pale green, highly rounded cores with a small but significant acmite component ($Na_2O \leq 2.5\%$). These compositions are inconsistent with the ultrapotassic nature of the carrier magma and may represent xenocrysts. They also occur as discrete rounded grains in the Outlet Bay breccia. The green clinopyroxene might originate from an eclogitic source, although a source in sodic, peralkaline magmas cannot be ruled out.

An unusually fresh, phlogopite-clinopyroxene lamprophyre dyke (sample PHA-89-K152) contains large, clear, poikilitic plates of potassium feldspar and calcite that include sprays and microphenocrysts of an olive-green to blue-green clinopyroxene (Fig. 51). Although not analyzed, they are optically identical to nonstoichiometric, Zr-bearing sodic pyroxene identified in the rind of a glimmerite xenolith (Peterson and LeCheminant, 1993). An earlier generation of equant clinopyroxene phenocrysts (?diopside) is entirely replaced by calcite in this sample. Other, more altered samples (particularly PHA-89-K8) appear to have had a similar groundmass assemblage.

Spinel

Magnetite mostly crystallized late in the lamprophyre, and occurs mainly as tiny (≤2 μm) microphenocrysts. These have very low Ti (Us_{0-25}-Ma_{75-99}). Larger (approx. 5 μm), rounded grains occur as inclusions in clinopyroxene. High-chromium spinel ($Cr_2O_3 \geq 55\%$), with compositions typical of macrocrysts in lamproite and Group II kimberlite (Fig. 52), and some diamond inclusions, occurs as dispersed euhedra in some phlogopite grains. They are fairly abundant in the Outlet Bay breccia, enclosed within lithic lapilli of the juvenile phlogopite-rich lamprophyre.

Feldspar and leucite

Alkali feldspar occurs in the groundmass of all samples and as phenocrysts in many felsic rocks. Groundmass potassium feldspar in the lamprophyre is rich in Ba and Fe, particularly in the cores (LeCheminant et al., 1987). Potassium feldspar and albite form void-filling masses and pseudomorphs in many samples.

Table 4. Electron-microprobe analysis of chromite and magnetite phenocrysts from flows and dykes of the Christopher Island Formation, Dubawnt Lake area.

	Chromite							Magnetite						
Grain	**1**	**1**	**1**	**2**	**2**	**3**	**3**	**4**	**5**	**6**	**7**	**8**	**9**	**10**
SiO_2	0.13	0.13	0.11	0.14	0.13	0.17	0.18	0.17	0.12	0.21	0.19	0.04	0.30	0.81
TiO_2	0.24	0.24	0.26	0.22	0.25	0.23	0.23	0.23	6.69	5.05	4.06	3.90	1.47	0.18
Al_2O_3	6.08	5.96	5.77	5.91	5.61	7.37	6.87	5.49	3.90	0.05	0.03	1.61	0.04	0.17
Cr_2O_3	63.38	63.37	61.21	61.59	62.28	56.77	57.31	54.93	0.03	0.03	0.04	0.05	0.04	0.04
FeO	12.11	12.50	17.09	16.37	17.07	23.03	23.06	28.87	77.85	85.31	87.06	82.57	89.69	89.72
MnO	0.21	0.19	0.33	0.29	0.41	1.80	1.68	3.74	0.34	0.02	0.03	0.35	0.02	0.00
MgO	16.25	16.17	12.91	13.35	12.81	8.68	8.15	0.98	2.04	0.07	0.07	2.03	0.02	0.36
CaO	0.01	0.01	0.01	0.04	0.04	0.08	0.05	0.05	0.04	0.15	0.15	0.08	0.06	0.10
V_2O_3	0.00	0.00	0.00	0.02	0.01	0.01	0.04	0.03	0.11	0.05	0.06	0.04	0.05	0.04
NiO	0.32	0.33	0.27	0.22	0.19	0.18	0.17	0.14	0.10	0.06	0.08	0.09	0.10	0.07
ZnO	0.09	0.04	0.11	0.07	0.07	0.11	0.17	2.73	0.00	0.00	0.00	0.00	0.00	0.00
Total	98.82	98.94	98.07	98.22	98.87	98.43	97.91	97.36	91.22	91.00	91.77	90.76	91.79	91.49
$MgCr_2O_4$	0.648	0.645	0.529	0.545	0.528	0.345	0.334	0.048	0.000	0.000	0.000	0.000	0.000	0.000
$MgAl_2O_4$	0.093	0.090	0.074	0.078	0.071	0.067	0.060	0.007	0.011	0.000	0.000	0.005	0.000	0.000
$FeCr_2O_4$	0.171	0.174	0.287	0.272	0.298	0.426	0.454	0.761	0.002	0.001	0.002	0.001	0.001	0.001
$FeAl_2O_4$	0.024	0.024	0.040	0.039	0.040	0.082	0.081	0.113	0.094	0.001	0.001	0.036	0.001	0.004
$MgFe_2O_4$	0.051	0.052	0.045	0.044	0.040	0.035	0.030	0.004	0.087	0.011	0.011	0.105	0.007	0.027
Fe_3O_4	0.013	0.014	0.024	0.022	0.023	0.044	0.041	0.066	0.768	0.964	0.972	0.840	0.989	0.967
Mg_2TiO_4	0.002	0.002	0.002	0.002	0.002	0.001	0.001	0.000	0.012	0.001	0.001	0.007	0.000	0.000
Fe_2TiO_4	0.001	0.001	0.001	0.001	0.001	0.002	0.002	0.003	0.103	0.086	0.066	0.056	0.022	0.003

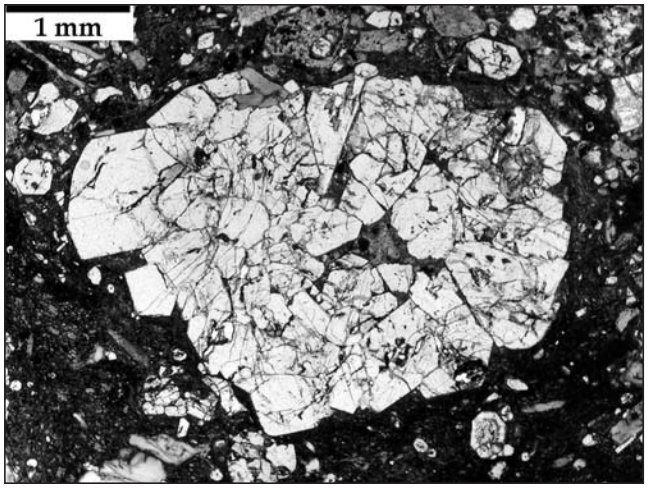

Figure 50. *Pyroxenite xenolith in a phlogopite-diopside lamprophyre clast from the Outlet Bay breccia (sample PHA-91-150).*

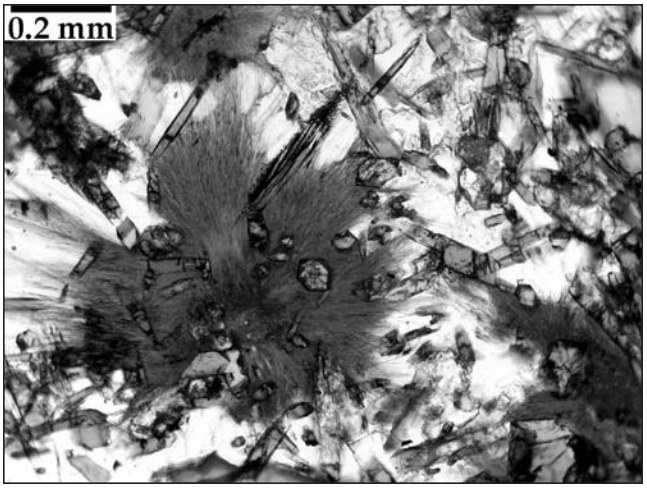

Figure 51. *Clinopyroxene microphenocrysts in poikilitic potassium feldspar of a phlogopite-clinopyroxene lamprophyre dyke (sample PHA-89-K152). The pyroxene has strong olive-green–blue-green pleochroism.*

Feldspar phenocrysts in relatively felsic rocks, and microphenocrysts in lamprophyre, are elongated and display Carlsbad twinning typical of sanidine (e.g. Fig. 53a). In relatively mafic samples, the feldspar phenocrysts are equant and typically altered. Twinning is difficult to discern but, where present, is crosshatched, typical of anorthoclase. Resorbed anorthoclase phenocrysts are also present in some samples of unit PBCva.

Phenocrystic plagioclase is a very uncommon constituent of the Christopher Island Formation. Feldspar porphyry may contain a small amount of low-An plagioclase as phenocrysts or inclusions in sanidine (Fig. 53b). An exception is some samples of the lower felsic unit PBCvf that contain partially melted tonalite xenoliths (Fig. 53c, 54). The groundmass of these flows is rich in microphenocrysts of plagioclase that, judging from their swallowtail morphology, grew rapidly in response to sudden saturation resulting from mixing with melted tonalite.

At least four occurrences of probable leucite, now pseudomorphed by quartz and feldspar, were noted in the Dubawnt Lake area. A medium-grained rock, consisting of olivine pseudomorphs, clinopyroxene, and phlogopite, contains rounded masses (≤2 mm) of interlocking potassium feldspar crystals with overgrowths of albite (Fig. 55); these are interpreted as former leucite phenocrysts. Euhedral microphenocrysts with an icositetrahedral habit, replaced by quartz and albite, are present in some samples of unit PBCva (upper felsic flows; Fig. 53d). These commonly contain the symmetry-controlled, spherical melt inclusions that are characteristic of leucite. The presence of leucite does not necessarily imply an unusual composition, but only that some crystallization occurred at low pressure before eruption.

Minor phases

Titanite never occurs as phenocrysts, but is commonly present as brownish, irregular grains in the groundmass. Secondary titanite recrystallized in lamprophyres adjacent to Nueltin

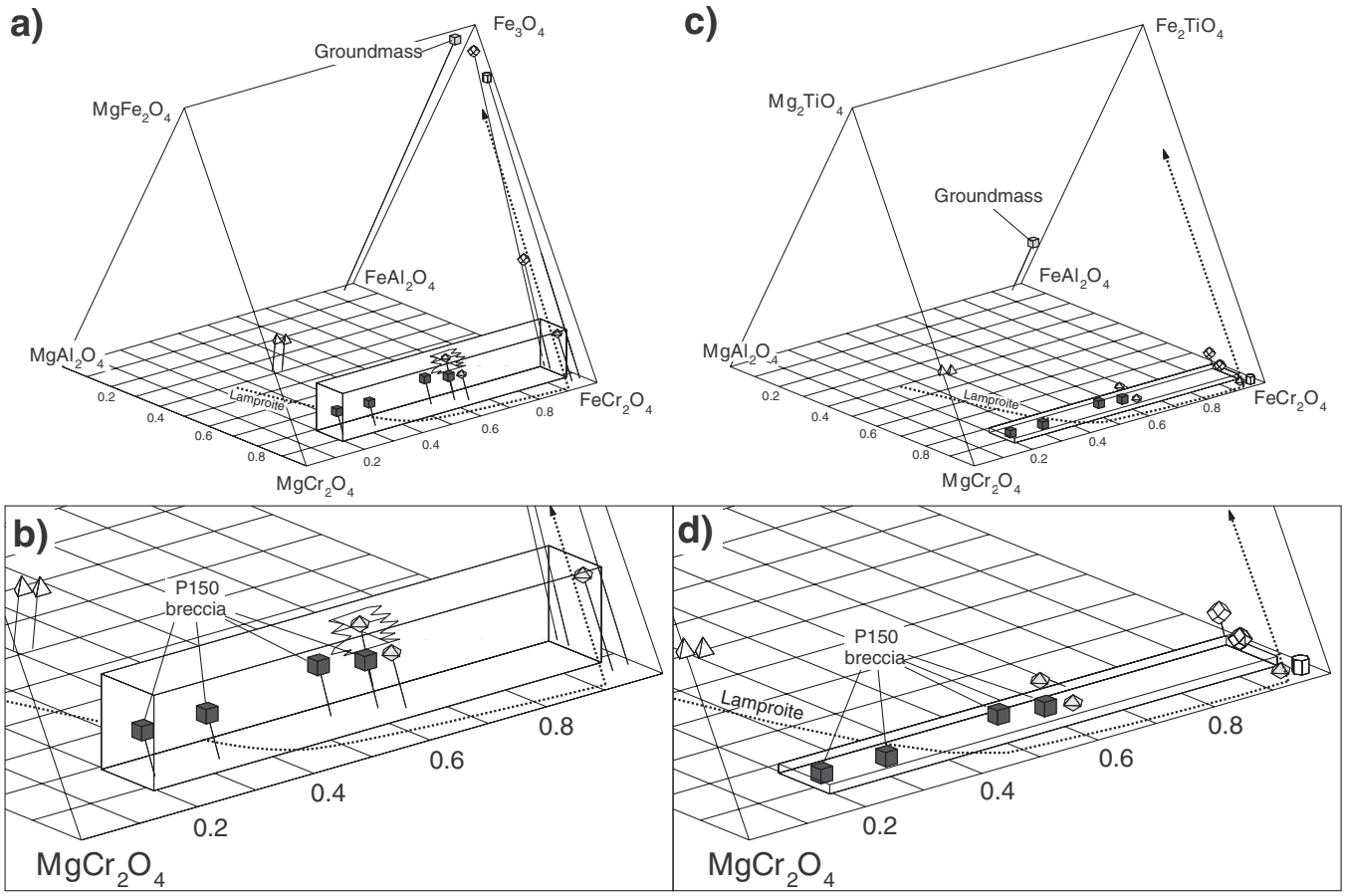

Figure 52. *Spinel prism plots: a) and b) oxidized prism; c) and d) reduced prism. The rectangular box encompasses the range of chromite compositions documented as diamond inclusions. The analyses labelled 'P150 breccia' are of magnesiochromite inclusions in phlogopite from the Outlet Bay breccia. Other analyses near the diamond inclusion box are of chromite from glimmerite xenoliths in the Christopher Island Formation (Peterson and LeCheminant, 1993). The groundmass analysis is from a phlogopite-clinopyroxene lamprophyre clast in the Outlet Bay breccia. The trend line labelled 'lamproite' represents phenocrysts in lamproite (Mitchell and Bergman, 1991).*

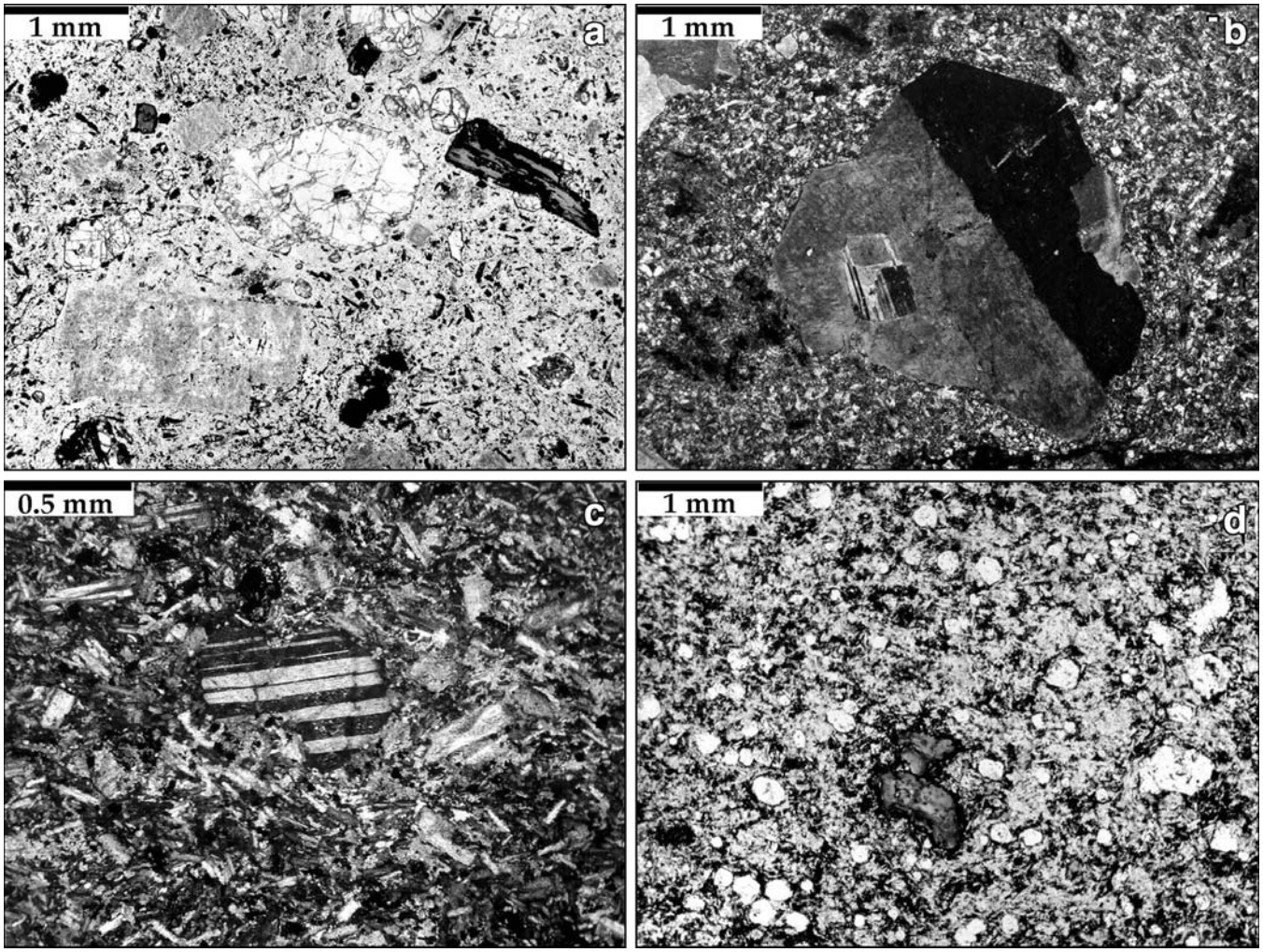

Figure 53. *Feldspar- and leucite-bearing rocks of the Christopher Island Formation: a) unit PBCvf lava with sanidine, clinopyroxene, olivine, and phlogopite (sample PHA-89-231), Kamilukuak basin; b) sanidine porphyry dyke (sample PHA-91-Q33) under crossed polars, Outlet Bay; c) unit PBCvf lamprophyre lava contaminated by melted tonalite xenoliths, with abundant groundmass plagioclase (sample PHA-89-84) under crossed polars, western Dubawnt Lake; large rounded plagioclase in the centre is a xenocryst from the tonalite; d) unit PBCva leucitite with a resorbed phenocryst of phlogopite (sample PHA-89-LBIF), Lost Boat island.*

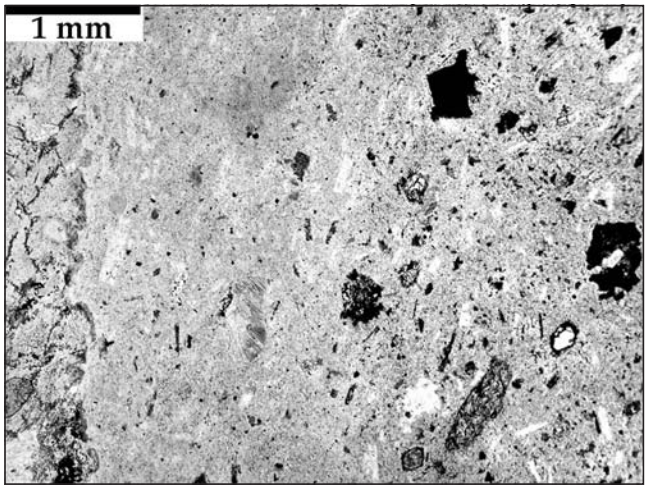

Figure 54. *Melt zone between a tonalite xenolith on the left and a lamprophyre with oxidized and resorbed phenocrysts of phlogopite and clinopyroxene on the right (sample PHA-89-84), west Dubawnt Lake. The melt layer is quenched to nearly pure plagioclase.*

granite plutons. Colourless rutile occurs in the groundmass of mafic lamprophyre flows and dykes. Both titanite and rutile are probably secondary after primary Ti-rich groundmass phases, such as phlogopite or alkali amphibole.

Calcite is a very common constituent of the lamprophyre and can be prominent in mafic rocks. It occurs as void-filling patches, as a replacement product of clinopyroxene phenocrysts and groundmass, and as inclusions in phlogopite. In some lamprophyre flows and dykes, it partially replaces clinopyroxene phenocrysts in optically continuous lobate masses that do not extend beyond the crystal boundaries. These may have developed in a plutonic environment, and were subsequently entrained by another magma. Ribbon-like calcite inclusions in phlogopite occur within the cleavage (Fig. 56) and are commonly boudinaged or folded with the phlogopite grain, especially in glimmerite xenoliths (Peterson and LeCheminant, 1993). This calcite is likely a product of the replacement of clinopyroxene inclusions.

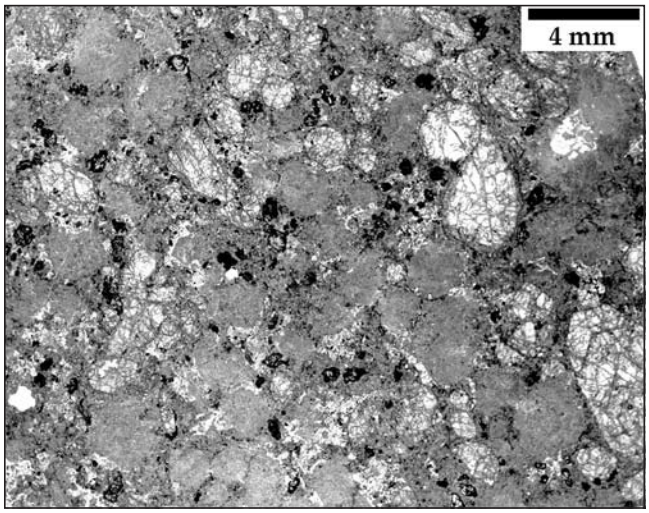

Figure 55. *Olivine-clinopyroxene-leucite cumulate from a (?)dyke (sample PHA-91-137), northern Outlet Bay. The leucite has been replaced by round, grey masses of potassium feldspar with albite rims.*

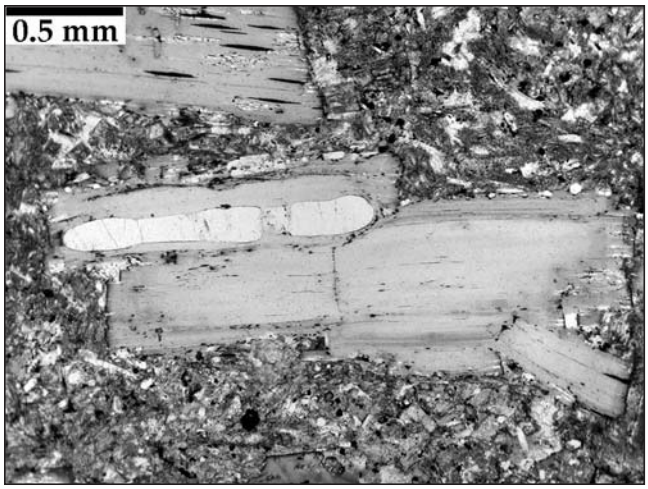

Figure 56. *Inclusions of calcite in a phlogopite phenocryst from a lamprophyre dyke (sample PHA-89-K146), Kamilukuak basin.*

Apatite, a prominent phenocryst phase in most samples of the Christopher Island Formation, can occur as inclusions in olivine, demonstrating that it was an early-crystallizing phase. In some samples that are enriched in highly incompatible elements, such as PHA-89-K8, it forms unusually large phenocrysts and approaches rock-forming proportions (Fig. 57).

An unidentified, dark brown, elongated microphenocryst phase that optically resembles aenigmatite is present in sample PHA-91-LBIF, which is enriched in highly incompatible elements. A partial microprobe analysis (Table 5) shows that it is a Ti-rich, Al-poor silicate mineral with substantial Na+K and 6% ZnO.

Epidote is widespread in the Christopher Island Formation. Allanite occurs as bright yellow to yellow-brown blades within the cleavage planes of some phlogopite crystals, which also contain calcite inclusions. Allanite also occurs in the groundmass of mafic lamprophyre. Secondary epidote, which is usually weakly pleochroic, replaces clinopyroxene and patches of groundmass, particularly in samples close to younger granite plutons.

Mantle xenocrysts

Two rounded grains of Mg- and Al-rich spinel, one with an attached phlogopite grain, were found in thin sections of the Outlet Bay breccia. They are identical to spinel in mantle lherzolite. Numerous mantle xenocrysts from this breccia were identified by drill sampling, heavy-mineral separation, and NaOH fusion (Chisholm, 1993). These include G9 (lherzolitic) and G10 (harzburgitic) garnets, magnesiochromite, magnesio-ilmenite, and chrome diopside.

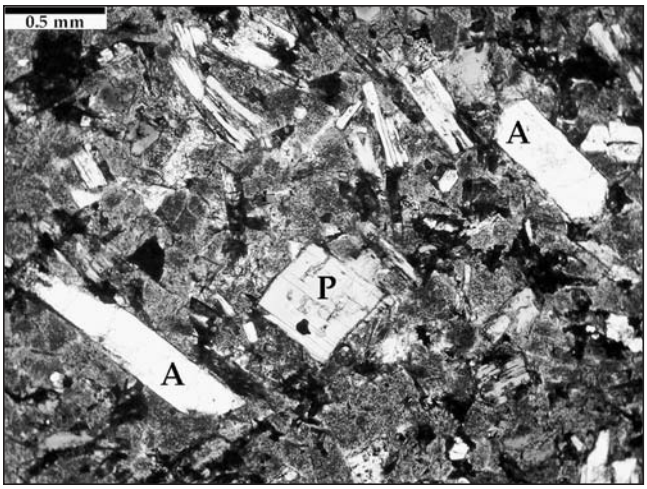

Figure 57. *Apatite (A) and phlogopite (P) phenocrysts in a lamprophyre dyke (sample PHA-89-K8), central Dubawnt Lake. The matrix consists of blocky, altered potassium feldspar phenocrysts; the interstitial minerals are altered but appear similar to those of sample PHA-89-K152 (Fig. 51).*

Table 5. Electron-microprobe analysis of groundmass, phenocrysts, and inclusions of minor phases from flows and dykes of the Christopher Island Formation, Dubawnt Lake area.

PHA-	89-16	89-16	89-81	89-82	89-82	89-77A	89-77A	91-150	91-150	91-137	91-137	P89/81	91-LBIF	91-LBIF
Sample type	**gmass**	**gmass**	**pheno**	**pheno**	**pheno**	**pheno**	**pheno**	**pheno**	**inclsn**	**pheno**	**pheno**	**Fe-Ln**	**aen**	**aen**
SiO_2	54.03	53.47	53.40	53.31	53.38	54.10	53.72	54.36	55.30	54.39	53.40	36.03	70.393	70.74
TiO_2	0.14	0.43	0.28	0.18	0.15	0.15	0.22	0.15	0.18	0.24	0.39	0.08	3.917	3.886
Al_2O_3	0.13	0.88	1.21	0.75	0.85	0.54	0.69	0.94	0.64	1.38	2.79	2.81	4.578	4.448
Cr_2O_3	0.01	0.03	0.22	0.10	0.09	0.00	0	0.02	0.06	0.09	0.08	0.00	0	0
FeO	8.40	10.45	5.26	5.37	4.73	5.38	5.50	5.39	4.26	5.01	5.15	24.58	0.169	0.234
MnO	0.66	0.62	0.14	0.22	0.16	0.42	0.35	0.18	0.13	0.14	0.15	0.47	0.036	0
MgO	12.22	10.68	15.83	16.36	17.05	15.50	15.17	16.82	18.89	16.29	15.08	0.00	0.008	0.038
CaO	20.43	19.01	22.78	22.27	22.18	22.41	22.46	21.93	21.24	22.80	22.32	34.09	0.042	0.022
Na_2O	2.41	3.12	0.47	0.52	0.48	0.73	0.74	0.34	0.38	0.53	0.77	0.00	3.641	2.467
K_2O	0.05	0.07	0.00	0.00	0.00	0.03	0.04	0.00	0.00	0.00	0.00	0.00	6.028	4.712
ZnO	NA	NA	NA	NA	NA	NA	NA	NA	NA	NA	NA	0.00	5.947	5.959
Total	98.48	98.76	99.57	99.08	99.07	99.26	98.89	100.13	101.08	100.87	100.13	98.06	88.812	86.547

Abbreviations: gmass, groundmass; pheno, phenocryst; inclsn, inclusion; Fe-Ln, Fe-larnite; aen, unknown dark red-brown microphenocryst that resembles aenigmatite

Geochemistry

A suite of samples was selected to cover the observed petrographic variety in dykes, and the complete stratigraphic range of lavas. All samples were selected for optimum freshness and weathered surfaces were trimmed by hammer, but a small degree of alteration is present in most samples. The principal effects of the net metamorphism and alteration were to reduce K/Na and Rb/Sr, and increase Si, Al, and Ca.

Whole-rock elemental analyses are given in Appendix 1. Major elements and Rb, Sr, Ba, Nb, Y, and Zr were analyzed by X-ray fluorescence (XRF) at the Geological Survey of Canada between 1988 and 1992. Detection limits for these trace elements are 20 to 30 ppm, with estimated errors of ±10%. Analysis of Nb, Pb, Th, and U was done by inductively coupled plasma–optical emission spectroscopy (ICP-OES). All rare-earth element (REE) analyses before 1991 were by ICP and have relative errors of ±5%; REE after 1991 were analyzed by inductively coupled plasma–mass spectrometry (ICP-MS). Samples selected for isotopic analysis were also analyzed for Rb, Sr, Sm, and Nd by isotope dilution (Table 6).

Geochemical characteristics of the Christopher Island Formation

If mafic volcanic and dyke rocks are defined as having greater than 5% MgO and Mg/(Mg+Fe^t) ³ 0.6 (n = 39), then all lamprophyre is mafic (Appendix 1). The remaining rocks are divided into high-SiO_2, low-MgO flows that are all from the lower felsic unit PBCvf (n = 7), and flows with intermediate SiO_2 and exceptional enrichments in incompatible elements, all from the upper felsic unit PBCva (n = 7). The averages of each group are given in Table 7. Selected elements are plotted against stratigraphic position for samples of lava flows in Figure 58, and selected elements are plotted against Mg# in Figure 59.

The mafic rocks are ultrapotassic (average wt. % K_2O/Na_2O = 4.3, excluding values of 10 or more that may reflect phlogopite accumulation), and one in five samples is peralkaline (average molecular [Na+K]/Al = 0.88). In major-element discriminant diagrams (e.g. Foley et al., 1987; Rock, 1991), most of the mafic rocks plot in or near the lamproite field, mainly due to their high K_2O/Na_2O and low CaO values, but some extend into fields characteristic of minette (Peterson, 1994). The average Christopher Island Formation lamprophyre differs from the average lamproite of Bergman (1987) in having higher contents of Al_2O_3 (9.1% in lamproite) and lower contents of TiO_2 (3.0% in lamproite). For all major elements except TiO_2 and P_2O_5, the average Christopher Island Formation lamprophyre is transitional between average lamproite and minette. The Christopher Island Formation is depleted in all high-field-strength elements (HFSE), particularly Ti, relative to both lamproite and minette.

The lower felsic unit (PBCvf) samples, including one dyke of similar petrography, are much higher in SiO_2, Al_2O_3, and Na_2O, and lower in MgO, CaO, Sr, Ni, and Cr than the lamprophyre. With average K_2O/Na_2O = 2.1, they do not fit any definition of ultrapotassic rocks. In the lamprophyre discriminant diagram of Rock (1991), samples of unit PBCvf mainly plot in the calc-alkaline lamprophyre field, which includes true minette as well as some hornblende-bearing lamprophyre.

All samples of unit PBCva are enriched in HFSE and large-ion lithophile elements (LILE) relative to both the lower felsic flows and average lamprophyre, and they are slightly more rich in SiO_2 than the lamprophyre. Two samples from the upper portion of the Lost Boat island section (PHA-89-16 and PHA-91-LBIF) contain 1000 ppm Zr and 200 ppm Th. This extreme enrichment in HFSE is typical of

Table 6. Isotopic analysis of samples selected for radiometric dating, Dubawnt Lake area.

Sample	Map unit	Rb	Sr	$^{87}Rb/^{86}Sr$	$^{87}Sr/^{86}Sr$	$Sr_{(T)}$	$T_{Sr,DM}$	ε_{Sr}	Sm	Nd	$^{147}Sm/^{143}Nd$	$^{143}Nd/^{144}Nd$	$Nd_{(T)}$	$T_{Nd, DM}$	ε_{Nd}
Snow River gneiss (T=2.7 Ga)															
PHA94-73	ARn	165	264	1.74819	0.77581	0.7075	2953	88	5.2	34.5	0.08928	0.51083	0.50924	2825	2.1
PHA94-98	ARo	14	516	0.07414	0.70590	0.7030	----	24	5.5	32.4	0.10194	0.50904	0.50925	2830	2.2
Snow Island suite (T=2.6 Ga)															
PHA94-77	ASgd	147	233	1.70905	0.76967	0.7054	2767	56	5.4	33.7	0.09603	0.51097	0.50932	2807	1.2
PHA94-125	ASm	395	645	1.71380	0.75415	0.6897	2117	-167	2.9	15.9	0.10823	0.51112	0.50926	2918	0.0
PHA94-126a	ASgd	83	262	0.88890	0.73682	0.7034	2768	28	7.7	45.5	0.10091	0.51109	0.50936	2762	2.0
Hudson granite (T=1.84 Ga)															
PHA94-108	Pg	240	366	1.84006	0.75340	0.7047	1933	34	8.4	61.7	0.08075	0.51070	0.50973	2788	-10.4
Christopher Island Formation (T=1.83 Ga)															
PHA88-214B	PBCva	121	1022	0.34360	0.71389	0.7048	2489	35	16	98	0.09010	0.51101	0.50992	2630	-6.8
PHA88-500C	PBCva	338	470	2.09400	0.75678	0.7014	1807	-13	19	160	0.08490	0.51094	0.50991	2601	-6.8
PHA89-111	PBCvm	640	1185	1.56800	0.74557	0.7041	1921	25	20	130	0.09850	0.51106	0.50987	2747	-7.6
PHA89-16	PBCva	385	1787	0.62380	0.72285	0.7064	2348	57			0.09510	0.51099	0.50984	2756	-8.2
PHA89-231	PBCvf	107	538	0.57510	0.71969	0.7045	2139	31			0.10500	0.51115	0.50988	2792	-7.5
PHA89-27A	PBCvm	683	815	2.42900	0.77375	0.7095	2048	103	32	170	0.11760	0.51124	0.50982	3011	-8.7
PHA89-27B	PBCvm	378	624	1.76000	0.75199	0.7055	1966	45	28	170	0.10830	0.51119	0.50988	2815	-7.4
PHA89-27B (repeat)	PBCvm	395	645	1.71380	0.75415	0.7089	2112	93	27.5	160.8	0.10198	0.51113	0.50989	2746	-7.2
PHA89-81	PBCvf	401	334	3.50700	0.79233	0.6996	1783	-38	7	50	0.10070	0.51108	0.50986	2777	-7.8
PHA89-82	PBCvf	386	415	2.70800	0.77298	0.7014	1813	-13	9.5	69	0.10670	0.51119	0.50990	2780	-7.1
PHA89-K8	dyke	232	2676	0.25120	0.71070	0.7041	2545	24	26	140	0.10610	0.51122	0.50994	2719	-6.3
PHA89-Q1A	dyke	131	625	0.58447	0.72045	0.7050	2203	38	2.7	12.0	0.13466	0.51158	0.50996	3000	-6.0
PHA91-150F	OBB	157	1132	0.38818	0.71778	0.7075	2997	74	5.8	32.1	0.10778	0.51130	0.51000	2642	-5.1
PHA91-150M	OBB	278	1150	0.68162	0.72745	0.7094	2649	101	5.1	28.2	0.10734	0.51117	0.50987	2823	-7.7
PHA91-LB1F	PBCva	291	1039	0.78366	0.72938	0.7087	2456	90	24.6	126.7	0.11565	0.51109	0.50969	3174	-11.1
PHA91-Q37	dyke	285	337	2.57391	0.78558	0.7176	2255	217	3.9	22.6	0.10161	0.51102	0.50979	2882	-9.3
Nueltin granite (T=1.75 Ga)															
PHA94-124b	PNg	281	53	15.18550	1.10089	0.7188	1824	233	6.11	39.21	0.092968	0.510981	0.50991	2721	-9.1

Abbreviations: DM, depleted mantle; OBB, clast from Outlet Bay breccia

Elemental concentrations in ppm

$Sr_{(T)}$, $Nd_{(T)}$ are calculated initial ratios

Depleted mantle assumed present-day ratios: $^{143}Nd/^{144}Nd$ =0.513151, $^{147}Sm/^{143}Nd$=0.2138

lamproite, and both samples contain abundant leucite, which is also typical for evolved lamproite (Mitchell and Bergman, 1991). They have relatively high Al_2O_3 contents, however, that are characteristic of minette.

The overall trace-element pattern for all samples conforms closely to that considered typical of some subduction-zone magmas. Trace-element plots normalized to mid-oceanic ridge basalt (MORB) in Figure 60 have negative anomalies in Nb and Ti, and strong positive anomalies in K, Rb, Ba, and Th. The high average contents of Ba (4000 ppm) and particularly Rb (327 ppm) in the lamprophyre are typical of lamproite but less so of minette. Figure 61 shows that light rare-earth elements (LREE) are strongly enriched over heavy rare-earth elements (HREE; Ce/Yb = 67–200). Several samples have distinct negative Eu anomalies, but no sample has a positive Eu anomaly.

Magma evolution

Interelement correlations among Christopher Island Formation rocks are typically very weak. This is not surprising, since the samples come from many different eruptive centres, and most have undergone some alteration. Within units PBCvf and PBCvm, K_2O correlates positively with Mg# and Al_2O_3, SiO_2, and Na_2O correlate negatively (Fig. 59). There is a positive correlation of Ni, Cr, K, and Rb with Mg# that is consistent with fractional crystallization of olivine and phlogopite, and the depletion in Ba in all siliceous rocks relative to lamprophyre is consistent with fractionation of potassium feldspar.

The lower felsic (unit PBCvf) samples are depleted in P and REE relative to lamprophyre, consistent with fractionation of apatite, which formed phenocrysts early in the crystallization sequence. Partially melted crustal xenoliths are common in unit PBCvf, and contamination of magmas by crustal rocks is partly responsible for the spectrum of compositions observed

Table 7. Average compositions of volcanic units in the Christopher Island Formation.

Unit	PBCvf	PBCva	PBCvm
n	7	7	39
SiO_2	63.39	54.83	53.23
TiO_2	0.47	1.24	0.79
Al_2O_3	13.56	13.53	11.62
FeO_t	4.04	8.86	6.76
MnO	0.06	0.12	0.1
MgO	3.14	5.64	9.18
CaO	3.31	3.83	5.19
Na_2O	2.96	2.43	1.75
K_2O	6.07	5.76	6.67
P_2O_5	0.49	0.88	0.75
H_2O	1.07	1.67	1.73
CO_2	0.37	0.04	0.85
Total	98.93	98.84	98.63
Rb	322	222	327
Be	5.1	9.4	7.3
Sr	619	1007	1363
Ba	2347	3369	4039
Y	16	46	28
Zr	295	533	320
V	55	126	117
Nb	17	36	26
Cr	116	115	301
Co	19	37	41
Ni	42	63	144
Cu	43	46	31
Zn	44	126	84
La	68	124	97
Ce	130	237	206
Nd	58	119	105
Sm	8.3	18.1	17
Eu	2.2	4.2	3.9
Gd	6	12.2	11.7
Dy	3.6	6.8	6.2
Ho	0.5	1.7	0.9
Er	1.3	3.4	2
Tm	0.23	0.58	0.32
Yb	1.42	1.68	1.78
Th	45	78.6	34.1
U	22.3	8.7	6.2
Pb	44	44	35
ε_{Sr}	68	42	51
ε_{Nd}	-8.2 (n = 3)	-8.2 (n = 4)	-7.7 (n = 8)
Oxide concentrations in per cent; trace-element concentrations in ppm			

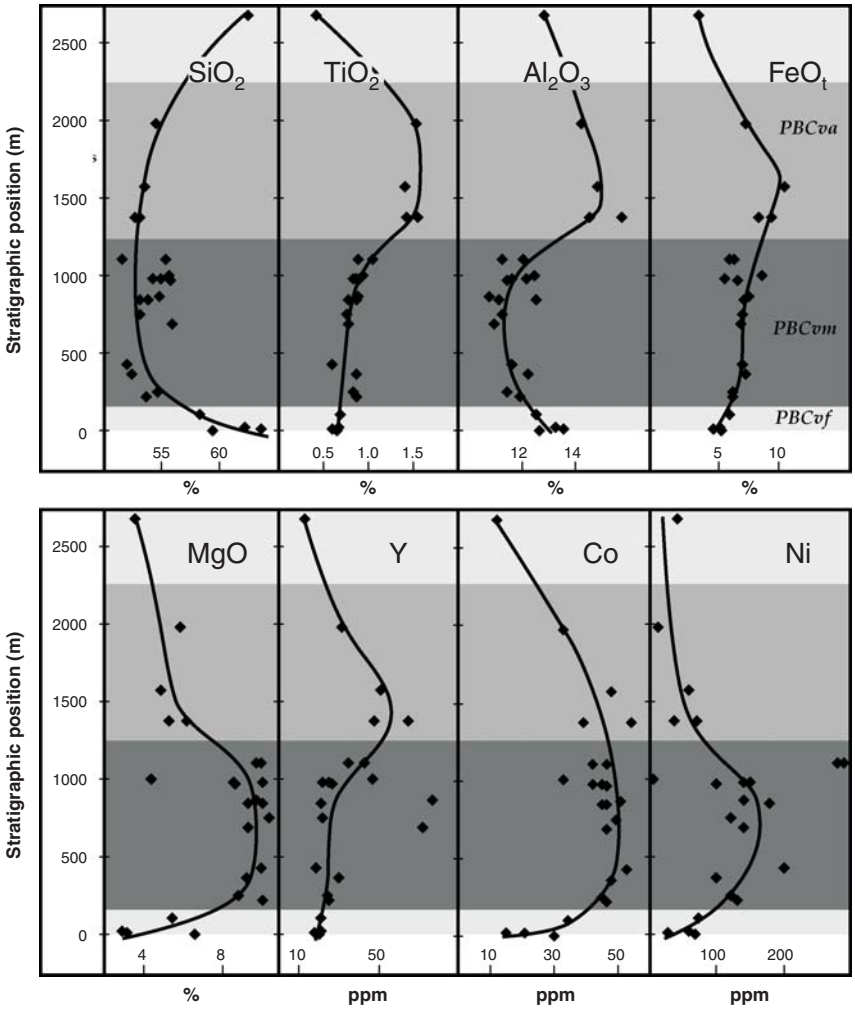

Figure 58. *Composition versus stratigraphic position for Christopher Island Formation lava samples, using the composite section of Figure 9 as a model. Petrographic types: PBCvf, light grey; PBCvm, dark grey; PBCva, medium grey. The bottom portion, where lower felsic minette flows are on the unconformity, is obtained from the Slow River section (NTS 65 N/3, UTM 400700E, 6993000N). The uppermost sample is of a flow within the upper PBCs conglomeratic unit of Lost Boat island, and has a composition like that of the lower felsic lavas.*

in high-SiO_2 rocks of the Christopher Island Formation. Identifying specific crustal contaminants is impossible because the Christopher Island Formation itself has incompatible trace-element patterns and concentrations similar to those of average upper crust.

The unit PBCva samples that are enriched in highly incompatible elements must have undergone some crystallization at low pressure, since some samples contain abundant leucite. The magmas may have formed by fractionation of a primary magma similar to mafic lamproite, which ponded within the upper crust. Although the high Ti contents typical of the unit PBCva flows are not commonly recorded in the mafic lamprophyres, there is one notable exception. Dyke sample PHA-89-K8 has anomalously high Ti and V (Appendix 1), and is the most plausible sample of parental magma for the unit PBCva flows. This dyke strongly resembles the diamondiferous Akluilâk minette dyke in both composition and petrography (MacRae et al., 1996).

Isotopic composition

Strontium and neodymium isotopic compositions were determined on 12 flows of known stratigraphic position, one dyke (sample PHA-89-K8), two juvenile fragments from the Outlet Bay breccia, and one conglomerate cobble from the top of the Lost Boat island section. Strontium and neodymium compositions were also determined for selected samples of Snow River gneiss and Archean and Proterozoic granitoid rocks. Analytical methods are given by Thériault (1990).

Strontium and neodymium data are given in Table 7, and epsilon values are plotted in Figure 62. The initial $^{87}Sr/^{86}Sr$ ratios for the Christopher Island Formation show a very wide range; the average value of ε_{Sr} is +15 (relative to bulk Earth), but three samples have $^{87}Sr/^{86}Sr$ ratios less than bulk Earth and some are strongly radiogenic. Cousens (1999) has shown that Rb and Sr are decoupled in lamprophyre (with Rb concentrated in silicate phases and Sr in carbonate), and that primary Sr compositions are probably best preserved in the carbonate fraction. These yield much less variable values of ε_{Sr} that are close to the mean of the data (Fig. 62). For the whole-rock samples, this Rb-Sr separation was mimicked by natural differentiation and alteration processes, resulting in two groups that are distinguished on an Rb-Sr isochron plot (Fig. 63). One group, which includes strongly enriched and less altered samples with high Sr/Rb ratios, yields an isochron age of ca. 2.3 Ga and an initial Sr composition close to that of bulk Earth. The other, which includes less enriched rocks and those collected close to a Nueltin granite pluton, yields an

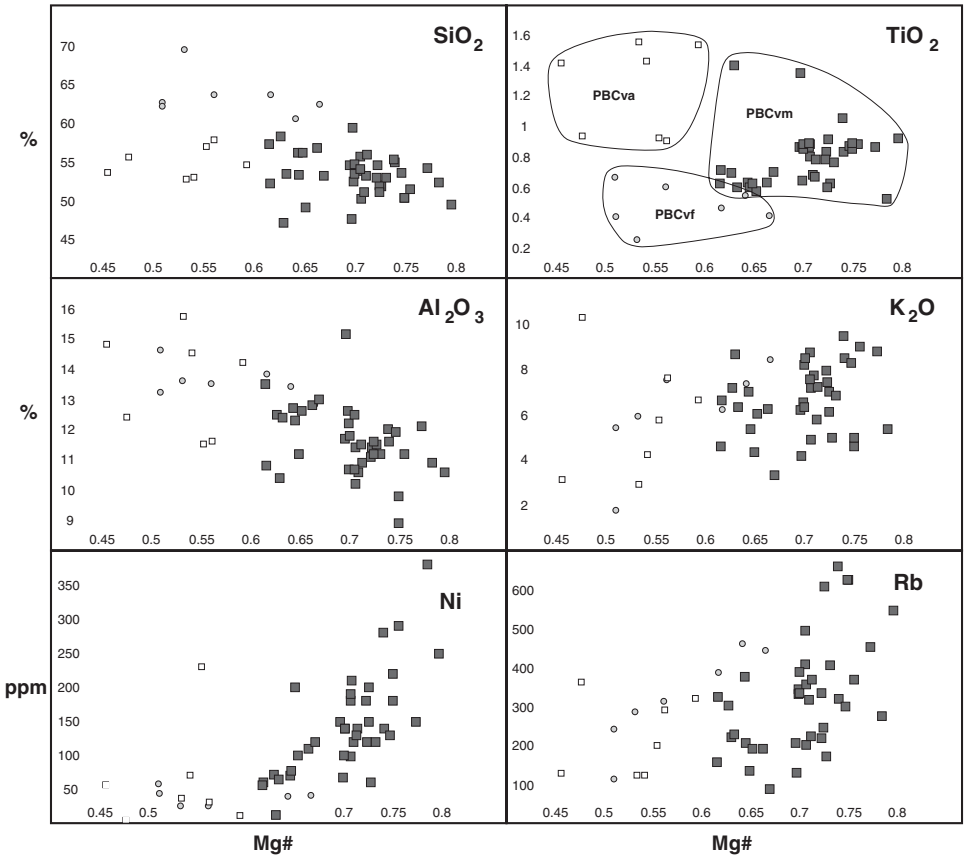

Figure 59. *Selected elements plotted against Mg# (Mg/[Mg+Fe_t]) for all analyses of Christopher Island Formation flows and dykes. Note the exceptional enrichment of unit PBCva samples in TiO_2 (matched by other high-field-strength elements). Symbols: circles, unit PBCvf; open squares, unit PBCva; solid squares, unit PBCvm.*

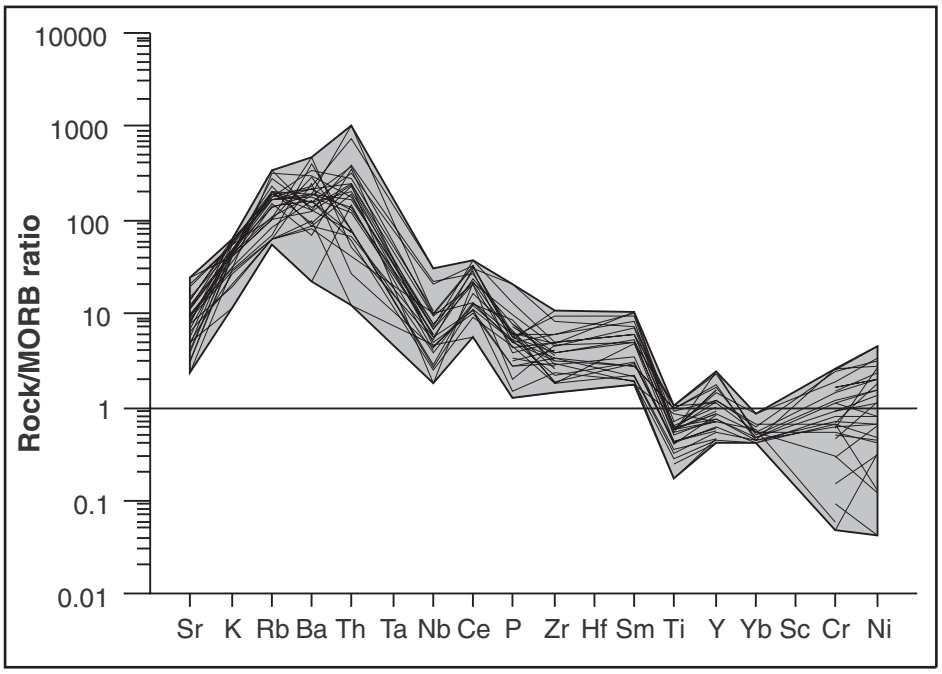

Figure 60. *Trace-element compositions, normalized to mid-oceanic ridge basalt (MORB), for all analyzed samples of the Christopher Island Formation.*

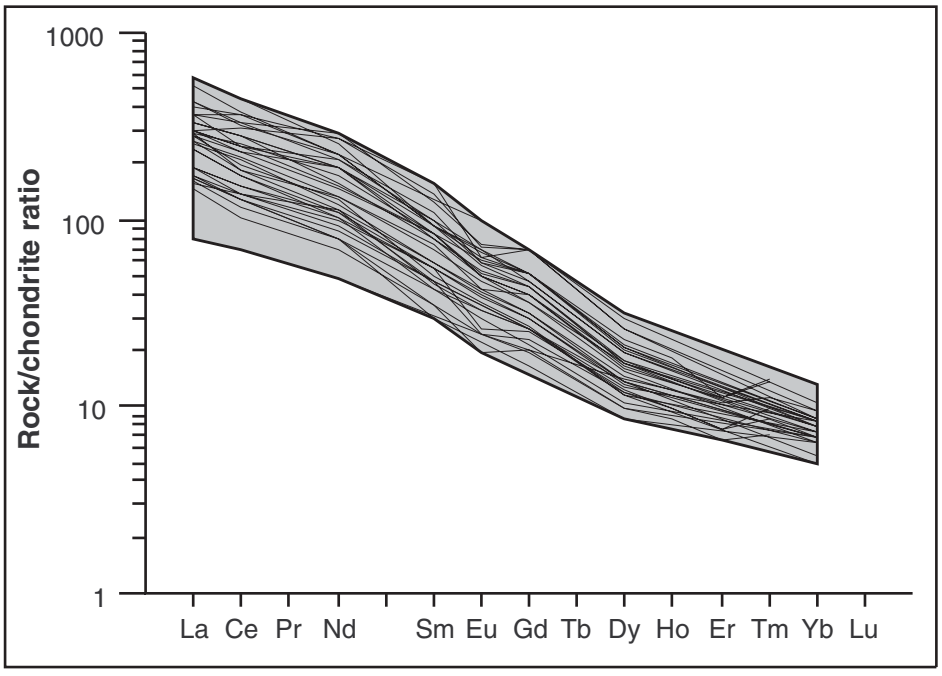

Figure 61. *Rare-earth element compositions, normalized to chondrite, for all analyzed samples of the Christopher Island Formation.*

isochron age of ca. 1.7 Ga, close to the emplacement age of the granite. The older age is in better agreement with depleted mantle Nd model ages and is presumably a more accurate Rb-Sr model age for the source region.

The range in ε_{Nd} values for the Christopher Island Formation is also large (–6 to –11, relative to chondritic uniform reservoir [CHUR]), although the variation is less than that for many other ultrapotassic suites (e.g. Fraser et al., 1985). There is no correlation between Sr and Nd isotopic compositions. As noted elsewhere (Peterson et al., 1994), the Christopher Island Formation has a Nd composition very similar to that of average crust of the western Churchill Province (Thériault et al., 1994). Depleted mantle Nd model ages average about 2.8 Ga. These accord well with the depleted mantle model age of both the Snow River gneiss (assumed to be ca. 2.7 Ga) and the Snow Island granitoid suite (ca. 2.6 Ga), as well as both Proterozoic granitoid suites (units Pg and PNg). The Archean Snow Island suite had a positive ε_{Nd} at the time of emplacement and presumably contained a substantial juvenile component.

Nature and origin of the Christopher Island Formation

The similarity in Nd composition between the Christopher Island Formation, the local Archean crust, and the Proterozoic granitoid rocks is remarkable. It is straightforward to interpret the isotopically enriched Proterozoic granite bodies as crustal melts, but the Christopher Island Formation lamprophyre flows and dykes are clearly mantle derived, since they contain mantle xenocrysts and typically have very high Mg#, Ni, and Cr. The REE content of the Christopher Island Formation is too high to be affected by any reasonable amount of crustal contamination, and there is little difference in Nd composition between mafic and felsic samples (Table 6). Hence, the lamprophyre must have a source component, with a long-term enrichment history, that resembles Archean continental crust. Lead in the lamprophyre is extremely nonradiogenic (Peterson et al., 1994), requiring a source with long-term low U/Pb. The Mg/Fe ratios and Ca contents are, respectively, higher and lower than those of most basaltic rocks, suggesting a second source component with a long-term history of depletion relative to convecting mantle. This component presumably lies in depleted lower crust or lithospheric upper mantle.

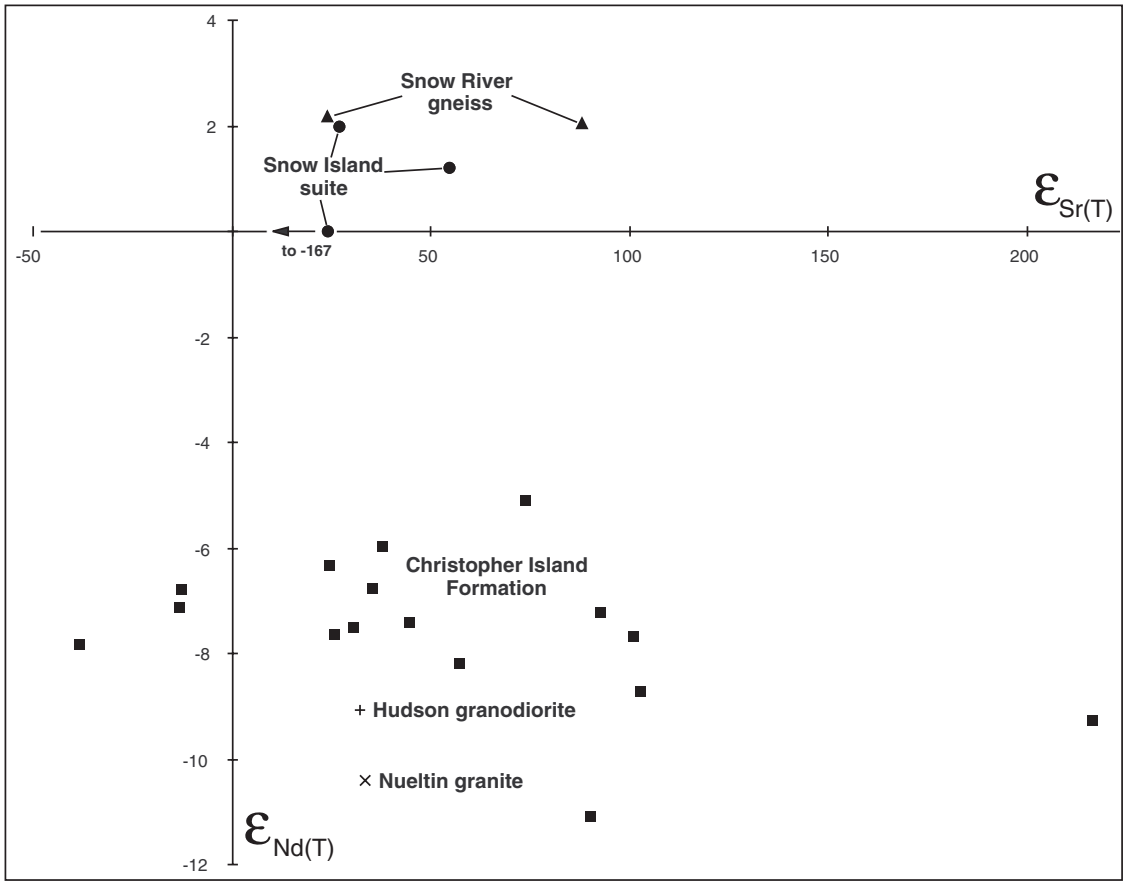

Figure 62. *Strontium-neodymium isotope compositions for samples of Christopher Island Formation and Archean and Proterozoic granitoid rocks. Epsilon values were calculated at the times indicated in Table 7. Strontium compositions were not measured for the Proterozoic granitoid rocks. Average Nd compositions for the Hudson granitoid and Nueltin granitic rocks are from Peterson et al. (2002).*

The isotopic composition of the Christopher Island Formation is very similar to that of lamproite, which typically has strongly enriched Nd, very nonradiogenic Pb, and highly variable Sr (e.g. Fraser et al., 1985). Diamonds are not known to occur in true minette bodies, but the Akluilâk lamprophyre dyke, which is part of the feeder dyke swarm for the Christopher Island Formation (MacRae et al., 1996), has a rich microdiamond content that is strikingly similar in size range and composition to some lamproite bodies, such as the Argyle phreatomagmatic intrusive breccia (Deakin and Boxer, 1989). The conflicting geochemical and mineralogical features of the Christopher Island Formation are difficult to reconcile with the current nomenclature of ultrapotassic rocks.

Detailed comparison of the Christopher Island Formation with other suites of ultrapotassic rocks around the world has been made by petrochemical cluster analysis. The ultrapotassic rocks that most closely resemble the Christopher Island Formation are from suites with characteristics transitional to lamproite, such as relatively high K/Na, Rb, and Zr, but with some minette-like characteristics, such as high Al and low Nb. In decreasing order of similarity, these suites are: sills and dykes of the Gondwana coalfields, India (Paul and Potts, 1981); Cenozoic postorogenic lamproite bodies of southern Spain and northern Italy (Venturelli et al., 1988); postorogenic minette bodies from the Bohemian massif (Nemec, 1988); Eocene anorogenic Sweetgrass hills minette bodies of southern Alberta (Kjarsgaard and Davis, 1994); and minette bodies from the Colorado Plateau (Jones and Smith, 1983). Most ultrapotassic suites associated with late syn- to postorogenic granitoid activity in collisional hinterlands strongly resemble the Christopher Island Formation in composition and mineralogy (e.g. trans-Amazonian ultrapotassic rocks of Brazil; Rosa et al., 2000).

True lamproite is thought to originate in subduction-enriched, metasomatized mantle (Nelson, 1992), and typically erupts through poorly consolidated sedimentary cover lying over continental orogens (Mitchell and Bergman, 1991). There is no consensus regarding its relationship to minette, which is disputed by some (e.g. Mitchell, 1994). Foley et al. (1987) identified transitional rocks, by factor analysis of a database of analyses of potassic rocks. This transitional group is broadly equivalent to the calc-alkaline lamprophyre (i.e. minette) association of Rock (1991). The majority of these minette bodies are associated in time and space with calc-alkaline granitoid rocks that are typically postorogenic, and distinct from the less enriched minette bodies that erupt in many active subduction zones, such as the Mexican Volcanic Belt (Wallace and Carmichael, 1989). A detailed discussion of the

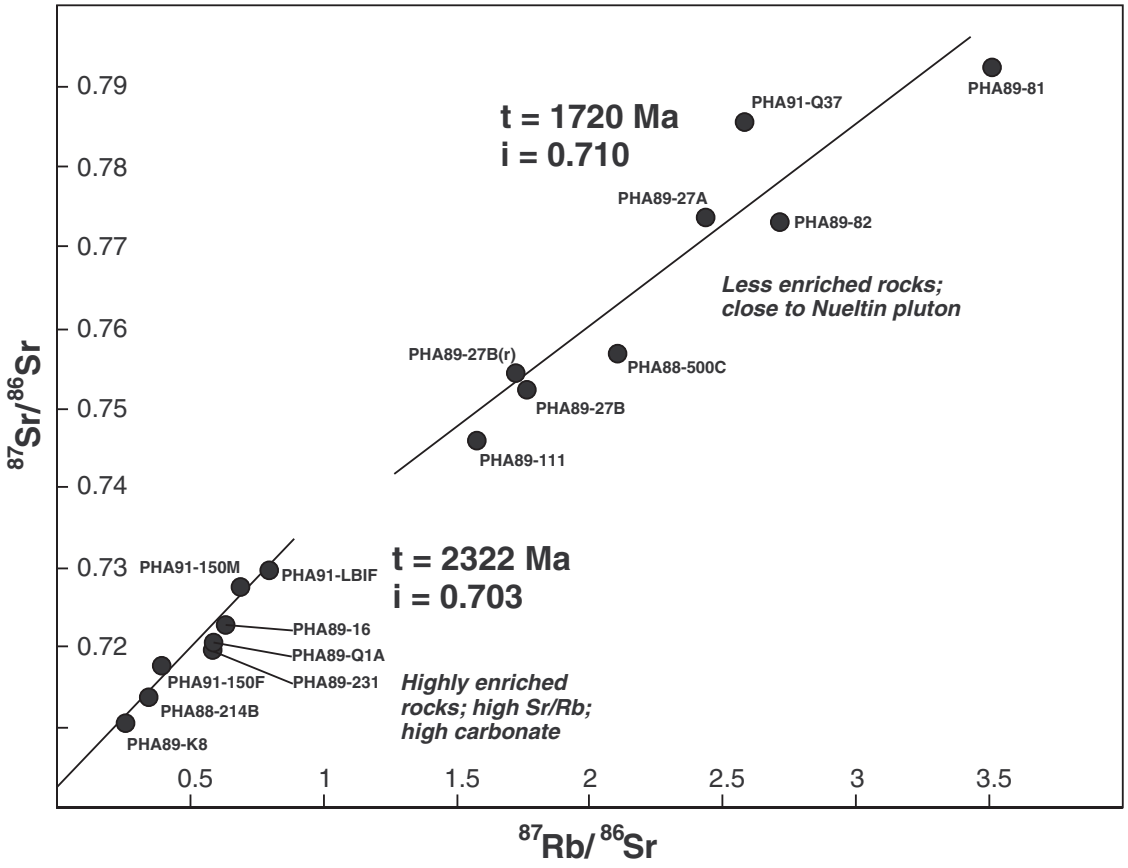

Figure 63. *Rb-Sr isochron plots for Christopher island Formation samples. i=initial Sr ratio, t=isochron age. The samples fall into 2 groups based on the degree of low-grade thermal metamorphism and alteration produced by younger Nueltin granites.*

petrogenesis of the Christopher Island Formation, in the context of postorogenic magmatism in collisional hinterlands, is given by Peterson et al. (2002).

Pitz Formation and Nueltin suite

Petrography

Rhyolite (unit PDWPv) and granite (unit PNg)

The Pitz Formation rhyolite in the study area is invariably altered, with a hematized groundmass. Alkali-feldspar phenocrysts are commonly replaced by clay minerals. Samples are typically dominated by subhedral phenocrysts of quartz with large (≤2 cm) phenocrysts of alkali feldspar that either do not display recognizable twinning or contain a recognizable Carlsbad twin (Fig. 64). In samples from a silicic dome in the Kamilukuak basin (*see* Fig. 26), about 50% of the phenocrysts show crosshatched twinning, characteristic of anorthoclase (Fig. 65). Rhyolite-porphyry dykes cutting the Snow River gneiss have phenocrysts with sanidine twin planes, as well as plagioclase inclusions in the sanidine. Feldspar minerals in granite (unit PNg; Fig. 66) are similar to those in the porphyry but display complex exsolution textures, and the granite is clearly hypersolvus. Some feldspar crystals have patchy cores that show albite twinning with rims of coarsely perthitic alkali feldspar, consistent with symmetry transformation in cooling anorthoclase crystals. These features suggest that the crystallization sequence in the silicic Pitz magmas was quartz → quartz+anorthoclase → quartz+plagioclase → quartz+sanidine+plagioclase.

Mafic minerals do not form phenocrysts in the rhyolite, but late biotite (partially replaced by chlorite) is a common phase in the granite, where it occurs with magnetite, titanite, zircon, and fluorite (Fig. 67). Biotite is typically riddled with pleochroic haloes surrounding zircon, and many sizeable patches of fluorite are strongly blue-purple and pleochroic.

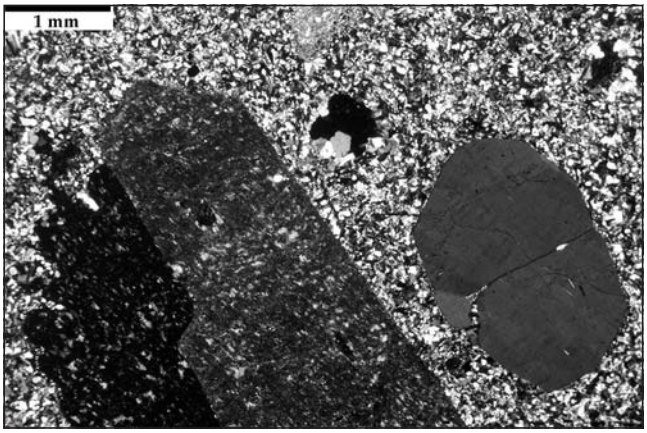

Figure 64. *Quartz phenocryst, and part of a sanidine phenocryst, in extrusive rhyolite (sample PHA-88-PZ, glacial erratic).*

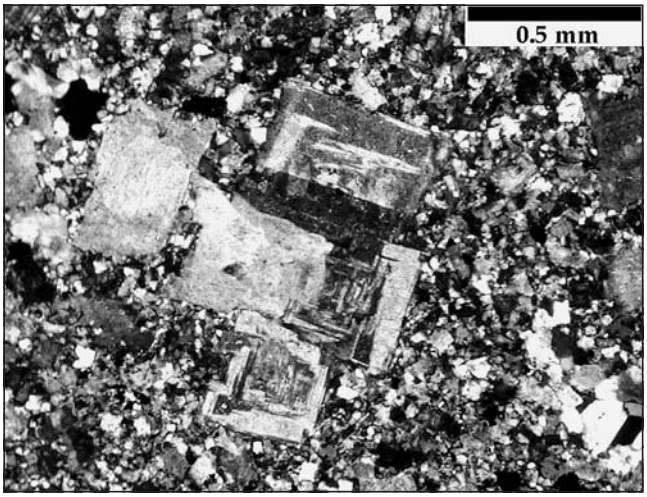

Figure 65. *Alkali-feldspar phenocrysts under crossed polars, showing an equant habit and crosshatched twinning characteristic of anorthoclase, from an extrusive dome in the Kamilukuak basin (sample PHA-89-303). The sample is atypical in its lack of quartz phenocrysts.*

Figure 66. *Complexly decomposed feldspars under crossed polars in Nueltin granite (sample PHA-88-500G), Lost Boat island. Note albite twinning in the ragged core of a tabular alkali-feldspar phenocryst (centre), suggesting it initially consisted of anorthoclase.*

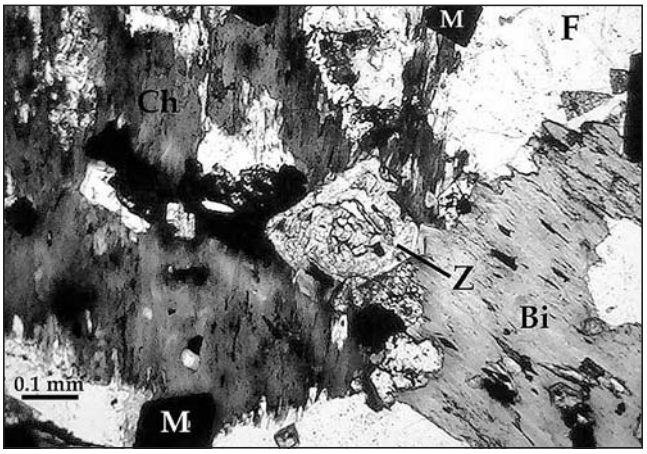

Figure 67. *Late fluorite (F), biotite (Bi; altered to chlorite, Ch), magnetite (M) and zircon (Z) in Nueltin granite under crossed polars (sample PHA-88-500G, Lost Boat island).*

A precise U-Pb zircon age has not been obtained for a Nueltin granite from the study area. A minimum age of 1745 Ma was obtained from a single zircon separate from sample PHA-89-23 (Lost Boat island; Roddick, unpub. data, 1989).

Mesocratic diabase (unit PNb)

Small blebs (0.1–1 cm) of chilled mafic magma are ubiquitous in the rhyolite (Fig. 31). These rocks are petrographically identical to diabasic dykes associated with small stocks of Nueltin granite in Snow River gneiss. They consist of phenocrysts or glomerocrysts of plagioclase (approx. An_{60}) with inclusions of clinopyroxene, in a groundmass consisting of subequal amounts of plagioclase and clinopyroxene with magnetite microphenocrysts. There is a population of plagioclase macrocrysts (approx. 1 cm in size) that are typically rounded. Amphibole is not present and chloritization of clinopyroxene is minimal.

Geochemistry

The Nueltin granite is peraluminous (average Na+K+Ca)/Al = 0.93) and potassic (average K/Na = 1.14). In geochemical discriminant diagrams (e.g. Pearce et al., 1984), they occupy the within-plate granite fields. Their trace-element patterns are very similar to those of the Christopher Island Formation, particularly in having strong depletions in Ti and P and strong enrichments in K and Th (Fig. 68). Barium is depleted in the granite, presumably due to fractionation of alkali feldspar. Prominent negative Eu anomalies (Fig. 69) are consistent with fractionation of Ca-bearing feldspar. One sample (PHA-94-124B), has ε_{Nd} = -9.1 at 1.76 Ga (Table 6, Fig. 62), and is similar to Nueltin granite elsewhere in the western Churchill Province (Peterson et al., 2002).

A whole-rock analysis of a mesocratic diabase (PHA94-124c, unit PNb, Appendix 1) shows it to be an intermediate rock rich in incompatible elements, with a K_2O/Na_2O ratio of approximately 1. It resembles benmoreite (a rock intermediate between alkali basalt and trachyte). Its trace-element pattern follows the top of the Christopher Island Formation envelope, but lacks the negative Ti and P anomalies that are so prominent in most other Proterozoic igneous rocks of the area. Compatible trace elements are at concentrations similar to those in MORB. Both composition and petrography (plagioclase-clinopyroxene-magnetite) are consistent with derivation from a mildly potassic alkali-basalt parent magma.

Kuungmi Formation

The single analysis of Kuungmi Formation lava (PHA89-R5, Appendix 1) shows it to be an Fe-rich, intermediate potassic rock with high Al_2O_3, similar to shoshonite. Although slightly less enriched in LILE than other rocks of the area, it is strongly depleted in compatible elements, which results in a steep negative slope in its trace-element pattern (Fig. 68). A modest negative P anomaly is present, but Ti is not depleted. There is no negative Eu anomaly (Fig. 69), suggesting that plagioclase was not an early-crystallizing phase.

SYNTHESIS: LAURENTIAN TECTONICS AND THE DUBAWNT SUPERGROUP

The Baker Lake Group and the Hudson granitoid rocks (which have no known extrusive equivalents) have an age range (ca. 1850–1800 Ma) that coincides with terminal collision between the Superior and Churchill provinces (Peterson and van Breemen, 1999; Peterson et al., 2002). Despite being situated in the heart of the Churchill Province and well removed from its bounding orogens (Fig. 70), the Dubawnt Supergroup overlies several important fault zones active at this time, such as the extrapolations of the MacDonald and Bathurst faults in the Thelon Tectonic Zone (the Thelon basin overlies their intersection), and the Snowbird Tectonic Zone. Peterson et al. (2000) concluded that the Hudson granitoid rocks were emplaced at mid-crustal levels, probably as a result of crustal heating shortly following lithospheric shortening and thickening. Where the Hudson granitoid rocks are close to sedimentary or volcanic rocks of similar age, they appear to be separated from them by major strike-slip faults, such as the Thirty Mile Lake shear zone southeast of Baker Lake (LeCheminant et al., 1979), or brittle extensional faults, such as the one bounding the northwest edge of a large exposure of Kunwak Formation near Tebesjuak Lake (LeCheminant et al., 1981). Some motion on these faults must therefore be younger than about 1800 Ma, and the motions probably coincide with emplacement of the Nueltin granite bodies (1760–1745 Ma), which are mostly flat lying and not affected by the faults (Rainbird et al., 2001). The Dubawnt minette swarm extends eastward as far as Hudson Bay (Fig. 71), suggesting the possibility that basins of the Baker Lake Group were once much more extensive but have been removed by post–1800 Ma uplift southeast of the Snowbird Tectonic Zone. Deposition of the middle and upper Dubawnt Supergroup at ca. 1760 to 1700 Ma coincided with additional collisional orogenies on the southern margin of the Superior Province (Hoffman, 1988). It therefore seems clear that the Dubawnt Supergroup and contemporaneous plutonic rocks were closely related to intracontinental hinterland deformation and partial melting during the latter stages of the amalgamation of Laurentia.

The literature on Proterozoic continental sedimentary rocks and ultrapotassic igneous rocks contains numerous examples with strong parallels to the Dubawnt Supergroup. These are summarized by Peterson et al. (2002); references on the following examples are contained in that paper. Notable among these examples are

1) minette intrusions and contemporaneous granitic rocks, of identical age and petrology to the Dubawnt minette and Hudson granitoid rocks, in the Nagssugtoqidian Orogen of western Greenland;
2) the ca. 1.7 Ga Espinhaço basin of Brazil, which contains lithofacies very similar to the middle and upper Dubawnt Supergroup and similarly overlies Proterozoic, mixed granite-minette plutons; and
3) the MacArthur basin of northwestern Australia, which is of identical age and lithofacies to the Thelon Formation and very close to outcrops of ca. 1850 Ma ultrapotassic intrusions.

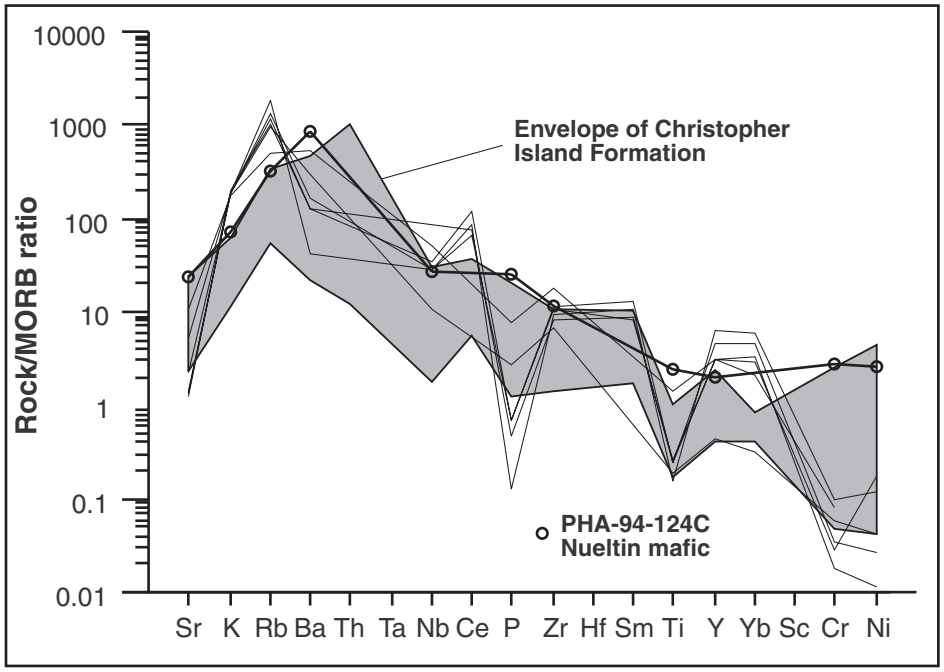

Figure 68. *Trace elements normalized to MORB for all analyzed samples of Nueltin granite and porphyry dykes, and extrusive rhyolite of the Pitz Formation (thin lines). Also shown is a mesocratic diabasic sample (PHA-94-124C, dark line with circles).*

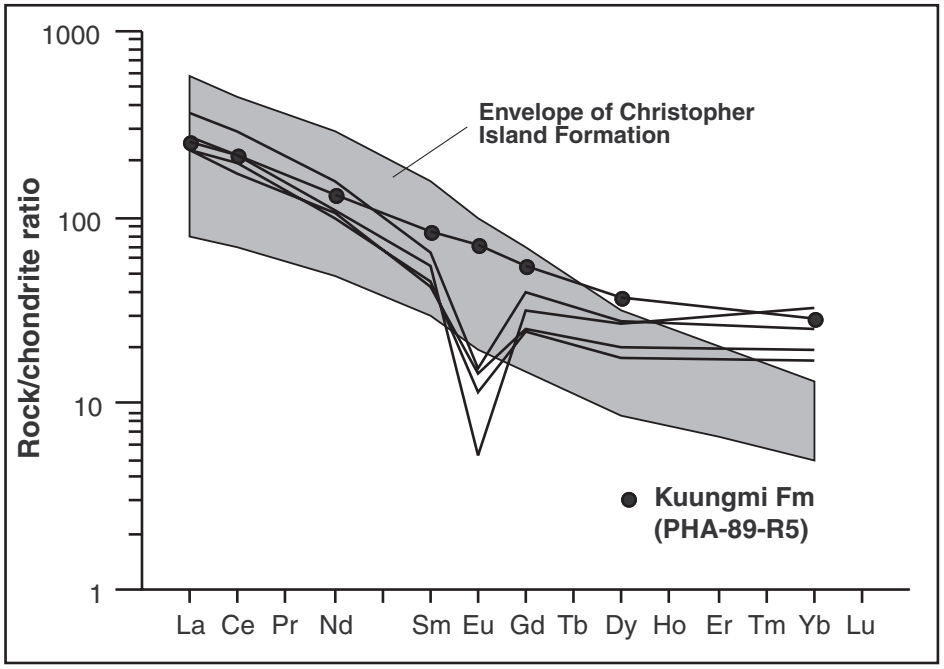

Figure 69. *Rare-earth elements normalized to chondrite for the Pitz Formation and Nueltin granite, and a Kuungmi Formation lava flow (sample PHA-89-R5), normalized to chondrite.*

In addition, the association of minette bodies similar to the Dubawnt swarm with minimum-melt granitoid rocks resembling the Hudson granitoid bodies in geology and petrology, is one that has appeared repeatedly in postorogenic environments from the early Proterozoic to the present day (e.g. the Hercynian Orogeny). A notable present-day example, which appears to be at a point in its development equivalent to late Baker Lake Group times, is the Tibetan plateau. There, ultrapotassic volcanic rocks and alluvial-fluvial sediments are currently being deposited on the western extensional flank of the plateau (the Karakorum fault zone), while mixed ultrapotassic, shoshonitic, and granitic rocks are being emplaced within the plateau proper. Post-minette, anorogenic bimodal rapakivi granite and rhyolite porphyry-basalt, indistinguishable from the Nueltin suite, are an important feature of the early Proterozoic Fennoscandian Orogen.

Although few examples with a completely preserved sequence of plutonic, volcanic, and sedimentary rocks have been described (the Espinhaço basin is the only one that approaches the Dubawnt Supergroup in this regard), the overall tectonic sequence that is characteristic of continental hinterlands to collisional orogenies is readily obtained from these examples. The sequence is

1) crustal thickening by pure shear, thrust stacking, or continental lithosphere subduction or underplating (equivalent to pre–Dubawnt Supergroup);

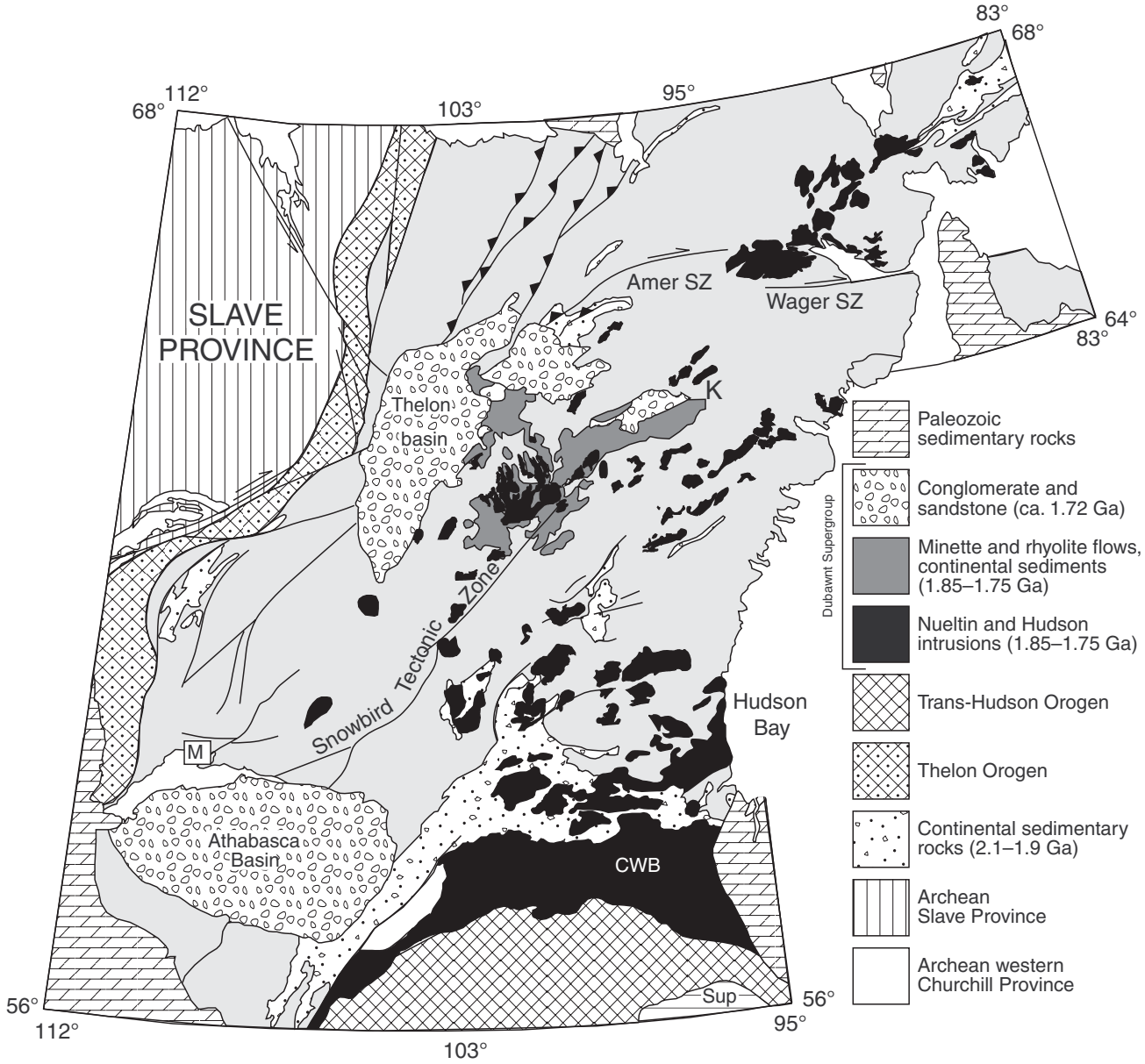

Figure 70. *Principal tectonic elements of the western Churchill Province. Abbreviations: CWB, Chipeweyan-Wathaman batholith; K, Kramanituar granulite complex; M, Martin Group; Sup, Superior Province; SZ, shear zone.*

2) partial melting of a metasomatized upper-mantle layer in the upper (hinterland) plate to produce minette, and in lower continental crust to produce contemporaneous granite magmas that often show mixing with the minette (equivalent to lower Dubawnt Supergroup and Hudson granitoid rocks); volcanism accompanies local fault-bounded basin formation;

3) major extensional faulting, which accompanies basalt melt production in asthenospheric mantle; the basalt invades the lower crust along the faults, triggering the production of anorogenic rapakivi granite and rhyolite-basalt extrusive rocks (equivalent to middle Dubawnt Supergroup); and

4) widespread sagging that produces large (ca. 105 km^2) terrigenous clastic basins with thin veneers of marine dolostone (equivalent upper Dubawnt Supergroup).

Steps (2) and (3) are typically separated by 50 to 100 Ma, and steps (3) and (4) by about 20 Ma.

The precise mechanisms that trigger subduction enrichment of the minette source region, and the later basalt-rapakivi event, cannot be directly deduced from the geology or petrology of the resulting rocks. In the case of the Baker Lake Group, the enrichment event could be Archean (Cousens et al., 2001), but the ubiquity of the minette-granitoid association implies that enrichment and melt generation are much more closely spaced (Peterson et al., 2002). The basalt-rapakivi event may be best explained as a product of lithospheric mantle delamination, with the final crustal sagging due simply to

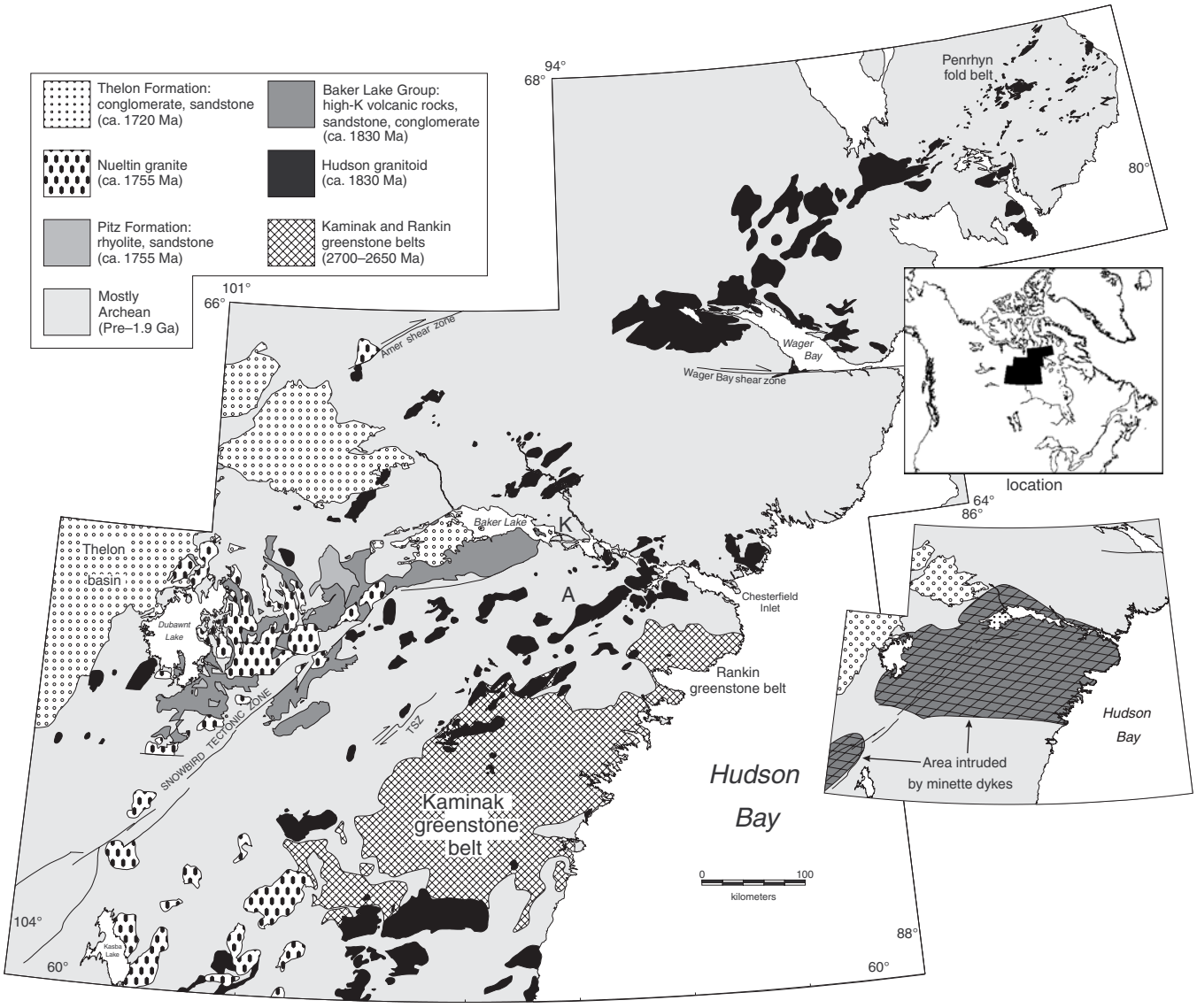

Figure 71. *Proterozoic sedimentary and volcanic rocks (Dubawnt Supergroup) and granitic plutonic rocks (Nueltin suite, Hudson suite) of the western Churchill Province. The lower inset shows the approximate extent of the Dubawnt minette dyke swarm.*

cooling and subsidence. These represent large-scale events in the lower lithosphere, and evidence for them must ultimately come from geophysical imaging of the lithosphere.

SUMMARY OF RESULTS

The results of this study can be summarized as follows:

1) The oldest rocks of the area are polydeformed, northwest-trending, quartzofeldspathic gneiss (Snow River gneiss), with minor amphibolite lenses, that are older than 2.6 Ga. They occupy the southwest corner of the map area, dip shallowly to the northeast, and are bounded on the northeast by a Proterozoic shear and intrusive zone. The gneiss is structurally overlain by biotite-rich schist and metapsammite, and minor iron-formation (Clarke River schist); the gneiss may have been a depositional basement for the schist, or may represent the lower part of a fining-upward clastic sequence.

2) The Snow River gneiss was intruded by a mafic to felsic, ca. 2.6 Ga, calc-alkaline plutonic suite (Snow Island suite), which is dominantly mafic (diorite, granodiorite) in the south half of the map area and felsic (monzonite, granite) to the north. The Clarke River schist, with minor mafic volcanic rocks, constitutes a large raft in Snow Island megacrystic monzonite and leucogranite north of the Snow River gneiss domain.

3) Quartz arenite and minor siltstone (Amer Group) were deposited unconformably over Archean rocks. Before ca. 1.85 Ga, the Amer Group and underlying Archean rocks were subjected to stretching along a south-southwest-trending, shallowly dipping vector, particularly along the northwest side of Dubawnt Lake. Shallowly dipping phyllotectonite beneath and within the Amer Group suggests that northeast-vergent thrust faulting may have occurred at about the same time.

4) At ca. 1.83 Ga, flat-lying flows of felsic minette (lower Christopher Island Formation) erupted onto Archean basement. They were followed by voluminous eruptions of mafic minette, and then siliceous ultrapotassic flows, within extensional basins bounded by active faults. Volcanic facies, ranging from subaerial, welded, proximal breccia and accretionary lapilli tuff to subaqueous flow breccia intercalated with turbiditic epiclastic deposits, suggest local damming of streams by volcanic cones and alluvial fans to produce small deep lakes in narrow valleys. As volcanism waned, faulting continued as alluvial fans were deposited along basin margins and fluvial deposits accumulated on the basin floors (Kunwak Formation).

5) At ca. 1.76 Ga, the eastern side of the map area was intruded by high-silica rapakivi granite (Nueltin granite). Lava flows of porphyritic rhyolite (Pitz Formation) are preserved as isolated domes. Small stocks and veins of Nueltin granite, and comagmatic diabase dykes, are present within the Snow River gneiss. Granite intrusion may have been accompanied by conjugate northeast-northwest faulting to give the basins of the Baker Lake Group their present configuration and orientation.

6) At ca. 1.72 Ga, pebbly quartz arenite of the Thelon Formation was deposited over an unconformity characterized by strong chemical weathering, with the depocentre lying west of Dubawnt Lake. Prior to lithification of the arenite, small volumes of shoshonitic magma erupted within the area (Kuungmi Formation). These are now preserved as small isolated outcrops of lava flows outside the Thelon basin, and phreatomagmatic tuff mixed with quartz sand within the basin.

7) The Dubawnt Supergroup reflects lithospheric deformation, heating, and subsequent cooling in a large continental hinterland during the latter stages of the Trans-Hudson Orogen. Although exceptional in its degree of preservation, it has numerous close parallels in other early Proterozoic sedimentary-volcanic packages that feature ultrapotassic and silicic igneous rocks, extensive basins of pebbly quartz arenite, and the minette-granite association that is characteristic of the late stages of collisional orogens from the early Proterozoic to the present.

REFERENCES

Baragar, W.R.A., Ernst, R.E., Hulbert, L., and Peterson, T.
1996: Longitudinal petrochemical variation in the Mackenzie dyke swarm, northwestern Canadian Shield; Journal of Petrology v. 37, p. 317–359.

Bergman, S.C.
1987: Lamproites and other potassium-rich igneous rocks: a review of their occurrence, mineralogy and geochemistry; *in* Alkaline Igneous Rocks, (ed.) J.G. Fitton and B.G.J. Upton; Geological Society of London, Special Publication 30.

Blake, D.H.
1980: Volcanic rocks of the Paleohelikian Dubawnt Group in the Baker Lake–Angikuni Lake area, District of Keewatin, N.W.T.; Geological Survey of Canada, Bulletin 309, 39 p.

Booth, G.W.
1983: The petrology and geochemistry of the Pamiutuq Lake Batholith, Northwest Territories; M.Sc. thesis, University of Toronto, Toronto, Ontario, 168 p.

Chafetz, H.S. and Guidry, S.A.
1999: Bacterial shrubs, crystal shrubs, and ray-crystal shrubs: bacterial vs. abiotic precipitation; Sedimentary Geology, v. 126, p. 57–74.

Chisholm, R.E.
1993: Diamond drilling report on the DUB 1 + 2 mineral claims; TAIGA Consultants Ltd. Calgary.

Cousens, B.
1999: Geochemistry and geologic setting of the Baker Lake Group, Angikuni Lake to Yathkyed Lake; Indian and Northern Affairs Canada, Geology Division, Open File 1999-05.

Cousens, B.L., Aspler, L.B., Chiarenzelli, J.R., Donaldson, J.A., Sandeman, H., Peterson, T.D., and LeCheminant, A.N.
2001: Enriched Archean lithospheric mantle beneath western Churchill Province tapped during Paleoproterozoic orogenesis; Geology, v. 29, p. 827–830.

Deakin, A.S. and Boxer, G.L.
1989: Argyle AK1 diamond size distribution: the use of fine diamonds to predict the occurrence of commercial size diamonds; *in* Kimberlites and Related Rocks, (ed.) J. Ross, A.L. Jacques, J. Ferguson, D.H. Green, S.Y. O'Reilly, R.V. Danchinn, A.J.A. Danse; Geological Society of Australia, Special Publication 14, v. 2, p.1117–1122.

Donaldson, J.A.
1965: The Dubawnt Group, District of Keewatin and Mackenzie; Geological Survey of Canada, Paper 64-20, 11 p.
1967: Two Proterozoic clastic sequences: a sedimentological comparison; Geological Association of Canada, Proceedings, v. 18, p. 33–54.
1969: Descriptive notes (with particular reference to the Late Proterozoic Dubawnt Group) to accompany a geological map of central Thelon Plain, Districts of Keewatin and Mackenzie; Geological Survey of Canada, Paper 68-49, 4 p.

Eade, K.E.
1972: Geology of Nueltin Lake and Edehon Lake (west half) map areas, District of Keewatin; Geological Survey of Canada, Paper 72-21, 29 p.

Foley, S.F., Venturelli, G., Green, D.H., and Toscani, L.
1987: The ultrapotassic rocks: characteristics, classification, and constraints for petrogenetic models; Earth Science Reviews, v. 24, p. 81–134.

Fraser, K.J., Hawkesworth, C.J., Erlank, A.J., Mitchell, R.H., and Scott-Smith, B.H.
1985: Sr, Nd, and Pb isotope and minor element geochemistry of lamproites and kimberlites; Earth and Planetary Science Letters, v. 76, p. 57–70.

Gall, Q., Peterson, T.D., and Donaldson, J.A.
1992: Early Proterozoic stratigraphy of the Thelon and Baker Lake basins, District of Keewatin: a proposed revision; *in* Current Research, Part C; Geological Survey of Canada, Paper 92-1C, p. 129–137.

Geological Survey of Canada
1972: Dubawnt Lake, District of Keewatin, Northwest Territories; Geological Survey of Canada, Geophysical Series Map 7843G, scale 1:253 440.

Hoffman, P.F.
1988: United Plates of America, the birth of a craton: early Proterozoic assembly and growth of North America; Annual Reviews in Earth Science Letters, v. 16, p. 543–603.

Jones, A.P. and Smith, J.V.
1983: Petrological significance of mineral chemistry in the Agathla Peak and The Thumb minettes, Navajo volcanic field; Journal of Geology v. 91, p. 643–656.

Kjarsgaard, B.K. and Davis, W.J.
1994: Eocene magmatism, southwest Sweetgrass Hills: expression and tectonic significance; *in* LITHOPROBE Alberta Basement Transects, Report of Transect Workshop, Feb. 14–15, 1994; LITHOPROBE Secretariat, University of British Columbia, Report 37, p. 234–237.

LeCheminant, A.N. and Heaman, L.M.
1989: Mackenzie igneous events, Canada: Middle Proterozoic hotspot magmatism associated with ocean opening; Earth and Planetary Science Letters, v. 96, p. 38–48.

LeCheminant, A.N. and Roddick, C.
1991: U-Pb zircon evidence for widespread 2.6 Ga felsic magmatism in the central District of Keewatin, Northwest Territories; *in* Radiogenic Age and Isotope Studies: Report 4; Geological Survey of Canada, Paper 90-2, p. 91–99.

LeCheminant, A.N., Ianelli, T.R., Zaitlan, B., and Miller, A.R.
1981: Geology of Tebesjuak Lake map area, District of Keewatin: a progress report; *in* Current Research, Part B; Geological Survey of Canada, Paper 81-1B, p. 113–128.

LeCheminant, A.N., Jackson, M.J., Galley, A.G., Smith, S.L., and Donaldson, J.A.
1984: Early Proterozoic Amer Group, Beverly Lake map area, District of Keewatin; *in* Current Research, Part B; Geological Survey of Canada, Paper 84-1B, p. 159–172.

LeCheminant, A.N., Leatherbarrow, R.W., and Miller, A.R.
1979: Thirty Mile Lake map area, District of Keewatin; *in* Current Research, Part B; Geological Survey of Canada, Paper 79-1B, p. 319–327.

LeCheminant, A.N., Miller, A.R., and LeCheminant, G.M.
1987: Early Proterozoic alkaline igneous rocks, District of Keewatin, Canada: petrogenesis and mineralization; *in* Geochemistry and Mineralization of Proterozoic Volcanic Suites, (ed.) T.C. Pharaoh, R.D. Beckinsale, and D. Richard; Geological Society of London, Special Publication 33, p. 219–240.

Loveridge, W.D., Eade, K.E., and Roddick, J.C.
1987: A U-Pb age on zircon from a granite pluton, Kamilukuak Lake area, District of Keewatin, establishes a lower limit for the age of the Christopher Island Formation, Dubawnt Group; *in* Radiogenic Age and Isotope Studies: Report 1; Geological Survey of Canada, Paper 87-2, p. 67–71.

Loveridge, W.D., Eade, K.E., and Sullivan, R.W.
1988: Geochronological studies of Precambrian rocks from the southern District of Keewatin; Geological Survey of Canada, Paper 88-18, 36 p.

MacRae, N.D., Armitage, A.E., Miller, A.R., Roddick, J.C., Jones, A.L., and Mudry, M.P.
1996: The diamondiferous Akluilâk lamprophyre dyke, Gibson Lake area, N.W.T.; *in* Searching for Diamonds in Canada, (ed.) A.N. LeCheminant, D.G. Richardson, R.N.W. DiLabio, and K.A. Richardson; Geological Survey of Canada, Open File 3228, p. 101–107.

Miller, A.R., Cumming, G.L., and Krstic, D.
1989: U-Pb, Pb-Pb, and K-Ar isotopic study and petrography of uraniferous phosphate-bearing rocks in the Thelon Formation, Dubawnt Group, Northwest Territories, Canada; Canadian Journal of Earth Sciences, v. 26, p. 867–880.

Mitchell, R.H.
1994: The lamprophyre facies; Mineralogy and Petrology, v. 51, p. 2–4.

Mitchell, R.H. and Bergman, S.C.
1991: Petrology of Lamproites; Plenum Press, New York, New York, 447 p.

Nemec, D.
1988: Origin of syenite porphyries in the Central Bohemian Pluton by magma mixing; Neues Jahrbuch für Mineralogie, v.159, p. 59–71.

Nelson, D.R.
1992: Isotopic characteristics of potassic rocks: evidence for the involvement of subducted sediments in magma genesis; Lithos, v. 28, p. 403–420.

Paul, D.K. and Potts, P.J.
1981: Rare earth abundances and origin of some Indian lamprophyres; Geological Magazine, v. 118, p. 393–399.

Pearce, J.A., Harris, N.B.W., and Tindle, A.G.
1984: Trace element discrimination diagrams for the tectonic interpretation of granitic rocks; Journal of Petrology, v. 25, p. 956–983.

Peterson, T.D.
1994: Early Proterozoic ultrapotassic volcanism of the Keewatin Hinterland, Canada; *in* Proceedings, 5th International Kimberlite Conference, Vol. 1: Kimberlites, Related Rocks and Mantle Xenoliths, (ed.) H.O.A. Meyer and O.H. Leonardos; Campanhia de Pesquisa de Recursos Minerais, Brasilia, Brazil, p. 221–235.
1995: A potassic phreatomagmatic volcanic centre in the Thelon Basin, Northwest Territories: implications for diamond exploration; *in* Current Research 1995-C; Geological Survey of Canada, p. 19–26.

Peterson, T.D. and Born, P.
1994: Archean and lower Proterozoic geology of western Dubawnt Lake, Northwest Territories; *in* Current Research 1994-C; Geological Survey of Canada, p. 157–164.

Peterson, T.D. and LeCheminant, A.N.
1993: Glimmerite xenoliths in Early Proterozoic ultrapotassic rocks of the Churchill Province; Canadian Mineralogist, v. 31, p. 801–819.

Peterson, T.D. and Lee, C.
1995: Pre-Dubawnt plutonism and deformation in the Nicholson Lake–Dubawnt Lake area, Northwest Territories; *in* Current Research 1995-C; Geological Survey of Canada, p. 11–18.

Peterson, T.D. and Rainbird, R.H.
1990: Tectonic and petrological significance of regional lamproite-minette volcanism in the Thelon and Trans-Hudson hinterlands, Northwest Territories; *in* Current Research, Part C; Geological Survey of Canada, Paper 90-C, p. 69–79.

Peterson, T.D. and van Breemen, O.
1999: Review and progress report of Proterozoic granitoid rocks of the Western Churchill Province, Northwest Territories (Nunavut); *in* Current Research 1999-C; Geological Survey of Canada, p. 119–127.

Peterson, T.D., Esperança, S., and LeCheminant, A.N.
1994: Geochemistry and origin of Early Proterozoic ultrapotassic rocks of the Churchill Province, Canada; Mineralogy and Petrology, v. 51, p. 251–276.

Peterson, T.D., van Breemen, O., Sandeman, H.A., and Cousens, B.
2002: Proterozoic (1.85–1.75 Ga) igneous suites of the Western Churchill Province: granitoid and ultrapotassic magmatism in a reworked Archean hinterland; Precambrian Research, v. 119, p. 73–100.

Peterson, T.D., van Breemen, O., Sandeman, H.A., and Rainbird, R.H.
2000: Proterozoic (1.85–1.75 Ga) granitoid plutonism and tectonics of the Western Churchill Province; Geological Association of Canada–Mineralogical Association of Canada, Joint Annual Meeting, GeoCanada 2000, Program and Abstracts, v. 25 (CD-ROM).

Pognante, U.
1990: Shoshonitic and ultrapotassic post-collisional dykes from northern Karakorum (Sinkiang, China); Lithos, v. 26, p. 305–316.

Rainbird, R.H. and Peterson, T.D.
1990: Physical volcanology and sedimentology of lower Dubawnt Group strata, Dubawnt Lake, District of Keewatin, N.W.T.; *in* Current Research, Part C; Geological Survey of Canada, Paper 90-1C, p. 207–217.

Rainbird, R.H., Hadlari, T., Aspler, L.B., Donaldson, J.A., LeCheminant, A.N., and Peterson, T.D.
2003: Sequence stratigraphy and evolution of the Paleoproterozoic intracontinental Baker Lake and Thelon basins, western Churchill Province, Nunavut, Canada; Precambrian Research, v. 125, no. 1-2, p. 21–53.

Rainbird, R.H., Hadlari, T., and Donaldson, J.A.
1999: Stratigraphy and paleogeography of the Paleoproterozoic Baker Lake Group in the eastern Baker Lake basin, Northwest Territories (Nunavut); *in* Current Research 1999-E; Geological Survey of Canada, p. 43–53.
2001: Evolution of the Paleoproterozoic intracratonic Baker Lake and Thelon basins, Western Churchill Province, Canada; *in* Cassidy, J.M. Dunphy, and M.J. Van Kranendonk; AGSO-Geoscience Australia Record 2001/37, p. 259–260.

Rock, N.M.S.
1991: Lamprophyres; Blackie Son Ltd., Glasgow, United Kingdom, 285 p.

Rosa, M.L.S., Conceiçâo, H., Oberli, F., Meier, M., Martin, H., Macambira M.J.B., Conceiçâo, R.V., Barreto dos Santos, E., Paim, M., Leahy, G.A.S., and Leal, L.R.B.
2000: Geochronology (U-Pb/Pb-Pb) and isotopic signature (Rb-Sr/Sm-Nd) of the Paleoproterozoic Guanambi batholith, southwest Bahia state (NE Brazil); Reviews of Brasilian Geology, v. 30, p. 62–65.

Tella, S. and Eade, K.E.
1980: Geology of the Kamilukuak Lake map area, District of Keewatin, a part of the Churchill structural province; *in* Current Research, Part B; Geological Survey of Canada, Paper 80-1B, p. 39–45.
1985: Geology, Kamilukuak Lake, District of Keewatin, Northwest Territories; Geological Survey of Canada, Map 1629A, scale 1:250 000.

Thériault, R.J.
1990: Methods for Rb-Sr and Sm-Nd isotopic analyses at the Geochronology Laboratory, Geological Survey of Canada; *in* Radiogenic Age and Isotopic Studies: Report 3; Geological Survey of Canada, Paper 89-2, p. 3–6.

Thériault, R.J., Henderson, J.B., and Roscoe, S.M.
1994: Nd isotopic evidence for early to mid-Archean crust from high grade gneisses in the Queen Maud Block and south of the McDonald Fault, Western Churchill Province, Northwest Territories; *in* Radiogenic Age and Isotopic Studies: Report 8; Geological Survey of Canada, Current Research 1994-G, p. 37–42.

Tippet, C.R and Heywood, W.W.
1978: Stratigraphy and structure of the northern Amer Group (Aphebian), Churchill structural province, District of Keewatin; *in* Current Research, Part B; Geological Survey of Canada, Paper 78-1B, p. 7–11.

Tyrrell, J.B.
1898: Report on the Dubawnt, Kazan, and Ferguson rivers and the north-west coast of Hudson Bay and on two overland routes from Hudson Bay to Lake Winnipeg; Geological Survey of Canada, Annual Report, 1896, v. 9, pt. F, p. 1–218.

Venturelli, G., Mariani, E.S., Foley, S.F., Capedri, S., and Crawford, A.J.
1988: Petrogenesis and conditions of crystallization of Spanish lamproitic rocks; Canadian Mineralogist, v. 26, p. 67–79.

Wallace, P. and Carmichael, I.S.E.
1989: Minette lavas and associated leucitites from the western front of the Mexican volcanic belt: petrology, chemistry, and origin; Contributions to Mineralogy and Petrology, v. 103, p. 470–492.

Wright, G.M.
1955: Geological notes on central District of Keewatin, Northwest Territories; Geological Survey of Canada, Paper 55-17, 219 p.
1967: Geology of the southeastern barren grounds, parts of the districts of Mackenzie and Keewatin; Geological Survey of Canada, Memoir 350, 91 p.

APPENDIX A

Whole-rock elemental analyses

Sample (PHA-)	88/214A	88/214B	88/216B	88/217	88/303A	88/303B	88/303C	88/500C	88/500D	89/16	89/17	89/18	89/27A
Map unit	PBCva	PBCva	PBCvm	PBCvm	PBCvm	PBCvm	PBCvm	PBCva	PBCva	PBCva	PBCvm	PBCvm	PBCvm
NTS area	65 N/6	65 N/6	65 N/6	65 N/6	65 N/6	65 N/6	65 N/6	65 N/6	65 N/6	65 N/6	65 N/6	65 N/6	65 N/3
UTM easting	389019	389019	388512	389001	397398	397398	397398	390158	390158	389921	389627	389715	391342
UTM northing	7020994	7020994	7020012	7020358	7021664	7021664	7021664	7021749	7021749	7020849	7020699	7020425	7009350
SiO_2	53.00	52.70	55.90	54.70	54.00	50.30	51.10	54.50	53.50	55.50	55.70	53.00	55.30
TiO_2	1.42	1.55	0.78	0.88	0.89	0.89	0.91	1.53	1.41	0.93	0.88	0.76	1.05
Al_2O_3	14.50	15.70	10.90	10.70	10.70	8.90	11.20	14.20	14.80	12.40	11.40	11.20	12.00
Fe_2O_3t	10.32	9.17	7.49	8.29	9.11	8.92	8.74	7.94	11.47	9.47	7.13	7.60	6.82
Fe_2O_3	2.40	4.00	6.50	6.20	7.90	7.60	7.20	4.20	3.00	7.60	4.60	4.30	6.60
FeO	7.20	4.70	0.90	1.90	1.10	1.20	1.40	3.40	7.70	1.70	2.30	3.00	0.20
MnO	0.15	0.14	0.09	0.10	0.07	0.12	0.12	0.08	0.16	0.14	0.09	0.12	0.04
MgO	6.20	5.32	9.36	9.74	11.00	13.41	11.60	5.87	4.88	4.36	8.65	10.43	9.73
CaO	5.38	4.95	2.80	3.85	1.47	6.41	5.37	3.15	6.86	3.31	3.96	4.51	1.54
Na_2O	3.40	5.20	2.40	2.50	2.50	2.50	1.70	2.60	2.50	1.10	2.30	2.50	1.00
K_2O	4.19	2.92	7.21	6.33	7.52	4.95	6.11	6.61	3.12	10.24	7.16	6.82	9.45
P_2O_5	0.62	0.93	0.24	0.70	0.42	0.89	0.98	1.52	0.57	0.68	0.38	0.66	0.72
H_2O	1.60	1.50	1.50	1.30	1.60	1.50	1.60	1.50	1.50	0.80	1.30	1.50	1.40
CO_2	0.10	0.00	0.90	0.10	0.10	0.10	0.10	0.10	0.00	0.00	0.10	0.10	0.00
Total	100.16	99.61	99.48	99.00	99.27	98.77	99.39	99.26	100.00	98.76	98.82	98.90	99.03
Mg#	0.54	0.53	0.71	0.70	0.71	0.75	0.72	0.59	0.46	0.48	0.71	0.73	0.74
F													
Cl													
Rb	123	123	370	337	497	628	612	322	128	364	359	409	664
Be	1.5	1.5	10.0	11.0	13.0	9.6	9.4	3.5	1.6	28.0	13.0	10.0	13.0
Sr	1044	953	817	1102	630	1339	1340	492	775	1720	1738	1359	916
Ba	4943	1718	4249	4676	5930	4251	3471	4156	1635	4748	6913	3002	2575
Y	48	65	72	77	40	76	32	32	51	47	27	22	35
Zr	303	343	415	402	429	367	439	429	283	1051	368	344	523
V	160	150	94	110	120	120	160	170	160	89	86	130	81
Nb	15	19	32					26	36	110	38	27	78
Cr	270	130	300	310	270	400	320	74	150	25	230	220	610
Co	46	36	41	44	61	54	48	32	42	32	41	43	38
Ni	70	36	140	140	190	220	150	11	57	4	99	120	280
Cu	83	19	53	16	35	19	18	21	64	52	7	12	4
Zn	120	140	140	120	140	110	120	130	140	150	60	80	44
La	52	110	98	120	120	140	110	190	63			95	100
Ce	120	240	200	310	290	280	240	380	130			220	270
Nd	71	98	120	140	180	140	120	160	65			110	170
Sm	9.1	16.0	16.0	19.0	25.0	19.0	17.0	19.0	8.7			17.0	32.0
Eu	2.50	3.90	4.10	4.80	5.70	5.30	4.60	5.10	2.50			3.80	4.80
Gd	7.10	10.00	12.00	14.00	19.00	14.00	14.00	14.00	7.10			11.00	19.00
Dy	3.90	5.80	5.80	7.20	9.00	7.00	7.40	6.80	4.60			5.60	8.90
Ho													
Er													
Tm													
Yb	1.60	1.80	1.70	1.90	1.90	1.70	1.90	1.80	1.50			1.60	2.10
U	1.1	2.2	4.5					5.0		17.0	6.8	3.2	11.0
Th	5.4	13.0	48.0					26.0		160.0	54.0	39.0	79.0
Pb	14.0	16.0	75.0					27.0		120.0	20.0	19.0	60.0
$^{87}Rb/^{86}Sr$		0.3436						2.094		0.6238			2.429
$^{87}Sr/^{86}Sr$		0.713888						0.756775		0.722846			0.773745
$^{147}Sm/^{143}Nd$		0.0901						0.0849		0.0951			0.1176
$^{143}Nd/^{144}Nd$		0.511005						0.51094		0.510992			0.511238
ε_{Sr}		35.1						-13.0		57.2			102.6
ε_{Nd}		-6.8						-6.8		-8.2			-8.7
$T_{Nd, DM}$		2630						2601		2756			3011
$T_{ND, CHUR}$		2327						2307		2460			2686

Appendix A (cont.)

Sample (PHA-)	89/27B	89/35A	89/35B	89/72	89/73	89/81	89/82	89/111	89/123	89/124	89/205	89/231	89/X1
Map unit	PBCvm	PBCvm	PBCvm	PBCvm	PBCvm	PBCvf	PBCvf	PBCvm	PBCvf	PBCvf	PBCvf	PBCvf	PBCvf
NTS area	65 N/3	6 5N/3	65 N/3	65 N/3	65 N/3	65 K/15	65 K/15	65 N/6	65 K/15	65 K/15	65 K/11	65 K/15	65 N/2
UTM easting	391342	391588	391588	391472	391472	411072	410027	397388	406957	406797	392500	406851	401034
UTM northing	7009350	7009126	7009126	7009099	7009092	6975667	6976107	7021724	6984852	6985967	6955000	6978832	6991874
SiO_2	51.50	53.00	53.80	54.90	54.20	63.50	56.10	50.30	62.30	52.20	60.5	62.50	59.30
TiO_2	0.88	0.78	0.86	0.83	0.86	0.46	0.63	0.85	0.41	0.71	0.54	0.40	0.64
Al_2O_3	11.20	11.10	12.50	11.60	12.10	13.80	12.70	9.80	12.80	10.80	13.40	14.60	12.60
Fe_2O_3t	6.45	7.74	7.73	6.02	5.89	4.78	6.88	8.30	3.50	6.53	4.41	5.26	5.63
Fe_2O_3	4.80	7.30	7.40	5.80	4.90	2.80	4.90	7.20	1.30	5.10	3.20	4.60	2.00
FeO	1.50	0.40	0.30	0.20	0.90	1.80	1.80	1.00	2.00	1.30	1.10	0.60	3.30
MnO	0.08	0.08	0.07	0.10	0.06	0.07	0.10	0.10	0.06	0.13	0.06	0.07	0.07
MgO	10.03	10.11	9.32	8.62	10.07	3.90	6.28	12.49	3.53	5.30	3.99	2.77	6.60
CaO	6.87	4.11	3.08	5.12	3.33	2.86	5.06	7.73	4.16	7.48	3.36	3.17	5.80
Na_2O	0.50	1.10	1.50	1.00	1.00	3.70	2.60	2.60	0.10	2.00	2.60	7.30	0.90
K_2O	8.95	7.93	8.72	8.45	8.74	6.21	7.01	4.60	8.38	6.61	7.33	1.77	6.53
P_2O_5	0.57	0.76	0.95	0.87	0.78	0.33	0.69	0.46	0.32	0.79	0.60	0.42	0.85
H_2O	1.40	1.40	1.40	1.50	1.50	0.90	1.30	1.20	1.80	1.40	1.30	0.70	1.40
CO_2	0.10	0.00	0.10	0.00	0.10	0.10	0.20	0.00	1.60	4.70	0.20	0.50	0.00
Total	98.38	98.07	100.00	98.99	98.54	100.43	99.37	98.33	98.76	98.52	98.18	99.40	99.99
Mg#	0.75	0.72	0.70	0.74	0.77	0.62	0.64	0.75	0.67	0.62	0.64	0.51	0.70
F													
Cl													
Rb	370	336	410	322	455	389	378	628	444	326	463	113	347
Be	10.0	7.4	10.0	7.8	6.8	7.5	4.0	8.7	3.7	5.3	7.6	6.4	3.6
Sr	687	2377	1705	1378	2077	368	463	1143	538	1330	619	625	1234
Ba	3030	3538	3816	3759	3907	1828	2593	5817	1719	1220	2359	466	4356
Y	43	21	21	25	22	16	18	26	13	17	16	13	20
Zr	541	223	285	321	259	307	169	442	262	219	372	254	348
V	57	190	200	120	130	66	110	140	58	110	67	46	83
Nb	74	21	21	27		19	13	24	17			15	
Cr	470	400	410	270	300	170	200	350	160	170	120	130	110
Co	41	41	40	38	40	21	34	49	18	30	22	17	30
Ni	290	180	180	140	150	59	70	180	41	61	40	43	68
Cu	6	18	6	5	5	32	28	22	170	58	14	24	14
Zn	75	77	76	87	78	50	62	83	25	61	41	28	59
La	130				97	55	62	140	53		55		78
Ce	320				210	110	130	290	100		110		150
Nd	170				96	50	69	130	50		50		65
Sm	28.0				17.0	7.0	9.5	20.0	6.1		8.5		11.0
Eu	5.50				4.00	1.90	2.70	5.30	1.70		2.30		3.10
Gd	19.00				12.00	5.30	7.20	13.00	4.60		6.00		8.10
Dy	11.00				6.00	3.40	4.10	6.60	2.90		3.60		4.60
Ho													
Er													
Tm													
Yb	2.90				1.80	1.50	1.40	1.80	1.40		1.50		1.50
U	12.0	3.0	3.6	7.3		22.0	4.6	9.5	17.0			12.0	
Th	65.0	24.0	27.0	34.0		46.0	15.0	36.0	37.0			31.0	
Pb	22.0	27.0	23.0	32.0		75.0	21.0	70.0	34.0			23.0	
$^{87}Rb/^{86}Sr$	1.76					3.507	2.708	1.568				0.5751	
$^{87}Sr/^{86}Sr$	0.751992					0.79233	0.772975	0.745574				0.719688	
$^{147}Sm/^{143}Nd$	0.1083					0.1007	0.1067	0.0985				0.105	
$^{143}Nd/^{144}Nd$	0.511191					0.511078	0.511186	0.511061				0.511146	
ε_{Sr}	44.6					-38.4	-13.3	25.5				30.5	
ε_{Nd}	-7.4					-7.8	-7.1	-7.6				-7.5	
$T_{Nd, DM}$	2815					2777	2780	2747				2792	
$T_{ND, CHUR}$	2485					2467	2450	2438				2470	

Appendix A (cont.)

Sample (PHA-)	89/X2	89/X3	89/X4	89/X5	89/X6	89/X7	89/X8	89/K8	89/K42	89/K95	89/K118B	89/K146	89/K149
Map unit	PBCvf	PBCvf	PBCvf	PBCvm	PBCvm	PBCvm	PBCvm	dyke	dyke	dyke	dyke	dyke	dyke
NTS area	65 N/2	65 N/2	65 N/2	65 N/2	65 N/2	65 N/2	65 N/2	65 N/4	65 N4	65 K/15	65 K/15	65 K/14	65 K/15
UTM easting	401058	401072	401143	401261	401247	401426	401568	369414	361100	410245	401210	382550	398212
UTM northing	6991892	6991902	6991963	6992100	6992086	6992143	6992147	6995531	7013725	6985860	6976950	6961142	6963252
SiO_2	63.50	62.10	58.20	54.60	53.60	52.40	52.00	47.10	51.80	56.70	53.20	50.20	53.40
TiO_2	0.60	0.66	0.69	0.83	0.87	0.86	0.60	1.40	0.62	0.63	0.70	0.80	0.60
Al_2O_3	13.50	13.20	12.50	11.40	11.90	12.20	11.60	10.40	11.50	12.80	13.00	10.20	12.40
Fe_2O_3t	4.87	5.51	6.44	6.74	6.77	7.90	7.56	6.04	7.11	6.78	7.52	5.86	7.24
Fe_2O_3	3.00	2.10	2.70	4.10	3.80	4.60	5.80	3.40	4.80	2.60	2.90	3.00	3.50
FeO	1.70	3.10	3.40	2.40	2.70	3.00	1.60	2.40	2.10	3.80	4.20	2.60	3.40
MnO	0.06	0.07	0.08	0.09	0.08	0.10	0.12	0.09	0.10	0.11	0.13	0.06	0.10
MgO	3.15	2.91	5.49	8.87	10.06	9.27	10.01	5.19	9.55	6.75	7.72	7.13	6.31
CaO	2.77	4.45	5.79	4.88	3.56	5.55	6.27	9.41	6.30	5.11	6.47	9.65	5.85
Na_2O	1.70	2.10	2.10	1.80	1.00	0.50	1.70	1.30	1.60	2.50	3.40	1.40	2.30
K_2O	7.50	5.41	7.17	7.39	8.25	8.16	6.99	8.64	4.98	6.24	3.33	4.87	6.32
P_2O_5	0.70	0.92	0.91	1.17	1.20	0.64	0.61	2.59	0.58	0.71	0.61	0.86	0.53
H_2O	1.20	1.00	0.90	1.60	1.80	1.70	1.70	1.50	3.10	1.70	2.40	2.60	1.60
CO_2	0.10	0.10	0.00	0.10	0.10	0.00	0.10	4.20	2.30	0.00	1.20	6.50	2.90
Total	99.48	98.12	99.93	99.23	98.92	98.98	99.10	97.62	99.33	99.65	99.26	99.87	99.21
Mg#	0.56	0.51	0.63	0.72	0.75	0.70	0.72	0.63	0.73	0.66	0.67	0.71	0.63
F													
Cl													
Rb	314	243	305	221	303	333	247	223	173	194	89	204	229
Be	3.6	2.5	5.7	6.3	6.6	9.0	3.0	8.6	5.2	6.6	3.0	5.8	3.4
Sr	616	1231	2001	1870	1821	1196	1712	2652	1959	976	1066	596	1008
Ba	4542	4154	4797	6317	6077	5632	3715	9957	3587	2760	2303	2512	2180
Y	18	21	21	24	25	30	19	38	17	19	20	20	19
Zr	331	336	299	314	354	423	180	803	237	286	223	346	186
V	23	99	110	93	100	99	110	95	120	90	110	94	100
Nb								20					
Cr	64	130	120	400	420	230	530	170	270	290	280	420	170
Co	20	24	33	40	41	42	45	34	44	37	40	39	36
Ni	26	58	72	120	130	100	200	12	61	110	120	210	65
Cu	6	31	49	61	37	27	10	61	24	29	52	61	46
Zn	59	57	66	75	80	94	70	86	75	110	86	59	71
La	93	85	86					170		78		87	
Ce	170	180	160					330		150		190	
Nd	80	76	72					140		68		83	
Sm	10.0	12.0	12.0					26.0		11.0		14.0	
Eu	2.80	3.30	3.20					7.60		3.00		3.60	
Gd	7.30	8.70	8.60					19.00		8.20		10.00	
Dy	3.90	4.90	4.70					10.00		4.50		5.30	
Ho													
Er													
Tm													
Yb	1.10	1.60	1.20					2.30		1.50		1.40	
U								3.5					
Th								11.0					
Pb								51.0					
$^{87}Rb/^{86}Sr$								0.2512					
$^{87}Sr/^{86}Sr$								0.7107					
$^{147}Sm/^{143}Nd$								0.1061					
$^{143}Nd/^{144}Nd$								0.511219					
ε_{Sr}								24.5					
ε_{Nd}								-6.3					
$T_{Nd, DM}$								2719					
$T_{ND, CHUR}$								2379					

Appendix A (cont.)

Sample (PHA-)	89/K152	89/K182	89/M32	89/Q1A	89/R16	89/R51	91/18	91/83	91/137	91/150F	91/150M	91/LBIF	91/Q33
Map unit	dyke	dyke	dyke	PBCvm	PBCvm	PBCvm	dyke	PBCva	PBCvm	PBCx	PBCx	PBCs2	dyke
NTS area	65 K/15	65 N/6	65 K/15		65 K/14	65 N/2				65 N/7	65 N/7	65 N/6	
UTM easting	398480	398108	400690		389919	407690		392330	414450	417820	417820	390000	411370
UTM northing	6963369	7021154	6972000		6970935	6989481		7037950	7048850	7037250	7037250	7022000	7016530
SiO_2	51.10	49.50	53.30	47.61	53.40	53.20	49.10	56.90	56.20	57.20	52.30	57.70	54.60
TiO_2	0.68	0.92	0.60	1.35	0.85	0.67	0.57	0.92	0.62	0.62	0.52	0.90	0.86
Al_2O_3	10.60	10.60	12.30	15.15	11.80	11.50	12.60	11.50	11.20	13.50	10.90	11.60	11.70
Fe_2O_3t	6.56	8.27	7.35	11.72	8.18	7.90	8.76	11.11	10.65	7.22	6.94	9.14	7.18
Fe_2O_3	3.70	7.50	3.50	11.72	7.30	3.50	5.90	8.80	10.10	4.80	3.20	8.70	1.90
FeO	2.60	0.70	3.50		0.80	4.00	2.60	2.10	0.50	2.20	3.40	0.40	4.80
MnO	0.10	0.06	0.11	0.16	0.08	0.13	0.16	0.11	0.04	0.08	0.11	0.07	0.13
MgO	8.08	16.19	6.76	13.56	9.62	9.86	8.28	6.97	9.91	5.84	12.71	5.91	8.31
CaO	6.11	1.87	6.01	1.84	3.93	7.35	8.54	1.55	1.01	4.69	6.86	1.60	7.06
Na_2O	2.00	2.00	2.60	1.53	1.00	1.40	1.30	0.10	0.10	4.00	1.30	2.10	1.00
K_2O	7.72	6.56	5.34	4.17	8.45	5.77	6.03	5.71	4.34	4.61	5.34	7.56	6.18
P_2O_5	0.86	0.51	0.50	0.16	0.76	0.79	0.97	1.14	0.74	0.58	0.51	0.72	0.73
H_2O	1.90	2.50	2.10		1.40	1.60	1.80	3.50	4.30	1.10	2.60	1.30	1.80
CO_2	3.50	0.10	3.40		0.00	0.00	1.10	0.00	0.00	0.00	0.10	0.10	0.10
Total	98.95	99.01	100.02	97.25	99.39	99.77	98.95	99.30	99.06	99.22	99.85	98.66	99.17
Mg#	0.71	0.80	0.65	0.70	0.70	0.71	0.65	0.55	0.65	0.62	0.78	0.56	0.70
F													
Cl													
Rb	320	549	208	131	391	225	193	200	136	158	278	292	208
Be	6.3	10.0	3.3		10.0	4.8	7.1	8.6	3.0	3.2	2.2	21.0	10.0
Sr	1797	1418	973	629	1950	1337	2744	1028	263	1137	1152	1040	1255
Ba	3173	2757	1807	2127	4042	3841	5424	2377	7641	3060	3151	4003	3539
Y	26	22	18	21	22	18	24	29	17	16	13	47	33
Zr	344	428	178	140	270	234	241	398	154	183	152	924	421
V	110	140	100	251	170	110	140	69	93	120	86	82	89
Nb		24		17			9	6	10	1	8	37	32
Cr	280	620	220	16	310	370	110	140	360	70	580	13	160
Co	41	57	38		44	48	43	45	58	24	41	28	35
Ni	120	250	77		140	130	100	230	200	56	380	31	150
Cu	59	10	43	6	3	59	91	28	10	34	44	52	58
Zn	68	90	78	105	79	73	97	64	69	43	64	140	150
La	110	98	57	26.1	91		63	120	95	57	48	210	170
Ce	240	210	120	60.2	200		120	210	160	110	87	340	310
Nd	120	120	59	30.2	92		62	130	84	55	43	190	200
Sm	20.0	19.0	9.5	6.14	17.0		11.0	22.0	15.0	9.4	7.1	34.0	34.0
Eu	4.50	4.40	2.70	1.85	3.80		2.00	4.50	3.30	1.90	1.50	6.60	4.60
Gd	13.00	12.00	7.10	5.56	11.00		7.00	14.00	11.00	6.20	5.50	21.00	19.00
Dy	6.70	5.90	4.30	4.84	5.50		4.20	7.90	6.00	4.10	3.40	12.00	8.60
Ho				0.87			0.70	1.30	1.00	0.70	0.61	2.00	1.30
Er				2.35			1.70	2.50	2.50	1.70	1.50	4.30	2.30
Tm				0.35			0.27	0.44	0.42	0.30	0.22	0.71	0.38
Yb	1.70	1.50	1.80	2.09	1.70								
U		5.6		0.50			5.3	11.0	1.8	6.7	3.9	16.0	19.0
Th		49.0		2.67			15.0	47.0	15.0	14.0	12.0	220.0	74.0
Pb		29.0		6.64									
$^{87}Rb/^{86}Sr$				0.58447						0.38818	0.68162	0.78366	
$^{87}Sr/^{86}Sr$				0.720445						0.717783	0.727454	0.72938	
$^{147}Sm/^{143}Nd$				0.13466						0.10778	0.10734	0.11565	
$^{143}Nd/^{144}Nd$				0.511583						0.511303	0.511167	0.511092	
ε_{Sr}				37.8						73.8	101.0	90.1	
ε_{Nd}				-6.0						-5.1	-7.7	-11.1	
$T_{Nd, DM}$				3000						2642	2823	3174	
$T_{ND, CHUR}$				2582						2281	2499	2893	

Appendix A (cont.)

Sample (PHA-) Map unit NTS area UTM easting UTM northing	91/Q37 PBCvf	88/500E PNg 65 N/6 390158 7021749	88/500G PNg 65 N/6 390158 7021749	89/23 PNg 65 N/6 391749 7020545	89/303 PWPv 65 K/15 399472 6966643	89/R37 PWPv 65 K/14 391390 6961170	89/PZ PWPv 65 K/15 boulder, Slow River	94/124C PNb 65 L/16	89/7 ACp 65 N/6 376259 7030829	89/R5 PRK 65 K/14 379050 6980210
SiO_2	69.30	76.10	76.80	75.70	71.30	63.70	75.70	56.46	42.50	49.50
TiO_2	0.25	0.15	0.21	0.23	0.17	0.93	0.22	1.45	0.25	1.79
Al_2O_3	13.60	12.30	12.00	12.30	14.10	14.60	11.80	13.81	5.20	16.20
Fe_2O_3t	2.95	1.29	1.15	1.38	1.91	6.02	1.95	8.46	19.02	11.62
Fe_2O_3	1.30	0.30	0.60	0.50	1.80	5.80	0.30	8.46	12.20	3.70
FeO	1.50	0.90	0.50	0.80	0.10	0.20	1.50		6.20	7.20
MnO	0.06	0.01	0.01	0.02	0.01	0.07	0.02	0.14	0.12	0.24
MgO	1.70	0.12	0.19	0.21	0.39	0.86	0.28	5.10	28.24	6.05
CaO	2.38	0.61	0.55	0.71	0.19	2.01	0.61	6.21	3.12	5.08
Na_2O	3.20	3.10	2.80	2.90	4.40	3.80	2.60	2.65	0.70	2.70
K_2O	5.88	5.46	5.56	5.45	5.34	5.29	5.65	2.40	0.44	3.17
P_2O_5	0.17	0.01	0.03	0.04	0.13	0.31	0.04	0.80	0.03	0.27
H_2O	0.60	0.60	0.60	0.50	0.70	1.30	0.70		1.60	4.00
CO_2	0.00	0.00	0.10	0.10	0.10	1.20	0.10		0.20	0.10
Total	99.94	99.66	99.95	99.46	98.73	100.07	99.52	97.49	100.80	100.00
Mg#	0.53	0.16	0.25	0.23	0.29	0.22	0.22	0.54	0.75	0.51
F		3377	2042							
Cl		313	393							
Rb	286	484	334	366	283	166	301	111	13	70
Be	4.5	4.6	4.8	7	5	3	3		.3	1.7
Sr	337	72	73	107	223	391	66	751	109	553
Ba	1363	206	529	651	1058	1742	523	2480	172	1238
Y	13	64	36	35	7	36.0	49	24	5	19
Zr	202	269	245	297	201	457	315	315	22	209
V	27	0	1	1	18	11	3	152	87	220
Nb	15	26	67	26	12	43	31	25	10	42
Cr	37	17	6	4	11	14	7	260	2400	34
Co	11	3	3	2	4	13	4		110	50
Ni	26	7	10	1	3	0	2	90	590	23
Cu	25	4	2	2	4	5	3	32	70	50
Zn	51	23	21	26	19	68.0	36	107	70	340
La	66	90	77	75	41	99	120		2	53
Ce	110	190	170	150			250			110
Nd	40	69.0	62.0	67.0			98.0			42
Sm	6.1	11.0	9.2	8.7			13.0			7.6
Eu	1.00	0.4	0.9	1.1			1.2			2.3
Gd	4.00	8.8	6.7	7.0			11.0			5.8
Dy	2.70	9.3	6	6.8			9.5			4.3
Ho	0.51									
Er	1.30									
Tm	0.23									
Yb		7.1	3.8	4.3	0.6	2.9	5.5		0.1	1.9
U	38.0									
Th	66.0									
Pb										
$^{87}Rb/^{86}Sr$	2.57391									
$^{87}Sr/^{86}Sr$	0.785575									
$^{147}Sm/^{143}Nd$	0.10161									
$^{143}Nd/^{144}Nd$	0.511016									
ε_{Sr}	216.5									
ε_{Nd}	-9.3									
$T_{Nd, DM}$	2882									
$T_{ND, CHUR}$	2589									

This is a Windows®-based autostart disk. If the autostart is not working, go to the CD-ROM root directory and double-click on the autoplay.exe file. If you read this CD-ROM with a Mac® or UNIX® operating system, the autostart will not work.

PDF files containing the full Bulletin contents are located in the \PDF folder on this CD.

Recommended minimum hardware/software:

PC	-	Pentium® processor with Windows® 98
MAC	-	Mac® OS X v. 10.2.2
UNIX	-	Go to adobe.com to download appropriate reader for your system
Monitor	-	17" colour monitor, video resolution of 1280 x 1024
RAM	-	64 MB

Adobe® Acrobat® Reader® v. 6.0 is required to view the contents of this CD-ROM. It is included on the CD-ROM in the \APPS directory.

Ceci est un disque à lancement automatique pour les systèmes d'exploitation Windows®. Si le lancement automatique ne fonctionne pas, allez au répertoire principal du CD-ROM et cliquez deux fois sur le fichier autoplay.exe. Si vous lisez ce disque à l'aide d'un système d'exploitation Mac® ou UNIX®, le lancement automatique ne fonctionnera pas.

Des fichiers PDF renfermant le contenu intégral du bulletin sont situés dans le dossier \PDF sur ce disque.

Configuration minimale recommandée :

PC	-	processeur Pentium® avec Windows® 95
MAC	-	Mac® OS X v. 10.2.2
UNIX	-	Connectez-vous au site « www.adobe.com» pour télécharger la version du logiciel dont vous avez besoin pour votre système
Moniteur	-	moniteur couleur de 17 po, avec résolution vidéo de 1280 x 1024
RAM	-	64 Mo

Le logiciel Acrobat® Reader® v. 6.0 d'Adobe® est requis pour visionner le contenu de ce CD-ROM. Il est fourni sur le disque dans le répertoire \APPS.